

---

Electronic Thesis and Dissertation Repository

---

12-5-2023 10:00 AM

## Elucidating the Relationships Between Spider Size, Joint Stiffness, and the Mechanical Frequency Response of the Body

Reese L. Gartly, *Western University*

Supervisor: Mhatre, Natasha, *The University of Western Ontario*

A thesis submitted in partial fulfillment of the requirements for the Master of Science degree in Biology

© Reese L. Gartly 2023

Follow this and additional works at: <https://ir.lib.uwo.ca/etd>



Part of the [Integrative Biology Commons](#)

---

### Recommended Citation

Gartly, Reese L., "Elucidating the Relationships Between Spider Size, Joint Stiffness, and the Mechanical Frequency Response of the Body" (2023). *Electronic Thesis and Dissertation Repository*. 9835.  
<https://ir.lib.uwo.ca/etd/9835>

This Dissertation/Thesis is brought to you for free and open access by Scholarship@Western. It has been accepted for inclusion in Electronic Thesis and Dissertation Repository by an authorized administrator of Scholarship@Western. For more information, please contact [wlsadmin@uwo.ca](mailto:wlsadmin@uwo.ca).

# Abstract

Spiders use vibrations to sense their surroundings. It has been suggested that the vibration perception in spiders may be altered by the mechanics of the body. I studied the biomechanics of spiders, at the level of leg joints and the whole body. To study joints, I quantified the allometry of leg joint stiffness in spiders. I found that the stiffness of spider joints increased nearly isometrically with increasing body mass, partly by having shorter and thicker leg segments and also by other unknown means. Using these data, I developed empirically validated biomechanical models which predicted the effects of mechanics on vibrational filtering within the body. Interestingly, both models and empirical data showed that the relatively linear increase in joint stiffness with mass meant that the mechanical filtering of spider bodies may be size independent, indicating that spiders of different masses or ecologies may sense the world in similar ways.

## Keywords

Vibrations, mechanical filtering, modes of vibration, vibration transmission, multi-body modeling, mechanoreception, biomechanics.

# Summary for Lay Audience

Spiders sense the world and communicate using vibrations. Vibrations are caused by forces that make a spider's web move up and down or side to side periodically. In a spider's world, vibrations can come from prey caught in the web, a male courting a female, or noise from wind and rain. Spiders sense these vibrations using sensors located near their leg joints. If the vibration makes the joint bend, then the sensor is activated, and the spider can sense that vibration.

I am interested in understanding whether different spider's bodies move differently when they are vibrated by large prey such as a moth in the web, by small prey such as a fruit fly, or by the wind blowing. Different properties of a spider's body determine what causes it to vibrate, what causes its leg joints to bend, and how it moves when it vibrates. Two of these are a spider's mass and the stiffness of its leg joints. Heavier spiders respond to low frequency vibrations, whereas spiders with stiffer joints respond to higher frequencies. But stiffer joints are needed to carry heavier spiders. So, my main questions are, do heavier spiders have stiffer joints? And do these two effects balance each other, or do heavier spiders vibrate differently than lighter spiders?

To answer the first question, I measured joint stiffness in 11 spider species and tested how it changed with spider mass. I incorporated these data into computer simulations of the bodies of three spider species. These simulations predicted how spiders of different sizes with different joint stiffnesses would move when vibrated. I tested simulation results against measurements of real spiders of all three species. I found that heavier spiders had stiffer joints,

balancing the effect of the increased mass. I found that the models and data from real spiders showed that the net effect of this was that spiders of different sizes vibrated in very similar ways. My thesis therefore suggests that even though spiders may come in various sizes, they may be perceiving the world in very similar ways.

# Co-Authorship Statement

Chapter Two is a version of a manuscript that has been submitted to the Journal of Comparative Physiology A. I am the first author of the manuscript with co-authors Dr. Natasha Mhatre, Dr. Benjamin D. Rubin, Lachlan Fisher, and Mouad Elganga. For this manuscript, I completed the research concept and design, sample collection, data collection, data analysis and writing. LG and ME contributed to sample and data collection. BDR contributed to statistical modeling and analysis. NM supervised the work.

Content from Chapter Three is planned to be included in a manuscript that will be submitted to a peer reviewed journal. The manuscript will be co-authored by myself, Dr. Natasha Mhatre, Dr. Senthurran Sivalinghem and Prof. Andrew C. Mason. For this manuscript, NM contributed to data collection, initial modeling and writing, SS contributed to data collection and AM supervised the work. I will be updating the models using my data from Chapter Three.

All work presented in this thesis was completed under the supervision of Dr. Natasha Mhatre. For all chapters, I contributed to all components of project completion including research conception and design, sample collection, data collection, model construction, data analysis, data interpretation and all writing. BDR contributed to statistical modeling and analysis for Chapter Two. LF and ME contributed to sample collection, data collection and animal care for Chapter Two. Data from the 2018 preprint (Mhatre et al., 2018) collected by NM was used as part of my dataset for Chapter Three.

# Acknowledgements

I would first like to thank my supervisor, Dr. Natasha Mhatre. It has been an honour to be one of your first graduate students and I am grateful that I had your guidance to help me navigate this journey.

Thank you to my advisors, Drs. Jim Staples and Chris Guglielmo for being insightful, enthusiastic, and supportive advisors. Thank you to Dr. Benjamin Rubin for your help with the statistical analyses in Chapter Two.

Thank you to my lab mates – Dr. Erin Brandt, Mika Little, Hossein Asgari, and all undergrads over the years – for your feedback, brainstorming sessions, and the laughs. A special thank you to Lachlan Fisher and Mouad Elganga for your tireless work in the summer. Chapter Two would not have been feasible in that time frame without you two.

Thank you to Aaron Mayordomo for lending me his pet tarantulas. Pumpkin and Samus were a treat to have in the lab.

Last, but not least, thank you to my family – Mom, Dad, Racheal, and Laine – and to Josh for always supporting me in this journey. For celebrating my highs with me, cheering me on in the lows, and for listening to me when I geek out about a spider I have found. Love you all!

# Table of Contents

Abstract .....	ii
Summary for Lay Audience.....	iii
Co-Authorship Statement.....	v
Acknowledgements .....	vi
List of Tables.....	xi
List of Figures .....	xii
List of Appendices .....	xiv
Chapter One: Introduction .....	1
1.1 Spider sensory ecology .....	1
1.1.1 Vibration sources differ in temporal pattern .....	1
1.1.2 Vibration sources can also differ in frequency .....	4
1.2 Spider slit sensillae and lyriform organs .....	5
1.2.1 How is mechanical strain sensed by the slit sensillae?.....	9
1.2.2 Which joints sense vibrations?.....	10
1.3 Signal filtering changes the frequency content of a vibration.....	12
1.3.1 Signal filtering depends on web type .....	13
1.3.2 Spider peripheral and central nervous systems filter signals differently .....	14
1.4 Filtering by the body.....	16

1.4.1 Using resonance principles to predict filtering by the body.....	16
1.4.2 Multi-body modeling predicts filtering by the body.....	20
1.5 What influences spider joint stiffness? .....	22
1.5.1 Spider leg anatomy.....	22
1.5.2 Scaling of joint stiffness with segment size .....	24
1.6 Thesis objectives .....	25
1.6.1 The relationship between spider joint stiffness and body size.....	25
1.6.2 Modeling mechanical filtering by a spider’s body .....	26
Chapter Two: the relationship between spider joint stiffness and body size.....	27
2.1 Introduction.....	27
2.2 Methods .....	31
2.2.1 Animal collection and care .....	31
2.2.2 Morphology measurements.....	34
2.2.3 Joint stiffness measurements.....	35
2.2.4 Statistical analyses.....	41
2.3 Results .....	43
2.3.1 Larger spiders have leg segments with a larger area-length ratio .....	43
2.3.2 Joint stiffness increases hypometrically and varies across joints and species.....	45
2.3.3 Baseline stiffness increases isometrically with mass .....	53

2.4 Discussion .....	55
2.4.1 Comparisons with known active and passive joint stiffnesses .....	55
2.4.2 Changing baseline stiffness across species and joints .....	57
2.4.3 Differences in joint stiffness between joint types .....	58
2.4.4 Assumptions and limitations .....	59
2.4.5 Conclusions .....	60
Chapter Three: modeling mechanical filtering by a spider’s body .....	61
3.1 Introduction.....	61
3.2 Methods .....	65
3.2.1 Web-dwelling species used in Chapter Three .....	65
3.2.2 Vibrometry measurement .....	68
3.2.3 Quantifying mechanical filtering .....	72
3.2.4 Building the multi-body models .....	76
3.2.5 Model parameter variation and simulation.....	81
3.2.6 Comparing model output to empirical measurements .....	87
3.3 Results .....	89
3.3.1 Empirically measured modes differed with spider orientation .....	89
3.3.2 Models predict similar modes of vibration.....	93
3.3.3 Model predictions of vibration transmission through a single leg .....	100

3.4 Discussion .....	107
3.4.1 Possible reasons for the lack of congruency between the <i>Araneus diadematus</i> model and real data .....	107
3.4.2 Poorer model fit for <i>Pholcus phalangioides</i> compared to <i>Latrodectus hesperus</i> .....	110
3.4.3 Assumptions and limitations: measuring spider mechanics.....	111
3.4.4 Assumptions and limitations: modeling spider mechanics .....	112
3.4.5 Conclusions .....	115
Chapter Four: Conclusions .....	117
4.1 Mass independent resonant frequencies of spider bodies .....	117
4.2 Future research directions .....	122
Appendices .....	133
Curriculum Vitae.....	151

# List of Tables

**Table 2.1** Species used in Chapter Two. .... 32

**Table 2.2** Mean and standard deviation of the mass in milligrams applied to the joints..... 39

**Table 2.3** Mean and standard deviation of calculated rotational joint stiffness of each joint type measured ..... 47

**Table 2.4** Mixed effects model fit comparisons using AIC. .... 49

**Table 2.5** Intercepts for each species predicted by the mixed effects model. .... 52

**Table 3.1** Species used in Chapter Three..... 66

# List of Figures

<b>Figure 1.1</b> Oscillograms and power spectra of vibrations from different sources measured in a western black widow cobweb .....	3
<b>Figure 1.2</b> Spider anatomy, slit sensillae and lyriform organs. ....	8
<b>Figure 1.3</b> Threshold curves of slits in the metatarsal lyriform organ in three species. ....	15
<b>Figure 1.4</b> A simple model for spider body mechanics. ....	18
<b>Figure 1.5</b> Anatomical structures within the leg that may contribute to leg joint stiffness. ....	23
<b>Figure 2.1</b> Eleven spider species used in Chapter Two.....	33
<b>Figure 2.2</b> Experimental apparatus for joint stiffness measurement .....	36
<b>Figure 2.3</b> Spider leg segment area-length ratio and mass .....	45
<b>Figure 2.4</b> Mixed effects model results .....	51
<b>Figure 2.5</b> Baseline stiffness increases and mass .....	54
<b>Figure 3.1</b> Species studied in Chapter Three and the corresponding multi-body models.....	67
<b>Figure 3.2</b> Vibrometry setup.....	69
<b>Figure 3.3</b> Monitoring data point quality .....	71
<b>Figure 3.4</b> Example data of the vibration velocity of the spider leg segments and abdomen showing peaks in the transfer function amplitude.....	76
<b>Figure 3.5</b> Main components of multi-body modeling.....	78
<b>Figure 3.6</b> Model parameter variation. ....	84
<b>Figure 3.7</b> Frequency range cutoff for model and empirical data .....	89
<b>Figure 3.8</b> <i>L. hesperus</i> empirical modes of vibration.....	91
<b>Figure 3.9</b> <i>P. phalangoides</i> empirical modes of vibration. ....	92

<b>Figure 3.10</b> <i>A. diadematus</i> empirical mode of vibration .....	93
<b>Figure 3.11</b> <i>L. hesperus</i> model predicted modes of vibration.....	95
<b>Figure 3.12</b> <i>P. phalangioides</i> model predicted modes of vibration. ....	97
<b>Figure 3.13</b> <i>A. diadematus</i> model predicted mode of vibration .....	99
<b>Figure 3.14</b> Probability density heatmaps of <i>L. hesperus</i> model predictions. ....	101
<b>Figure 3.15</b> Probability density heatmaps of <i>P. phalangioides</i> model predictions.....	104
<b>Figure 3.16</b> Probability density heatmaps of <i>A. diadematus</i> model predictions. ....	106

# List of Appendices

<b>Appendix 1.</b> Permissions for select figures in Chapter One. ....	133
<b>Appendix 2.</b> Dead spiders hanging in webs with legs fully extended .....	134
<b>Appendix 3.</b> Spider holders used in measurements for Chapter Two. ....	135
<b>Appendix 4.</b> Mean and standard deviation of the initial joint angle for each species .....	136
<b>Appendix 5.</b> Checking mixed effects model assumptions for the best model.....	137
<b>Appendix 6.</b> Tables of the parameters for the multi-body models for each species.....	138
<b>Appendix 7.</b> Multi-body model postural variation.....	142
<b>Appendix 8.</b> Effects of varying the stiffness of different joint types independently. ....	143
<b>Appendix 9.</b> Creating variable pulses for model stimulation .....	144
<b>Appendix 10.</b> Creating a probability density heatmap.....	146
<b>Appendix 11.</b> Modes of vibration observed from <i>L. hesperus</i> . ....	148
<b>Appendix 12.</b> Modes of vibration observed from <i>P. phalangioides</i> .....	149
<b>Appendix 13.</b> Modes of vibration observed from <i>A. diadematus</i> .....	150

# Chapter One: Introduction

## 1.1 Spider sensory ecology

In order to maximize fitness (survival and reproduction), animals need to obtain information about their surroundings. Sensory information can be particularly important in certain contexts such as when an animal is searching for food, avoiding predators, or finding a suitable mate for reproduction. Signals that relay crucial information to the animal can be obtained through several different sensory modes, such as olfaction, vision, hearing, and other forms of mechanoreception. Vibrations are the primary cues used by spiders to gather environmental information (Barth, 2001; Barth, 2002; Barth, 2012), and here I will focus on the reception of vibrations.

One of the best-known examples of vibrations that spiders sense are those generated when prey struggle in a spider's web. Vibrations that spiders encounter also include those generated by males signaling to females in courtship, or from environmental noise. The two features that may allow spiders to distinguish between these sources of vibrations are the temporal pattern (Fig. 1.1A-B) and the frequency (Fig. 1.1C-D) (Barth et al., 1988; Hergenröder and Barth, 1983; Klärner and Barth, 1982; Landolfa and Barth, 1996; Masters, 1984a; Masters, 1984b; Vibert et al., 2014; Wignall and Herberstein, 2021).

### 1.1.1 Vibration sources differ in temporal pattern

A vibration is an oscillation that displaces an object over time. We can visualize a vibration using an oscillogram, which shows the amplitude of the object's displacement over time, or in other words, the temporal pattern of the vibration. The temporal pattern of a vibration may be

important in allowing a spider to distinguish between vibrations made by potential conspecific mates and those made by a different species, or even by entirely different vibration sources such as prey. In some spider species, adult males will court females by creating vibration signals to relay information about their identity, mating status, quality and also to reduce the risk of the sexual cannibalism by the female (Mitoyen et al., 2019; Wignall and Herberstein, 2013; Wignall and Herberstein, 2021). During courtship, males will perform dances that include a vibratory component. How courtship vibrations are generated can vary among species (Wignall and Herberstein, 2021), but generally males will produce signals by vibrating their abdomen, drumming their legs and appendages near the mouthparts called pedipalps on the substrate, or by plucking the female's web (Baurecht and Barth, 1992; Elias et al., 2003; Sivalingham and Mason, 2021; Vibert et al., 2014; Wignall and Herberstein, 2021). Male courtship vibrations are meant to convey information and therefore contain distinct temporal patterns that are often repeated (Fig. 1.1A), compared to prey vibrations, which are caused by the struggling of the prey, and are therefore quite sporadic (Fig.1.1B). Prey vibrations are often shorter in duration and higher in amplitude in comparison to male courtship vibrations (Vibert et al., 2014). Female spiders may use the temporal differences between prey and courtship vibrations to differentiate between vibration sources (Barth, 1985a; Vibert et al., 2014; Wignall and Herberstein, 2021).

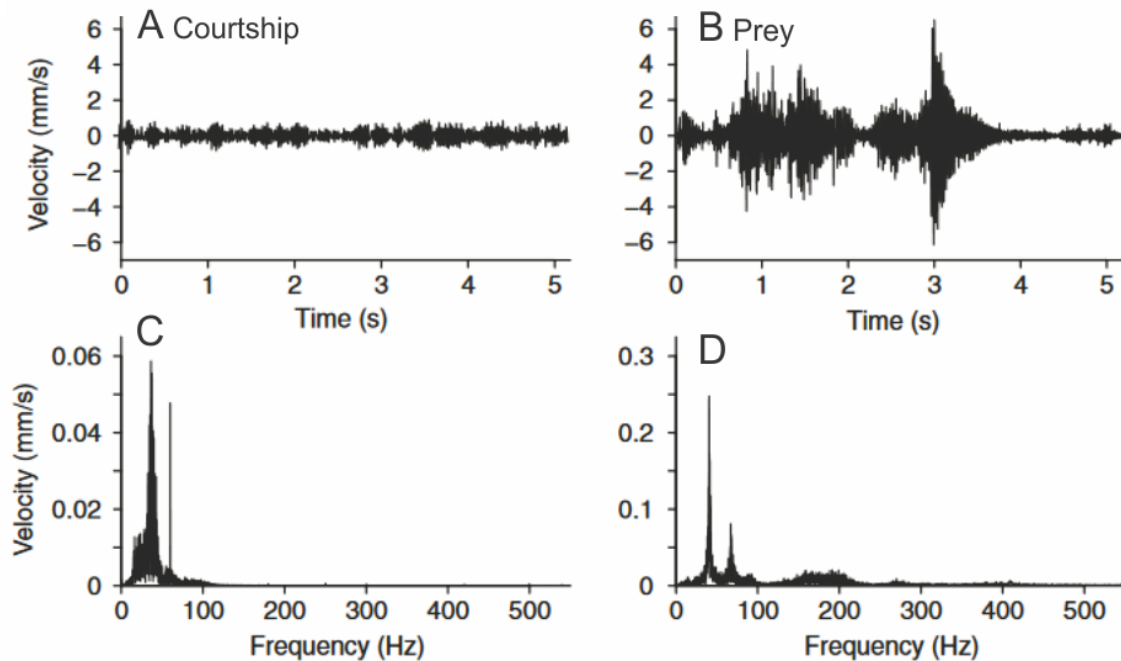


**Figure 1.1** Oscillograms (A-B) and power spectra (C-D) of vibrations from different sources measured in a western black widow cobweb. Oscillograms show the amplitude of the vibration velocity over time and power spectra show the amplitude of the vibration velocity of each frequency in the signal. (A) Male courtship vibrations have distinct patterns that are repeated over time. (B) Prey vibrations are more sporadic. Power spectra of both male courtship vibrations (C) and prey vibrations (D) show that these vibrations contain frequencies from 0-100 Hz, with very little signal above about 100 Hz. Prey vibrations, especially smaller prey such as flies shown here, have more higher frequencies in the signals in comparison to male courtship vibrations, but still little signal above 100 Hz. From Vibert et al. (2014) under a Creative Commons Attribution License (Appendix 1).

### 1.1.2 Vibration sources can also differ in frequency

Spiders may also identify vibration sources by a vibration's frequency content. For a sinusoidal signal, the frequency is simply the number of oscillations per second. Usually, signals are more complex and contain more than one sinusoidal frequency. In this case, the frequency content of a signal can be represented using a power spectrum (Fig. 1.1C-D), where each frequency is plotted on the horizontal and relative amplitude is on the vertical axis. A peak indicates which frequencies carry the most energy and is often also referred to as the dominant frequency of the signal. Environmental vibrations, such as wind, typically contain frequencies below 10 Hz (Barth et al., 1988; Masters, 1984a). Most vibrations that would be considered biologically relevant, such as vibrations from prey (Fig. 1.1D) or mates (Fig. 1.1C), range from 30-1000 Hz (Klärner and Barth, 1982; Masters, 1984b). In substrate communicating spiders such as *Cupiennius salei*, vibrations of 250 – 500 Hz have been reported in courtship vibrations (Baurecht and Barth, 1992), however in web-dwelling spiders like black widows, hobo spiders or orb weaving spiders, frequencies above 100 Hz do not excite the web substantially (Landolfi and Barth, 1996; Masters and Markl, 1981; Vibert et al., 2014; Vibert et al., 2016). Different components of male courtship vibrations, e.g., abdomen vibrations, leg drumming or web plucking, may have different dominant frequencies such as 50-100 Hz in *Latrodectus hesperus* or 30 Hz in *Argiope aetherea* (Sivalinghem and Mason, 2021; Wignall and Herberstein, 2021). Dominant frequencies in courtship vibrations often are species-specific and may aid females in identifying their own species; females are more likely to attack heterospecific males than conspecific males (Wignall and Herberstein, 2021). Prey vibrations often range from 20-100 Hz (Barth et al., 1988; Hergenröder and Barth, 1983; Landolfi and Barth, 1996; Masters, 1984a).

Interestingly, if a prey individual walks slowly on the web, i.e., does not generate high frequency vibrations commonly produced by struggling prey, a spider is less likely to attack the prey (Barth et al., 1988). This is likely because as the prey walks slowly, it produces vibrations that are low in amplitude and relatively low in frequency. These vibrations may resemble those from wind more than prey (Barth et al., 1988). For captured prey that are struggling in the web, the frequency component of the vibrations produced depends in part on prey size. Larger prey generate lower frequency vibrations than smaller prey (Landolfa and Barth, 1996), and spiders may be able to distinguish relative prey size by the vibration frequency. For instance, in black widow spider webs, small ants generate vibrations from 90-110 Hz whereas large crickets generate vibrations from 15-30 Hz (Mhatre et al., 2018). To sense these vibrations, spiders use mainly slit sensillae and the associated mechanoreceptors (Barth, 1985a).

## 1.2 Spider slit sensillae and lyriform organs

Spider legs have seven segments named proximal to distal from the cephalothorax: coxa, trochanter, femur, patella, tibia, metatarsus, and tarsus (Fig. 1.2A). Spiders sense vibrations using slit sensillae that are primarily found on the legs but also found on the pedipalps and abdomen (Barth, 2004; Barth and Stagl, 1976). Slit sensillae appear like cracks in the exoskeleton and are associated with mechanoreceptor cells. The organs used to sense vibrations in spider legs are called lyriform organs and are compound organs made of several slit sensillae arranged parallel to each other (Fig. 1.2B and D). In the case of the metatarsus-tarsus joint, the main lyriform organ involved in vibration sensing is placed directly on the hard cuticle of the joint hinge (Barth and Pickelmann, 1975; Morley et al., 2016). Other lyriform organs are typically placed on the hard cuticle of the leg segments, close to but not on the

articular membrane that inflates and deflates to allow joint rotation (Fig. 1.2D). The slits range from 1-2  $\mu\text{m}$  in width and 8-200  $\mu\text{m}$  in length (Fig. 1.2B) and respond to strains in the cuticle (Barth, 2004; Barth and Pickelmann, 1975; Blickhan and Barth, 1985).

As the spider moves or is moved by external forces, forces are applied to its exoskeleton. During walking, forces are generated by muscles pulling on the exoskeleton or from changes in hemolymph pressure generated by the hydraulic locomotion system pushing against the exoskeleton (Blickhan and Barth, 1985). Forces can also be caused by external vibrations impinging on the animal which cause the joints to rotate, generating both forces on joint muscles and changes in hemolymph pressure (Barth and Pickelmann, 1975; Blickhan and Barth, 1985; Hergenröder and Barth, 1983; Seyfarth and Barth, 1972). The force applied to the exoskeletal cuticle distributes over its surface area and generates strains in the cuticle. Strain is the change in length of an object in relation to its initial length, where in this instance the object is the cuticle. For example, when a joint bends, the forces generated against the leg muscle and changes in hemolymph pressure within the joint will cause the cuticle to be stretched slightly (Blickhan and Barth, 1985; Schaber et al., 2012) and this is the stimulus that is sensed by the slit sensillae.

The crack-like structure of the slit sensillae is crucial to their function of sensing cuticular strain. When a force is applied to a perfectly smooth object, stresses and strains are evenly distributed throughout the object (Ennos, 2012). However, if a crack or a ridge is present in the object, stresses concentrate around the imperfection (Ennos, 2012). When stresses are generated in spiders, either by internal or external forces, they concentrate around the slit

sensillae (Höböl et al., 2009). This increases the likelihood that small stresses in the cuticle are magnified into large strains and stimulating the slit sensillae mechanoreceptors, making them some of the most sensitive mechanoreceptors known in biology and allowing them to respond to the tiny stressors produced by external vibrations (Barth, 2004).

The arrangement of the slits in a lyriform organ impacts how the slits are deformed when forces are applied to the cuticle. Peripheral slits in an organ experience greater forces than those in the center of an organ (Barth and Pickelmann, 1975), resulting in different levels of slit deformation. Within an organ, slits can differ in length, curvature, and longitudinal shift relative to each other (Fig. 1.2D). These differences in slit patterns also cause different levels of slit deformation within an organ (Höböl et al., 2007; Höböl et al., 2009), possibly allowing a spider to sense variable magnitudes and directions of strain.

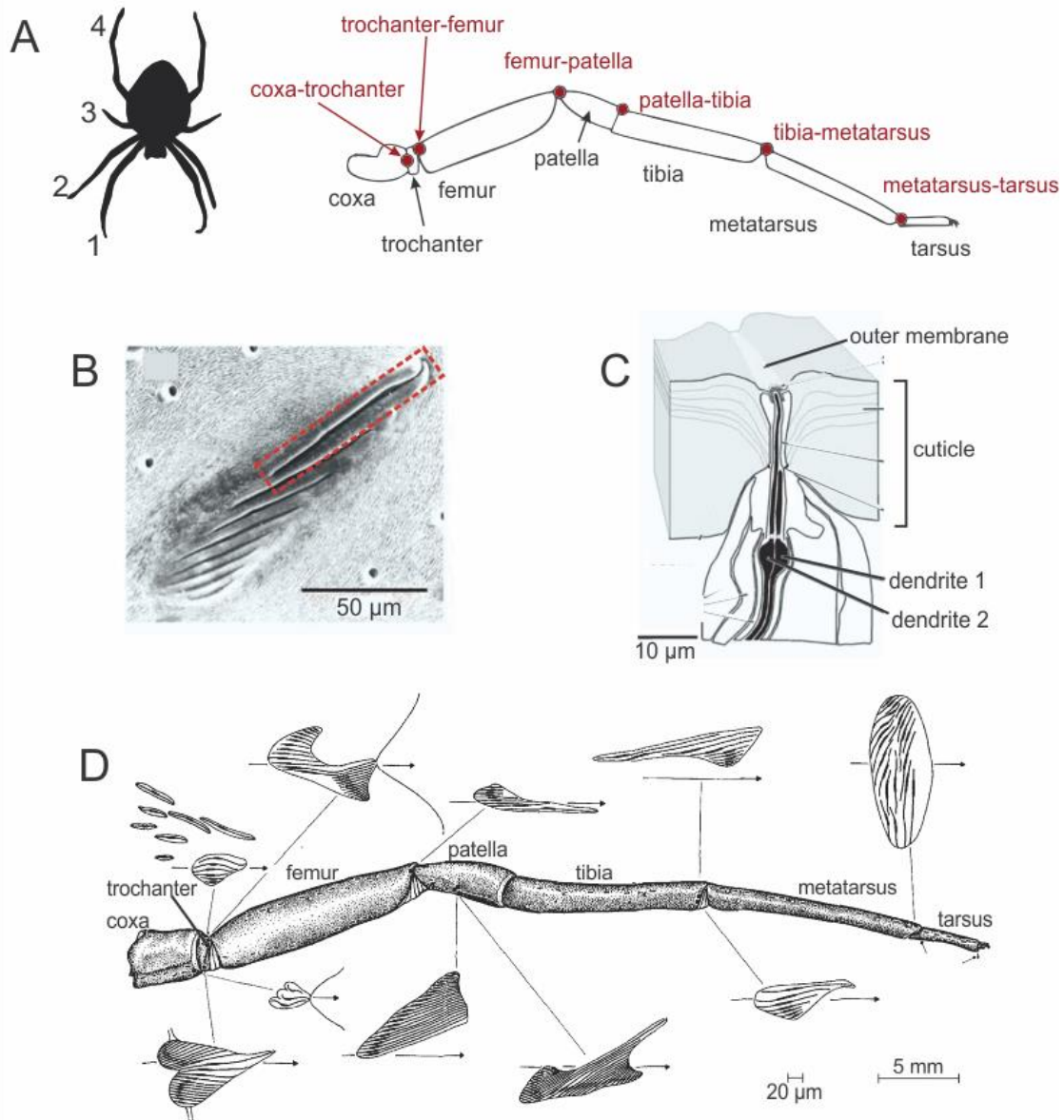


**Figure 1.2** Spider anatomy: (A) Spider legs are typically numbered from one to four for description. Each leg has seven segments named proximal to distal from the cephalothorax: coxa, trochanter, femur, patella, tibia, metatarsus, tarsus. The joints indicated here are all hinge-like joints that rotate in one plane. Spiders sense vibrations with slit sensillae. (B) shows a group of slit sensillae with a single slit highlighted. The slits in slit sensillae are cracks in the hard cuticle of the exoskeleton and can be found on the legs, pedipalps, and abdomen, and range from 1-2  $\mu\text{m}$  in width and 8-200  $\mu\text{m}$  in length. The slits respond to cuticular strains caused either during locomotion by muscle activity, changes in hemolymph pressure or joint rotation

due to vibrations. (C) Two bipolar neurons innervate each slit. The dendrites are attached to the inner and outer slit membranes and are physically deformed during slit compression. If the dendrite deformation exceeds the deformation threshold, an action potential is generated which can allow a spider to sense the vibration. (D) Lyriform organs are composed of groups of several slits and many are found close to the joint articular membrane. They are thought to be the principal organs used to sense external vibrations, especially the lyriform organs on the metatarsus-tarsus joints because of their high sensitivity. Different organs seem to have very specific slit patterns, which are thought to be structured so that the organs can respond to a wide range of strain directions and magnitudes. (B) from French et al. (2002), (C) from Barth (1971); French et al. (2002), (D) from Barth and Pickelmann (1975). Permissions listed in Appendix 1.

#### 1.2.1 How is mechanical strain sensed by the slit sensillae?

When slit sensillae are deformed, they transform the mechanical strain into a neural signal. Within each slit, there are two bipolar neurons (Fig. 1.2C). The dendrites of the neurons are attached to the inner and outer membranes of the slit (Fig. 1.2C, Barth, 1971; Barth, 1985b; French et al., 2002). When the slit experiences cyclic cuticular strain, this results in the slit membranes being physically stretched and compressed. Compression of the slit membranes causes the attached dendrite tips to be compressed as well (Barth, 1985b). The slit sensillae are deformed the most when the applied force is perpendicular to the long axis of the slit (Barth and Pickelmann, 1975). If the deformation of the dendrite tip exceeds the deformation threshold, then an action potential is generated by the mechanically activated receptors in the dendrite (Barth and Geethabali, 1982; Seyfarth and French, 1994) allowing a spider to sense the vibration. The specific ion channels have not been identified in spiders but piezo channels are currently the best candidates since they are expressed in the mechanosensory neurons

(Johnson et al., 2021). The two neurons innervating the slit have different responses to mechanical stimulus. One, called 'type A', only produces one or two action potentials in response to a single applied force whereas the other, 'type B', can produce successive bursts in response to prolonged stimulus (Seyfarth and French, 1994). The response differences of these two neurons may complement each other and allow a spider to sense multiple vibrations occurring simultaneously or distinguish between short and prolonged vibrations (Seyfarth and French, 1994).

### 1.2.2 Which joints sense vibrations?

Joints that have a large range of motion will likely have the greatest levels of joint bending and therefore are likely the most relevant joints for sensing vibrations. In the spider leg, the joints with the largest ranges of motion are the femur-patella (dorso-ventral range of motion: 150°), tibia-metatarsus (120°) and metatarsus-tarsus joints (125°) (Foelix, 2011; Hao et al., 2019; Reußenzehn, 2010) and the response characteristics of the lyriform organs associated with these three joints have been studied in the past (Barth and Geethabali, 1982; Blickhan, 1986; Bohnenberger, 1981). A large range of motion is more likely to generate greater strain in the cuticle. As the joint rotates more, the muscles associated with the joint will be stretched more and there will likely be greater changes in the hemolymph pressure in the leg segment. These greater forces generated during larger joint rotations will generate more strain in the exoskeleton, resulting in greater stimulation of the mechanoreceptors in the slit sensillae of the lyriform organs.

As mentioned previously, the metatarsus-tarsus lyriform organ is highly sensitive to vibrations (Barth and Geethabali, 1982). The metatarsus-tarsus joint has a large range of motion in ground dwelling spiders but in web-hanging spiders, the functional range of motion may differ. Nevertheless, the lyriform organ closest to the metatarsus-tarsus joint is important for sensing vibrations due to its unique orientation and sensitivity. The lyriform organ at this joint is perpendicular to the long axis of the leg (Fig. 1.2D, Barth and Geethabali, 1982; Morley et al., 2016). Due to the orientation of the organ with respect to the leg segment, the compressive forces generated by even slight upward deflections of the tarsus towards the metatarsus are in the optimal direction for slit stimulation (Barth, 2001), likely contributing to this organ's high sensitivity to vibrations (Barth and Geethabali, 1982).

Other joints, such as the femur-patella and tibia-metatarsus joints, have high ranges of motion and are likely also important for sensing vibrations. Lyriform organs near the tibia-metatarsus joint are arranged more parallel to the long axis of the leg segment. An organ in this orientation may be used to sense strains caused by the cuticle bending during flexor muscle activity or changes in hemolymph pressure during joint bending rather than direct segment contact like in the metatarsus-tarsus organ (Barth and Pickelmann, 1975; Landkammer et al., 2014).

Some lyriform organs are found in close proximity to each other, such as those found on the patella and tibia (Fig. 1.2D). These organs can interact and alter each organ's sensitivity to strains in different directions. For example, lyriform organs positioned close to each other on the tibia are predicted to be most sensitive to forces acting between  $60^\circ$  and  $135^\circ$  rather than

only forces acting perpendicular to the long axis of the organ's slits (Höböl et al., 2007; Höböl et al., 2009). The diverse arrangement of slits and locations of lyriform organs may allow spiders to sense signals causing strains of various magnitudes and directions. The vibrations that reach a spider may be different from the vibrations that were originally generated because they can be altered through signal filtering.

### 1.3 Signal filtering changes the frequency content of a vibration

Signal filtering occurs when a system is stimulated more by a particular frequency or frequency range, and by extension not stimulated by other frequencies (King, 2009; Rossing and Fletcher, 1995). Filtering can be mechanical, such as an object physically moving more at particular frequencies, or neurological, such as a neuron being stimulated by its relevant stimulus at particular frequencies (Miller and Mortimer, 2020; Mortimer, 2017). Filtering effectively alters the relative amplitudes of frequencies in a signal. The amplitudes of frequencies that a system is not stimulated by are decreased and the information that these frequencies may have contained is lost. As a vibration travels to a spider, there are several stages where it may be filtered (Miller and Mortimer, 2020): in the web or the substrate a spider stands on, in a spider's body, or in the nervous system. Each filtering stage is important as each has the potential to alter vibrations enough that information contained in certain frequencies is lost. Therefore, it would be ideal to consider each stage in succession. However, since the main focus of my thesis is the mechanical behaviour of a spider's body, I will discuss the first and the last stages, before describing filtering due to the body's mechanics.

### 1.3.1 Signal filtering depends on web type

Filtering in the web or on the substrate is the first stage where a signal may be altered. Here, I mainly consider web-based filtering since my thesis primarily deals with web building spiders. Of the web types studied thus far, filtering in the web appears to depend on the web type. Cobwebs are three-dimensional webs with irregular structure as opposed to two-dimensional orb webs with more regular structure. Since each silk thread in a cobweb has several connections in many directions, vibrations in cobwebs dampen faster than in more resonant orb webs (Challita et al., 2021). Orb webs dissipate high amplitude movements by moving much more than a cobweb when a flying prey hits it (Sensenig et al., 2012; Sensenig et al., 2013). There is minimal filtering in cobwebs as they generally allow equal transmission of frequencies from 0-1000 Hz (Vibert et al., 2016). In contrast, the filtering in orb webs changes in different areas of the web. The amplitude of frequencies above 100 Hz decreases as vibrations travel through the center of an orb web, in contrast to the edges of an orb web where all frequencies are transmitted equally (Landolfa and Barth, 1996; Masters and Markl, 1981). Similar to orb webs, it appears that transmission changes in different areas of the funnel web of the corner funnel weaver, *Hololena curta* (Naftilan, 1999). From behavioural studies, the corner funnel weaver would only approach the prey when it was generating vibrations in particular parts of the funnel web (Naftilan, 1999). Measurements of courtship signals on funnel webs found that funnel webs transmit vibrations from 1-30 Hz and filter out higher frequencies (Singer et al., 2000), suggesting that this web type filters vibrations more than cobwebs or orb webs. The differences in filtering seen across different web types may be due to web geometry. Web geometry impacts the tension on the silk strands which can influence vibration

transmission and thus, how vibrations are filtered through a web (Mortimer, 2019; Mortimer et al., 2016).

### 1.3.2 Spider peripheral and central nervous systems filter signals differently

Signal filtering can also occur at the level of the neurons, which is the final stage of processing. The slit sensillae in lyriform organs respond to vibrations like high-pass filters (Barth and Geethabali, 1982; Juusola and French, 1995). A high-pass filter allows relatively high frequencies to be transmitted and filters out lower frequencies. In lyriform organs, the dendrites attached to each slit require greater leg segment displacements to respond to frequencies below 100 Hz and lower displacements at higher frequencies from 100-1000 Hz (Fig. 1.3, Barth and Geethabali, 1982; Juusola and French, 1995). The response level of the dendrites drops strongly from ~100 to 400 Hz and dendrites respond equally to all frequencies within the high frequency range above 400 Hz (Fig. 1.3). The response is similarly flat within the lower frequency range, between about ~10-100 Hz.

In contrast to the behaviour in the sensory periphery, in the central nervous system of the tiger wandering spider, *Cupiennius salei*, neurons do appear to filter specific bands of frequencies. Low frequency interneurons respond more to lower frequencies from 10-400 Hz, which usually fall within the range of most substrate vibrations, whereas high frequency interneurons respond to higher frequencies between 700 - 900 Hz (Speck-Hergenr and Barth, 1986).

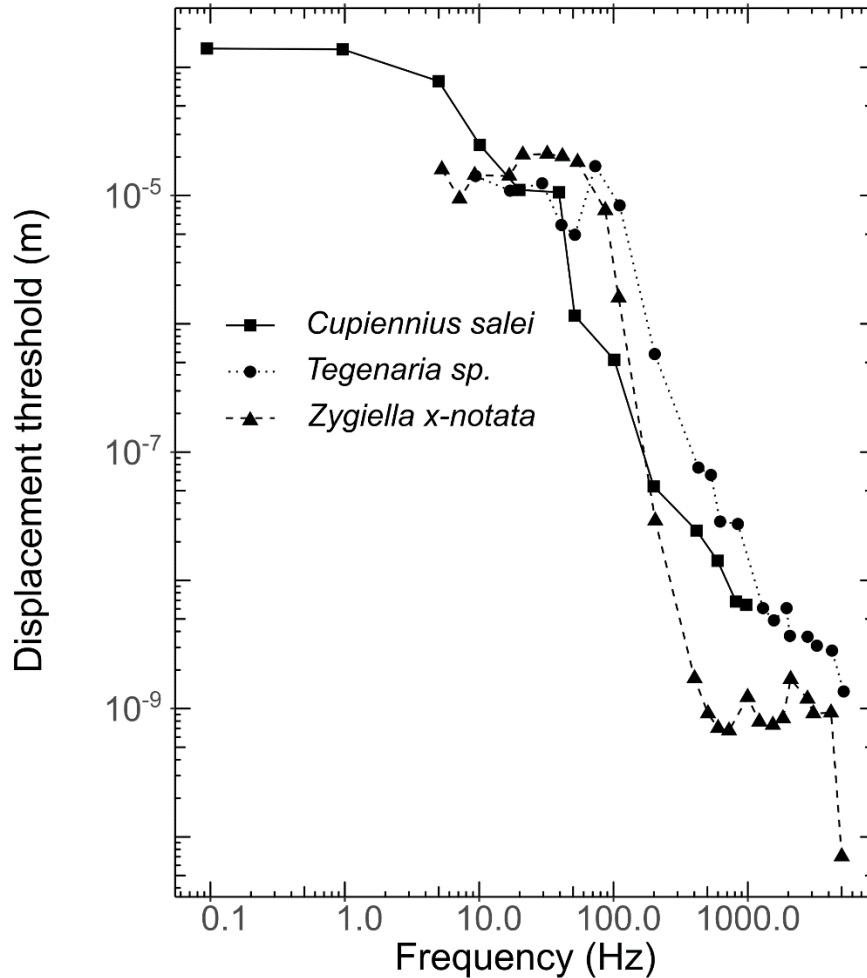


**Figure 1.3** Threshold curves of the slits in the metatarsal lyriform organ in three species of spider. The curves show that when isolated from the mechanical effects of the body, the slit sensillae respond similarly to frequencies below about 100-150 Hz which are common in most substrate and web vibrations. The threshold curve indicates the level of stimulus required to elicit an action potential in sensory neurons attached to a slit sensillae in a lyriform organ. In each species, similar leg segment displacement levels are required for all lower frequencies (0-150 Hz). Surprisingly, they are more sensitive to higher frequencies (150-1000 Hz), which are not observed in the web vibrations of most web-dwelling spiders and the function of which is unknown. Redrawn from Barth and Geethabali (1982).

## 1.4 Filtering by the body

There is a filtering stage prior to the nervous system: mechanical filtering by the body. For a spider to sense a vibration, the vibration must have sufficient energy to bend a spider's joints. Even if they arrive at the body with the same amplitude, the vibration frequencies that will cause relatively more joint bending will depend on the mechanical properties of the body, for example, the mass of the body or the stiffness of the joints. Therefore, these mechanical properties of a spider's body will influence what is sensed in the later stages by the peripheral and central nervous systems. Filtering by the body has been largely understudied but is clearly important for sensing vibrations.

### 1.4.1 Using resonance principles to predict filtering by the body

Past work has made predictions about how a spider's body morphology would influence vibration transmission within the body (Masters, 1984b). A heavier abdominal mass is predicted to cause a spider to move as a rigid object, e.g., in the species *Nuctenea sclopetaria* (200 mg), the abdomen and legs would vibrate together with the same amplitude at lower frequencies, about 12 Hz (Masters, 1984b). At higher frequencies above 100 Hz, the abdomen of a spider would remain relatively motionless and only the legs that are lower in mass would vibrate (Masters, 1984b). Thus, at the higher frequencies, vibrations would bend the distal leg joints, and not the more proximal leg joints since the abdomen is relatively motionless. At lower frequencies, joint bending is expected to extend across all leg joints. Since joint bending eventually leads to in lyriform organ stimulation, this pattern of lyriform organ stimulation could explain how spiders can make at least some frequency discriminations.

These intuitive predictions have been based on the concept of resonance. All objects vibrate naturally, even if at low amplitudes, and they can have one or more resonant frequencies. These resonant frequencies depend on many characteristics of the object such as its shape, material, mass, and boundary conditions (King, 2009). If an external force is applied at a resonant frequency, this will result in the object vibrating with a greater amplitude than at other non-resonant frequencies. If we consider a simple system, such as a mass suspended from a spring which can only move up or down (a system with a single degree of freedom), the resonant frequency of the system is fully determined by the object's mass and the spring constant of the suspension spring as shown in equation (1.1) (Rossing and Fletcher, 1995).

$$2\pi (f) = \sqrt{\frac{k}{m}}$$

(1.1)

Where  $f$  is the resonant frequency (Hz),  $k$  is the spring constant or stiffness (N/m), and  $m$  is the mass of the hanging mass (kg). As the mass of the system increases, the resonant frequency decreases. As the spring constant increases, the resonant frequency increases (Fig. 1.4A).

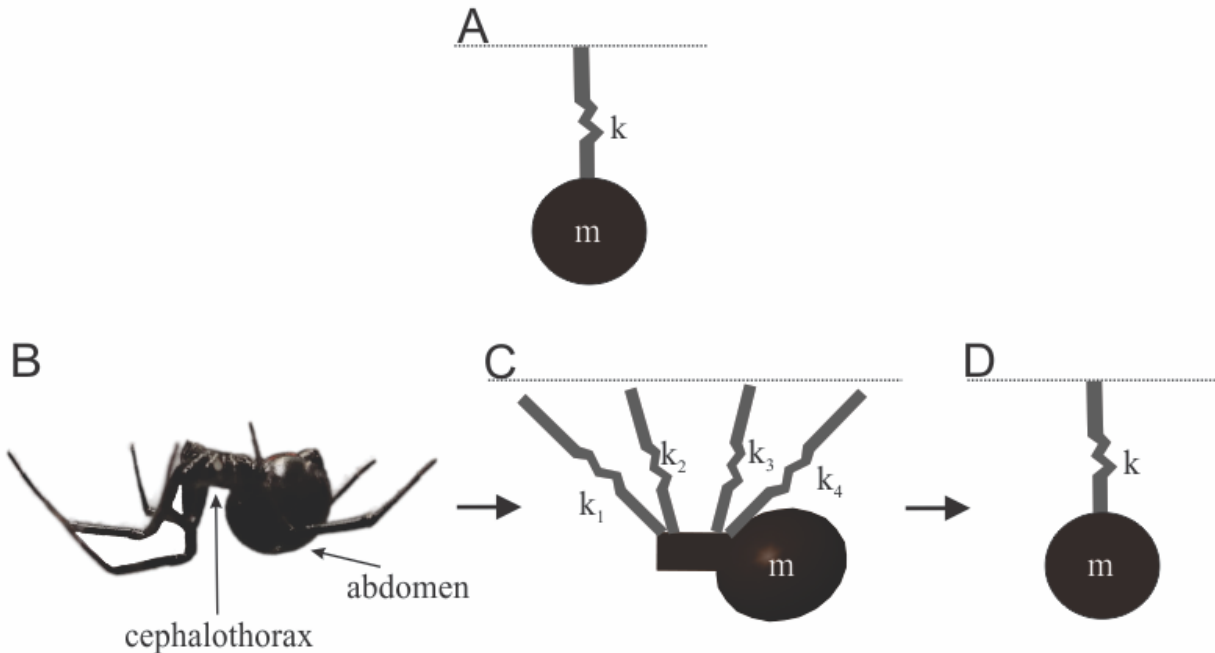


**Figure 1.4** Using simple models to develop an intuition about spider mechanics. (A) The resonant frequency ( $f$  (Hz) in equation 1.1) of a simple system, such as a mass suspended by a spring, depends on the mass ( $m$  (kg)) and the spring constant, or stiffness, ( $k$  (N/m)) of the spring. Stiffness is a measure of an object's resistance to deformation (Ennos, 2012), and in this case, is the resistance of the spring to stretching. As the mass increases, the resonant frequency decreases. As the spring constant increases, the resonant frequency increases. (B) A spider in its web is a complex system composed of several objects. The abdomen has the largest mass in this system and the legs can function as springs to support the mass. (C) We can simplify a spider by representing each leg as a spring, with a spring constant  $k_i$  for each leg, supporting the abdomen mass,  $m$ . (D) If we think of the eight springs representing each leg as being parallel with one another, then we can simplify the system further to an equivalent spring, resulting in the system acting as a single spring. The spring constant for such a spring is the sum of all the spring constants (Rossing and Fletcher, 1995). Therefore, we can simplify the complex spider to a simple mass-spring system for the purposes of intuition and use the resonant frequency of the simple system to make tentative predictions of the mechanical filtering by a spider's body.

A spider is a complex system composed of several objects that each vary in mass. For the purpose of simplification, we can represent the spider's cephalothorax and abdomen with a single mass and represent each leg as a spring (Fig. 1.4C). The stiffnesses of the leg joints that support the mass of a spider would determine each leg's spring constant. We can further simplify the eight parallel springs to an equivalent single spring (Fig. 1.4D). This simplification allows us to see that a spider's mass and the spring-like behaviour of its legs will influence its resonant frequency and thus, allow us to make predictions about the mechanical filtering by the body. Based on our simplification of a spider, as the mass of a spider increases, the resonant frequency will likely decrease resulting in the body filtering out higher frequencies. Likewise, as the leg joint stiffness increases, the resonant frequency will likely increase resulting in the body filtering out lower frequency vibrations.

Using resonance only gives a partial explanation of how a spider body filters vibrations. In particular, both previous verbal models (Masters, 1984b), and the more recent quantitative models (Mhatre et al., 2018; Wu et al., 2023), ignore possible variations in joint stiffness between or even within legs. As spider mass increases across species, the stiffness of leg joints may increase to support the mass of the abdomen during locomotion (Moya-Laraño et al., 2008). In this situation, it becomes difficult to predict all the resonant frequencies of a spider's body since the effects of increases in mass and stiffness may compensate each other. To make more detailed predictions, we need better data on how leg joint stiffnesses vary in spiders.

#### 1.4.2 Multi-body modeling predicts filtering by the body

More detailed predictions of mechanical filtering by the body can be made with quantitative modeling techniques. Multi-body modeling integrates the different factors influencing body vibration mechanics (Landkammer et al., 2016; Mhatre et al., 2018; Wu et al., 2023; Zentner, 2013). This approach treats a spider as a collection of rigid bodies, which do not deform or change shape when forces are applied. Since spiders are arthropods with a rigid exoskeleton, it is assumed that each body and leg segment does not deform and can be modeled as a rigid body. The exoskeleton is stiffer (Young's modulus of 18 GPa in *Cupiennius salei*) than the articular membrane (Young's modulus of 3-5 GPa in *Phidippus regius*) which allows the joint to rotate (Blickhan and Barth, 1985; Göttler et al., 2021; McConney et al., 2007; Schaber et al., 2012). Given that the stiffness of the exoskeleton and articular membrane are different by an order of magnitude, when a force is applied to a leg segment, the segment should rotate around the joint it is connected to rather than being bent itself. This is true for the macroscopic scale, however microscopic strains may occur within each segment (see section 1.2) (Strauß and Stritih-Peljhan, 2022). To allow motion in the system, the rigid bodies are connected to each other by joints.

The vibration mechanics of the multi-body system depends on three main factors: 1) the masses of the rigid bodies, 2) the stiffnesses of joints and 3) the damping at each of the joints (Landkammer et al., 2016; Mhatre et al., 2018; Schiehlen, 1997; Zentner, 2013). The mass and spatial extent of each rigid body is defined by its geometry and density. The stiffness is a joint's resistance to rotation, where a higher stiffness results in more resistance to joint bending and is entered as a parameter for each joint. In a system with only springs and masses, kinetic energy

is stored as potential energy and released over time and is not dissipated. Hence this system will oscillate indefinitely. Damping causes the dissipation of energy in an oscillation and only with damping will a system eventually stop oscillating (Rossing and Fletcher, 1995). A joint with higher damping results in more of the vibration's energy being dissipated as heat sooner than a joint with lower damping. Damping only changes the vibration magnitude of a system, but not the resonant frequency (Rossing and Fletcher, 1995) and is also a model input for each joint.

Recently, a multi-body modeling approach has been used to study the mechanical filtering of the body in the western black widow, *Latrodectus hesperus* (Mhatre et al., 2018). In line with previous verbal predictions, the leg segments located more distally from the body resonate at higher frequencies, around 60 Hz. The segments located more proximal to the body resonate at 17 Hz, i.e., higher frequencies are filtered out as vibrations travel closer to the abdomen (Mhatre et al., 2018). Interestingly, the posture of the spider influenced mechanical filtering. Spiders in a defensive 'crouch' posture resonated at higher frequencies than those in a more 'neutral' posture (Mhatre et al., 2018).

The value of the joint stiffness parameters in the black widow multi-body models were not measured, and were estimated by fitting the model to empirical data from real black widows (Mhatre et al., 2018). Additionally, all joints were treated as being equally stiff. As expected, the system was sensitive to changes in joint stiffness. As the stiffness parameter increased with all else, including mass, being held constant, the resonant frequencies predicted by the model also increased (Mhatre et al., 2018). Having a more accurate prediction of joint

rotational stiffness within and across legs would improve our ability to model the mechanical behaviour of a spider body and to apply this method to other species.

## 1.5 What influences spider joint stiffness?

### 1.5.1 Spider leg anatomy

As mentioned previously, spider legs are composed of seven segments named proximal to distal from the cephalothorax: coxa, trochanter, femur, patella, tibia, metatarsus, and tarsus (Fig. 1.2A). All joints are hinge-like joints that allow rotational motion in one plane except the coxa-trochanter joint which is a ball and socket like joint and allows three rotational degrees of freedom (Parry, 1957; Whitehead and Rempel, 1959). To move segments around their joints, spiders use flexor muscles and hemolymph pressure (Ellis, 1944). Joints are extended by increasing the pressure of hemolymph in the joint, which causes an expansion of a bellows-like joint articular membrane which extends the joint (Fig. 1.5). This increase in hemolymph pressure is achieved by the spider's open circulatory system and channels called hydraulic lacunae (Ellis, 1944). Joint flexion is achieved through the contraction of flexor muscles (Ellis, 1944). Of the hydraulic lacunae and flexor muscles, only the flexor muscles will likely contribute to joint stiffness.

During joint extension or flexion, the tissues attached to a joint will be stretched or compressed and resist this distortion of their natural resting length. There are many anatomical structures in the proximal segment that are attached to a joint, and all of these will be stretched and compressed during joint bending. These structures include muscles, hydraulic lacunae, nerves in the leg, and the articular membrane of the joint (Fig. 1.5). However, the

muscles that drive joint flexion are typically the largest structure within that leg segment and therefore I expect them to be the main contributor to joint stiffness (Fig. 1.5) (Siebert et al., 2010).

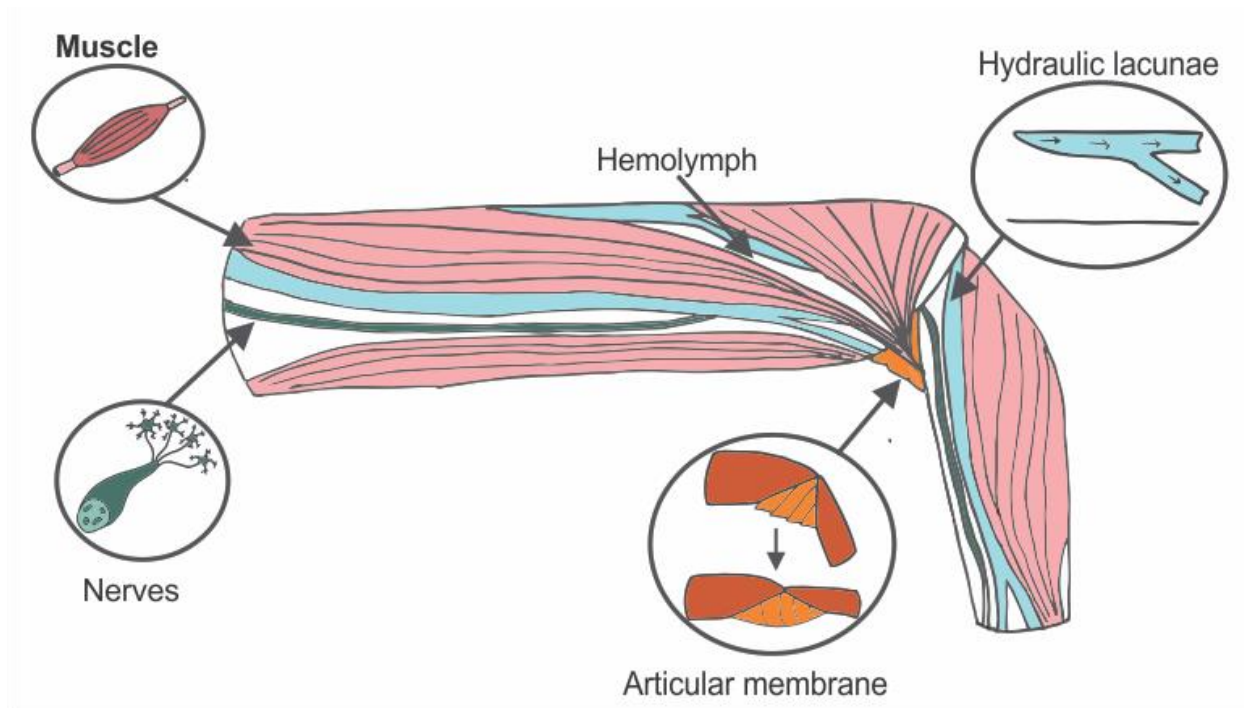


**Figure 1.5** Anatomical structures within the leg that may contribute to leg joint stiffness. A joint's stiffness is its resistance to rotation. Anatomical structures in the segment proximal to a joint are attached to the joint and will stretch during joint extension. These structures include the bellows-like articular membrane connecting the two leg segments at a joint, muscles, nerves, and the walls of hydraulic lacunae which extend a joint using hydraulic pressure. The linear stiffness of an object depends on the object's size (equation 1.2). Since muscle is typically the largest structure within the leg, it is therefore likely to contribute the most to joint stiffness. Anatomical structures are not drawn to scale and are based on anatomical drawings of *Cupiennius salei* by Blickhan and Barth (1985).

### 1.5.2 Scaling of joint stiffness with segment size

Given what we know about the main contributors to spider joint stiffness, we can make some predictions regarding the scaling of joint stiffness. Spiders have a rigid exoskeleton and as a result, the dimensions of the muscles supporting each joint are constrained by the leg segment. Muscle length is likely constrained, since the muscles attached to each joint remain confined to the proximal segment in all the species studied so far (Brown, 1939; Parry, 1957; Ruhland and Rathmayer, 1978; Whitehead and Rempel, 1959). Additionally, muscle cross-sectional area will be constrained by the cross-sectional area of the segment it is contained in. Given that most of the cross-section of segments like the tibia are composed of muscle (Blickhan and Barth, 1985; Liu et al., 2019), the dimensions of the muscle and leg segment are likely proportional, e.g., as the leg segment dimensions change across species, the dimensions of the muscle will change proportionally. In a homogenous structure, one where material properties are the same in all directions, stiffness changes with the structure's dimensions according to equation (1.2).

$$k \propto \frac{A}{L}$$

(1.2)

Where,  $k$  is the stiffness of the structure,  $A$  is the cross-sectional area ( $\text{m}^2$ ), and  $L$  is the length of the structure (m) (Ennos, 2012). I will hereon refer to the ratio of cross-sectional area to length as area-length ratio. This equation predicts that a short wide object would have a high area-length ratio and a higher stiffness while the inverse is true for a long thin object.

The same logic can be applied to a spider's muscle dimensions and joint stiffness. As the area-length ratio of the proximal muscle increases, the stiffness of the muscle will increase and thus, the rotational stiffness of the joint it attaches to will also increase.

However, muscle can also actively generate forces. When the muscle is activated, it could generate a force in the opposite direction of joint extension, thus further increasing the stiffness of the joint (Dorfmann et al., 2007; Ettema and Huijing, 1994). Different levels of muscle activation would give rise to actively modifiable and variable joint stiffness. The force production of a given muscle depends on its length with respect to its resting length (Biewener and Patek, 2018; Siebert et al., 2010). In *C. salei*, this force has been measured for the tibia-metatarsus joint and has been observed to be the highest at its joint angle in a normal, resting posture (about 130°) and remains similar from about 110 – 170° (Siebert et al., 2010).

## 1.6 Thesis objectives

### 1.6.1 The relationship between spider joint stiffness and body size

Given that we have an understanding of the determinants of joint stiffness, we may be able to generate and test a quantitative model to predict the stiffness of a joint which may improve quantitative models of spider body mechanics. In Chapter Two, I measure the rotational joint stiffness of four joints in 11 spider species of different sizes, and use these data to develop a quantitative model for spider joints. In this chapter, my first objective is to determine how area-length ratio changes with spider mass across species. My second objective is to test how rotational joint stiffness varies with the dimensions of the leg segment preceding the joint and with spider mass.

### 1.6.2 Modeling mechanical filtering by a spider's body

As we have seen, several factors may influence the mechanical filtering by a spider's body. Spiders vary greatly in posture, orientation, and body morphology, from large tarantulas with relatively short and thick legs to small cellar spiders with long, thin legs. My first objective in Chapter Three is to parameterize and improve the existing multi-body model of mechanical filtering in a spider's body using data from Chapter Two. My second objective is to test if this modeling approach can capture the natural variation observed across different individuals from a species. I will test predictions of mechanical filtering at the level of the whole-body and the leg by comparing outputs from a multi-body model to empirical measurements of vibration transmission through a spider's body for three species of web-dwelling spiders.

# Chapter Two: the relationship between spider joint stiffness and body size

## 2.1 Introduction

The leg joints of spiders are multi-functional and are used for locomotion and sensing vibrations (Barth and Pickelmann, 1975; Blickhan and Barth, 1985). As a spider moves through its environment, joints are flexed by the contraction of flexor muscles and extended by increasing the pressure of hemolymph in the joint (Ellis, 1944). Similarly, joints experience torques in different directions caused by external vibrations being transmitted through the body. Joint stiffness will mechanically influence both which vibrational frequencies generate torques, and the level of the torque delivered to the joint. The level of the torque delivered to the joint determines how much the joint is rotated. Joint rotation is thought to be transformed through a variety of microscopic mechanical processes (Strauß and Stritih-Peljhan, 2022), such as strains on internal tissues such as muscles or changes in hemolymph pressure. These microscopic processes may eventually lead to a strain being generated in the exoskeletal cuticle, stimulating lyriform organs that are densely arranged near the leg joints (Barth and Bohnenberger, 1978; Barth and Geethabali, 1982; Barth and Pickelmann, 1975; Bohnenberger, 1981; Erko et al., 2015; Fratzl and Barth, 2009; Hößl et al., 2007; Hößl et al., 2009; McConney et al., 2007; Schaber et al., 2012; Young et al., 2014). Appropriate joint stiffness is therefore crucial for both functions.

Leg joints must be stiff enough for locomotor function, i.e., they must provide sufficient resistive force to support a spider's mass whether on the ground or in a web (Moya-Laraño et

al., 2008). Therefore, stiffness will likely scale positively with spider mass. When sensing vibrations, a spider body's resonant frequencies will cause the most joint bending and, therefore, stimulate lyriform organs (Barth and Geethabali, 1982; Masters, 1984b). In simple spring-mass-damper systems, the resonant frequency increases with increasing spring stiffness and decreases with increasing mass (Rossing and Fletcher, 1995). This general relationship between mass, stiffness, and resonant frequency likely holds for a spider's body as well (Masters, 1984b), therefore vibration sensing will also likely depend on spider mass and joint stiffness.

It is unclear how the needs of vibrational sensitivity balance with the requirements for locomotion. As a spider increases in mass, the stiffness of the leg joints must increase to support locomotion. As stiffness increases, a spider may become less sensitive to lower frequencies. This may be disadvantageous for larger spiders that likely prefer larger prey items which generate low frequency vibrations (Landolfa and Barth, 1996; Masters, 1984a). However, the increased mass would also moderate the effect of increased stiffness. Therefore, a precise balance between joint stiffness and body mass is likely crucial for maintaining the multifunctionality of spider joints. However, the actual scaling relationships between spider mass and joint stiffness are not well understood.

While I expect that joint stiffness will scale with spider mass, I also expect that more directly related morphological features can predict joint stiffness. Specifically, I expect joint stiffness to be influenced by the anatomical structure of the leg segment proximal to the joint. During joint extension, several structures within the leg segment proximal to the joint will be

stretched, will resist stretching, and therefore contribute to that joint's stiffness (Fig. 1.5).

Typically, muscles are the largest and densest structures in the leg and will likely contribute the most to the joint's stiffness. In spiders, leg muscle length is restricted since muscles are generally within a single leg segment (Blickhan and Barth, 1985; Parry, 1957; Ruhland and Rathmayer, 1978). In addition, because spiders have an exoskeleton, the cross-sectional area of the muscle is constrained by segment size. Therefore, I expect that the stiffness of the muscle will be related to joint stiffness. To estimate this stiffness, I need to account for the muscle's geometry, most importantly the ratio between its cross-sectional area and length which I term as the area-length ratio. In *C. salei*, the tibia is nearly completely filled with muscle (Blickhan and Barth, 1985) and in all spiders observed so far, this proportion does not vary greatly (Blickhan and Barth, 1985; Brown, 1939; Ellis, 1944; Foelix, 2011; Parry, 1957; Ruhland and Rathmayer, 1978; Whitehead and Rempel, 1959). Therefore, I assume that the size of the muscle is proportional to the size of the leg segment. The stiffness of structures with relatively isotropic, i.e., same material properties in different directions, and linear material properties increases linearly with area-length ratio (Ennos, 2012). If the muscle size is proportional to the segment size and if the stiffness is the same along the muscle length, I expect that joint stiffness will increase approximately linearly with the area-length ratio of the proximal leg segment. Thus, a joint with a short and wide proximal leg segment will likely be stiffer than one with a long thin proximal segment.

In this chapter, my first objective is to determine how area-length ratio changes with spider mass across species. My second objective is to test how rotational joint stiffness varies with the dimensions of the leg segment preceding the joint and with spider mass. To meet

these objectives, I measured joint stiffness at two different joints on two differently sized legs across 11 spider species covering a range of body and leg sizes. To measure joint stiffness, I displaced the segment distal to the joint of interest by loading it with a mass. I calculated the rotational stiffness from the change in angle due to the torque generated. I measured joint stiffness from spiders that were alive and awake to allow varying degrees of muscle activation. The stiffness properties of the muscle itself can also vary. In addition to muscle size and elasticity, joint stiffness will likely be affected by muscle activity since muscle stiffens when activated (Dorfmann et al., 2007; Ettema and Huijing, 1994). Measuring awake animals adds variation to my measurements but is a more representative measure of a joint's true stiffness in naturalistic behavioural conditions. I used a regression analysis to test the effect of spider mass on the area-length ratio of the proximal segment of each joint. I used Gaussian random intercept mixed effects modeling to test for the effects of spider mass, proximal leg segment area-length ratio, species identity and joint identity on rotational stiffness.

While my approach allows me to explore some aspects of the scaling of joint stiffness of spiders during naturalistic behaviour, it does not allow me to ascertain the independent contributions of muscle activity or elasticity. There are very few measurements of spider joint stiffness in awake spiders, especially across a range of body sizes. Measurements in awake spiders are relevant for understanding the joint mechanics required for locomotion and vibration sensing, and my data from this chapter will help fill this gap.

## 2.2 Methods

### 2.2.1 Animal collection and care

In this chapter, I used 11 species within the Araneae (Dimitrov and Hormiga, 2021; Garrison et al., 2016; Wheeler et al., 2017) listed in Table 2.1 and shown in Fig. 2.1. All species chosen for my study are monophyletic in Opisthothelae within the Araneae (Garrison et al., 2016; Wheeler et al., 2017). Two species in my sample are tarantulas (Mygalomorphae) whereas the other species are modern spiders (Araneomorphae) (Garrison et al., 2016; Wheeler et al., 2017). This is one of two main divergences in the spider phylogeny, the other being between the Mesothelae and Ophisthothelae (Dimitrov and Hormiga, 2021; Garrison et al., 2016; Wheeler et al., 2017). There are no known differences in the hydraulic mechanism of leg extension or muscle anatomy between Mygalomorphae and Araneomorphae (Brown, 1939; Ellis, 1944; Foelix, 2011; Parry, 1957; Ruhland and Rathmayer, 1978; Whitehead and Rempel, 1959). I chose these species because it allowed me to test a wide range of body and leg sizes and included both ground and web-dwelling spiders (Fig. 2.1).

**Table 2.1** Species used in this chapter all fall within the Araneae (Wheeler et al., 2017) and below I present their common name, family, where they were sourced and average body mass and standard deviation (§ = eight individuals per species, \*= one individual per species).

Common name	Family	Species	Source	Mass (mg)
Orchard spider§	Tetragnathidae	<i>Leucauge venusta</i>	Wild caught	17 ± 5.3
Yellow sac spider§	Cheiracanthiidae	<i>Cheiracanthium inclusum</i>	Wild caught	19 ± 9.0
False widow spider§	Theridiidae	<i>Steatoda grossa</i>	Lab reared	56 ± 19.2
Bold jumping spider§	Salticidae	<i>Phidippus audax</i>	Wild caught	109 ± 44.1
Western black widow spider§	Theridiidae	<i>Latrodectus hesperus</i>	Lab reared	327 ± 33.6
European garden spider§	Araneidae	<i>Araneus diadematus</i>	Wild caught	410 ± 54.9
Yellow garden spider§	Araneidae	<i>Argiope aurantia</i>	Wild caught	427 ± 198.8
Wetland giant wolf spider§	Lycosidae	<i>Tigrosa helluo</i>	Wild caught	667 ± 169.6
Striped fishing spider§	Pisauridae	<i>Dolomedes scriptus</i>	Wild caught	728 ± 355.2
Pumpkin patch tarantula*	Theraphosidae	<i>Hapalopus sp. Colombia</i>	Pet trade	7890
Curlyhair tarantula*	Theraphosidae	<i>Tliltocatl albopilosus</i>	Pet trade	25 273

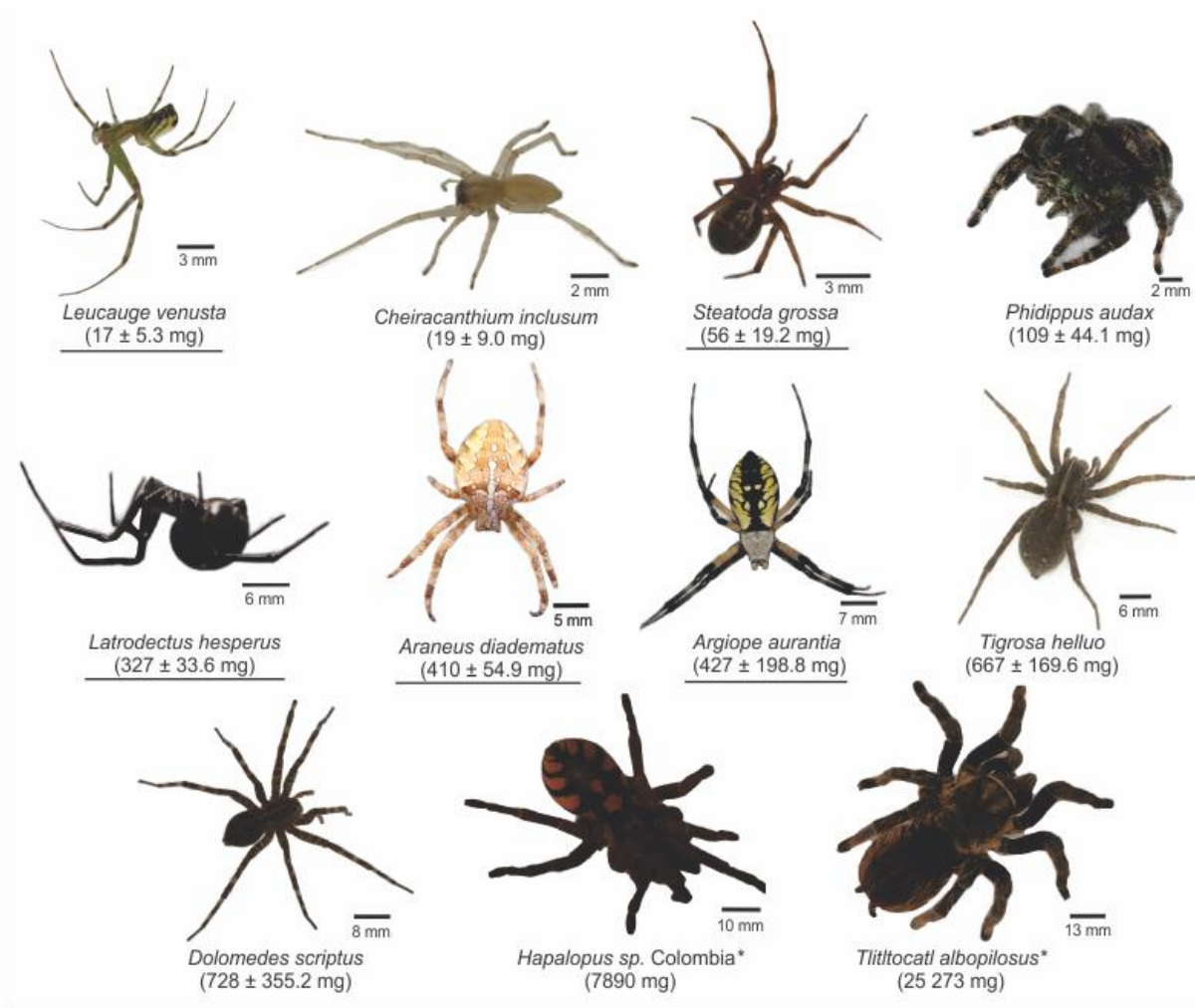


**Figure 2.1** Eleven spider species used in Chapter Two. Species are listed in order of increasing mass from left to right. Scale bars indicate the variation in size and the average and standard deviation of the body mass of each species is given. Species underlined are web-dwelling spiders. (n=8 individuals per species, n\*=1 individual).

I obtained *L. hesperus* and *S. grossa* spiders from a laboratory colony established from individuals collected in California in 2021. In the summer of 2022, I collected *D. scriptus* and *T. helluo* under large rocks and *L. venusta* in bushes along the Thames River on the University of Western Ontario campus, London, Ontario. I collected *P. audax* and *C. inclusum* on and around

human structures on the University of Western Ontario campus. I collected *A. diadematus* and *A. aurantia* in unused aviaries at the Environmental Sciences Western Field Station, Ilderton, Ontario. I measured eight adult females per species except *T. albopilosus* and *H. sp.* Colombia, which were pet animals obtained from a colleague. As a result, only one individual of each species was available.

Individuals collected were kept in the lab. I kept *L. hesperus*, *L. venusta*, *C. inclusum*, and *S. grossa* in 1.5 cm x 1.5 cm x 0.6 cm (length x width x height) AMAC clear polystyrene boxes (AMAC Plastic Products, California, USA). *D. scriptus*, *T. helluo* and *P. audax* were kept in 10.1 cm x 10.1 cm x 12.8 cm AMAC clear polystyrene boxes. *D. scriptus*, *T. helluo* and *L. venusta* were collected near water so, I placed a wet piece of floral foam in each container to increase the humidity. *A. diadematus* and *A. aurantia* were kept in 20 cm x 20 cm x 6 cm (length x width x height) picture frames to allow them to build vertical orb webs as they do in nature.

*L. venusta*, *C. inclusum*, and *S. grossa* were fed 3-5 *Drosophila melanogaster* weekly (Pet Paradise, London, Ontario). *D. scriptus*, *T. helluo*, *P. audax*, *A. diadematus*, *L. hesperus* and *A. aurantia* were fed one *Tenebrio molitor* larvae (Pet Paradise, London, Ontario) or a third instar *Gryllus veletis* (lab colony) weekly. After experiments were complete, I released collected specimens back at the site of collection. Other animals were returned to the colony or to their owner.

### 2.2.2 Morphology measurements

I narcotised each spider using CO<sub>2</sub>. I took photographs (DFK 37BUX273 USB camera, The Imaging Source, North Carolina, USA; FMA050 fixed microscope adaptor, Amscope, California,

USA) of each leg segment under a microscope (SZM-45T2, Amscope, California, USA) with a scaled slide. I used the dimensions of the leg segment as a proxy for the muscle dimensions, assuming that the two were proportional as mentioned in section 2.1. I measured the leg segment length in ImageJ (version 1.53k (Schneider et al., 2012)). I also measured the leg segment diameter at the proximal, midpoint, and distal ends of the segment. I used an average of the segment diameter at these three points on the leg to calculate the leg segment cross-sectional area, assuming the leg segment was a cylinder. For *T. albopilosus* and *H. sp.* Colombia, measurements of leg segment length and diameter were made with a Vernier caliper. This allowed me to better measure their larger leg segments by compressing the hair on their legs.

### 2.2.3 Joint stiffness measurements

I measured the rotational stiffness of the femur-patella and tibia-metatarsus joints of the first two legs on the same side of the body (Fig. 2.2A). I chose these joints as they have large, visually observable ranges of motion. I measured these two legs as it allowed me to include two leg segment sizes for each species. I measured from spiders that were alive and awake because the stiffness required for locomotion and vibration sensing will have active and passive contributions. In dead spiders hanging in the web, I have observed that the limbs hyperextend (Appendix 2). Therefore, the passive stiffness is unable to support the mass of the spider. Thus, passive stiffness would not inform me about the joint stiffness normally used and required for natural posture, locomotion, or vibration sensing.

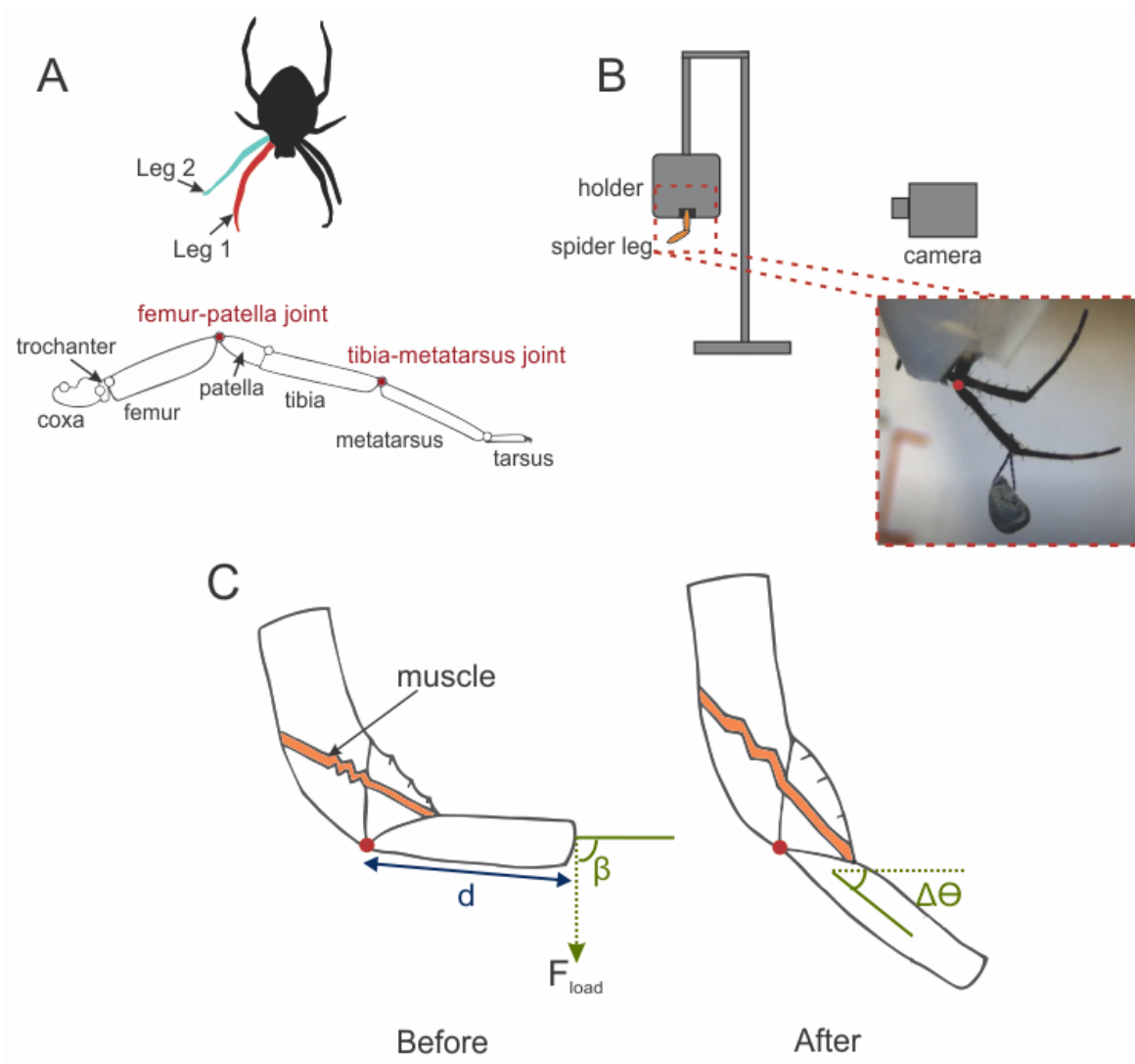


**Figure 2.2** Experimental apparatus for joint stiffness measurement. (A) The stiffness of the femur-patella and tibia-metatarsus joints were measured from legs one and two in each spider. (B) During the measurement, the spider was immobilised by being placed in a holder with the legs being measured outside the holder. A weight was placed on the segments distal to the joint of interest, generating a torque which caused the leg segment to rotate in a plane around the joint. The inset shows a photo of a spider during a trial with a mass applied to the segments distal to the femur-patella joint of interest, indicated in red. (C) Stills from trial videos were used to calculate rotational joint stiffness ( $k_r$ ). The distance from the joint pivot to where the mass was placed on the distal segment ( $d$ ), the change in joint angle ( $\Delta\theta$ ) and the angle between the

leg and the force vector ( $\beta$ ) were measured in ImageJ.  $k_r$  was then calculated using equation (2.1), where torque generated ( $\tau$ ) was calculated using equation (2.2).

**2.2.3.1 Experimental setup:** To immobilise the spider during the trial, I placed the spider in a holder based on its size (Appendix 3), so the whole body was fully contained except for the legs of interest (Fig. 2.2B). I narcotised spiders using CO<sub>2</sub>. The spiders were narcotised until they were secure in the holder, about 3-5 minutes. I placed cotton around the spider in the holder to restrict its movement and to prevent the spider from pulling the leg into the holder once awake. I immobilized the segment proximal to the joint of interest by gluing it to a mount using liquid latex. The segments distal to the joint of interest were immobilized by gluing a piece of wire to the leg using liquid latex, ensuring that only the joint of interest was free to move. I allowed the spiders to recover before testing, and the time between being placed in the holder and running the trial varied depending on the individual. If the spider reacted to the paint brush by flexing the joint when the brush touched the leg, then the trial was run.

The spider was held so that the leg segments distal to the joint of interest were parallel to the bench (Fig. 2.2B). The average initial angles of the femur-patella and tibia-metatarsus joints for each species are listed in Appendix 4. These joint angles reflect the positions of legs during naturalistic walking posture. For the tibia-metatarsus joint, the force produced by the muscle is similar between joint angles of 110-170° in *C. salei* and declines rapidly beyond that (Siebert et al., 2010). A single trial consisted of placing a mass on the segment distal to the joint of interest (Fig. 2.2C). This generated a torque on the joint of interest which caused the leg segment to rotate in a plane around the joint. I used different masses depending on the spider

species (Table 2.2) that ranged from 2% to 78% of the spider's body mass. The exact mass was chosen based on the individual's behaviour in the first trial. For example, if the leg did not extend when the mass was applied, a heavier mass was chosen. Conversely, if the leg fully extended when the mass was applied, a lighter mass was chosen. I did not want the leg to fully extend because at this end range of motion, the measured stiffness would be influenced by the cuticle of the two leg segments interacting rather than reflecting the natural stiffness of the joint. After this, the same mass was used for both subsequent trials. I completed three suitable trials with the same mass for each joint of interest. Trial suitability was assessed based on the spider's behaviour during the trial. For example, if the spider fully extended the leg once the mass was put on, that trial was discarded, and another was run. After each trial, I weighed both the spider and the mass applied to the leg using a microbalance (accuracy 0.1 mg, TR-204, Denver Instrument Company, New York, USA).

**Table 2.2** Mass applied to each joint type in each species (§= three trials with the same mass per joint from eight individuals, two joints per individual. \*= three trials from one individual, two joints per individual).

Species	Mass applied (% of mean body mass)	
	Femur-patella joint	Tibia-metatarsus joint
<i>L. venusta</i> §	22.6	11.3
<i>C. inclusum</i> §	25.6	10.2
<i>S. grossa</i> §	58.8	10.6
<i>P. audax</i> §	78.5	11.8
<i>L. hesperus</i> §	26.5	12.5
<i>A. diadematus</i> §	13.9	13.6
<i>A. aurantia</i> §	5.8	2.3
<i>T. helluo</i> §	22.4	2.8
<i>D. scriptus</i> §	19.2	3.9
<i>H. sp. Colombia</i> *	30.8	38.9
<i>T. albopilosus</i> *	36.0	19.1

**2.2.3.2 Rotational stiffness calculation:** I recorded each trial (DFK 37BUX273 USB camera, 3 Mega Pixel 8-50 mm lens, The Imaging Source, North Carolina, USA), using ICCapture (version 2.5.1547.4007, The Imaging Source, North Carolina, USA) at 100 frames per second using a 1 cm scale beside the holder as a reference length. Using video stills, I measured the initial and final joint angle, and the distance between the applied mass and the joint (Fig. 2.2C) in ImageJ. I defined the initial joint angle as the angle just prior to the mass being released on the leg. I defined the final joint angle as the angle held for a minimum of three seconds after joint extension. I calculated joint rotational stiffness ( $k_r$ , N·m/rad) using equation (2.1).

$$k_r = \frac{\tau}{\Delta\theta}$$

(2.1)

Where,  $\tau$  (N·m) is the torque rotating the joint and  $\Delta\theta$  (rad) is the change in joint angle. I calculated torque with equation (2.2).

$$\tau = F_{load} \cdot d \cdot \sin(\beta)$$

(2.2)

Where,  $F_{load}$  (N) is the force due to gravity acting on the mass applied (gravitational acceleration  $9.81 \text{ m/s}^2$ ),  $d$  (m) is the distance between the loading position and the joint and  $\beta$  (rad) is the angle between the lever arm and the force vector (Fig. 2.2C).

Assuming that the composite of the leg tissues is proportional to the size of the leg segment, then the linear spring constant of the tissues is expected to be,

$$k_t = E_{eff} \left[ \frac{A}{L} \right]$$

(2.3)

where,  $k_t$  is the tissue spring constant (N/m),  $E_{eff}$  is the effective elastic modulus of the material resisting joint extension (N/m<sup>2</sup>), and  $\frac{A}{L}$  is the area-length ratio (m<sup>2</sup>/m). This  $E_{eff}$  arises from a combined effect of both muscle elasticity and muscle activity, which cannot be differentiated in my approach.

As the joint extends, muscle and other tissues within the leg lengthen approximately linearly with respect to joint angle change (Siebert et al., 2010). Thus, I expected that joint

rotational stiffness also varies linearly with the tissue spring constant. Therefore, the expected relationship between the joint rotational stiffness, the effective elastic modulus of the composite of leg tissues, and area-length ratio is similar to equation (2.3), as expressed in (2.4).

$$k_r \propto E_{eff} \left[ \frac{A}{L} \right]^b \quad (2.4)$$

Where,  $k_r$  is the joint rotational stiffness (Nm/rad),  $E_{eff}$  is the effective elastic modulus that combines passive and active resistance to joint extension (N/m<sup>2</sup>), and  $\frac{A}{L}$  is the area-length ratio (m<sup>2</sup>/m). Importantly, here I add the parameter  $b$  which is a scaling exponent that allows for the possibility that stiffness does not scale linearly with the leg segment area-length ratio.

#### 2.2.4 Statistical analyses

Statistical analyses were conducted using R (version 4.2.1 (R Core Team, 2022)). I fit Gaussian random intercept mixed effects models (Zuur et al., 2009) using the package *glmmTMB* (Brooks et al., 2017). To compare nested model fits, I used Akaike information criterion (AIC). If two models were within two AIC units, the simpler model was chosen. I modeled the effects of segment area-length ratio, species identity, joint identity, and leg identity (fixed effects) on rotational stiffness (dependent variable) with individual identity as a random effect. Each species has a different mass however, here I included only species identity as a categorical variable and looked at the effects of mass in a separate analysis after accounting for the effects of the area-length ratio. Joint identity was initially separated by leg to test if the effects of area-length ratio on rotational stiffness differed between the same joint types on

different legs. Area-length ratio and rotational stiffness were  $\log_{10}$  transformed for testing the scaling exponent. A random intercept model had a lower AIC value than the equivalent random intercept and slope model ( $\Delta AIC = 5.3$ ). Proceeding with a random intercept approach, I used a top-down fitting strategy to determine the best fit model (Zuur et al., 2009).

Mixed effects modeling assumes that the residuals are normally distributed and have homogenous variance. I assessed the assumption of normally distributed residuals using a quantile-quantile plot (Appendix 5A). To test for homogenous variance across all included x-variables, I plotted the residuals against each x-variable in the model. Certain patterns, for example, a cone-shaped pattern, indicates systematic residual variance in the x-variable that is not accounted for by the model. If no pattern was seen, I concluded that the assumption was met (Appendix 5B-D). Spider mass was not included as a fixed effect in the final model, but the model residuals were plotted against spider mass to confirm that including mass would not further improve the fit of the slopes within each species (Appendix 5E). I used a separate analysis to test the effect of mass on the predicted intercepts for each species.

I showed the expected relationship between the joint rotational stiffness, the effective material elastic modulus and area-length ratio in 'linear space' in equation (2.4).

$$k_r \propto E_{eff} \left[ \frac{A}{L} \right]^b \quad (2.4)$$

However, I  $\log_{10}$  transformed my data. The log-transformation of equation (2.4) gives equation (2.5).

$$\log(k_r) \propto \log(E_{eff}) + b \log \left[ \frac{A}{L} \right] \quad (2.5)$$

The intercept is calculated from the regression at the point where the area-length ratio is equal to one. Therefore, the second term in equation (2.5) disappears giving the intercept, which I call the baseline stiffness. This baseline stiffness is proportional to the log-transform of the effective elastic modulus ( $\log(E_{eff})$ ) of the tissues being stretched. The slope predicted by the model estimates the scaling exponent,  $b$ .

After assessing the mixed effects model results, I fit a weighted multiple regression using *lm* (R Core Team, 2022) to investigate the effects of the segment length, cross-sectional area, mass and joint identity on the predicted species intercepts from the mixed model. I averaged segment length, cross-sectional area, and spider mass within each species so that each species was represented by two data points (one each for the femur-patella and tibia-metatarsus joint). Regression weights were the sample size for each species (Montgomery et al., 2021), and the continuous explanatory variables were  $\log_{10}$  transformed. I applied the same top-down approach as described previously to determine the model of best fit and compared nested models using AIC.

## 2.3 Results

### 2.3.1 Larger spiders have leg segments with a larger area-length ratio

As expected, spiders with a higher body mass generally had leg segments with a higher area-length ratio, which should enable stiffer joints (Fig. 2.3). I found that the area-length ratio

scaled positively with the mass in an allometric fashion (slope = 0.41, 95% CI = [0.36, 0.45]), i.e., heavier spiders had shorter and thicker leg segments. In a linear regression model, I observed that some web-dwelling spiders had longer and thinner leg segments than expected for their mass suggesting that morphological changes may drive joint stiffness changes with habitat type (Fig. 2.3). To contrast, all points for *P. audax* lie above the line, indicating that this ground dwelling species has shorter and thicker segments than expected for its mass (Fig. 2.3). These observations are similar to previous data (Moya-Laraño et al., 2008).

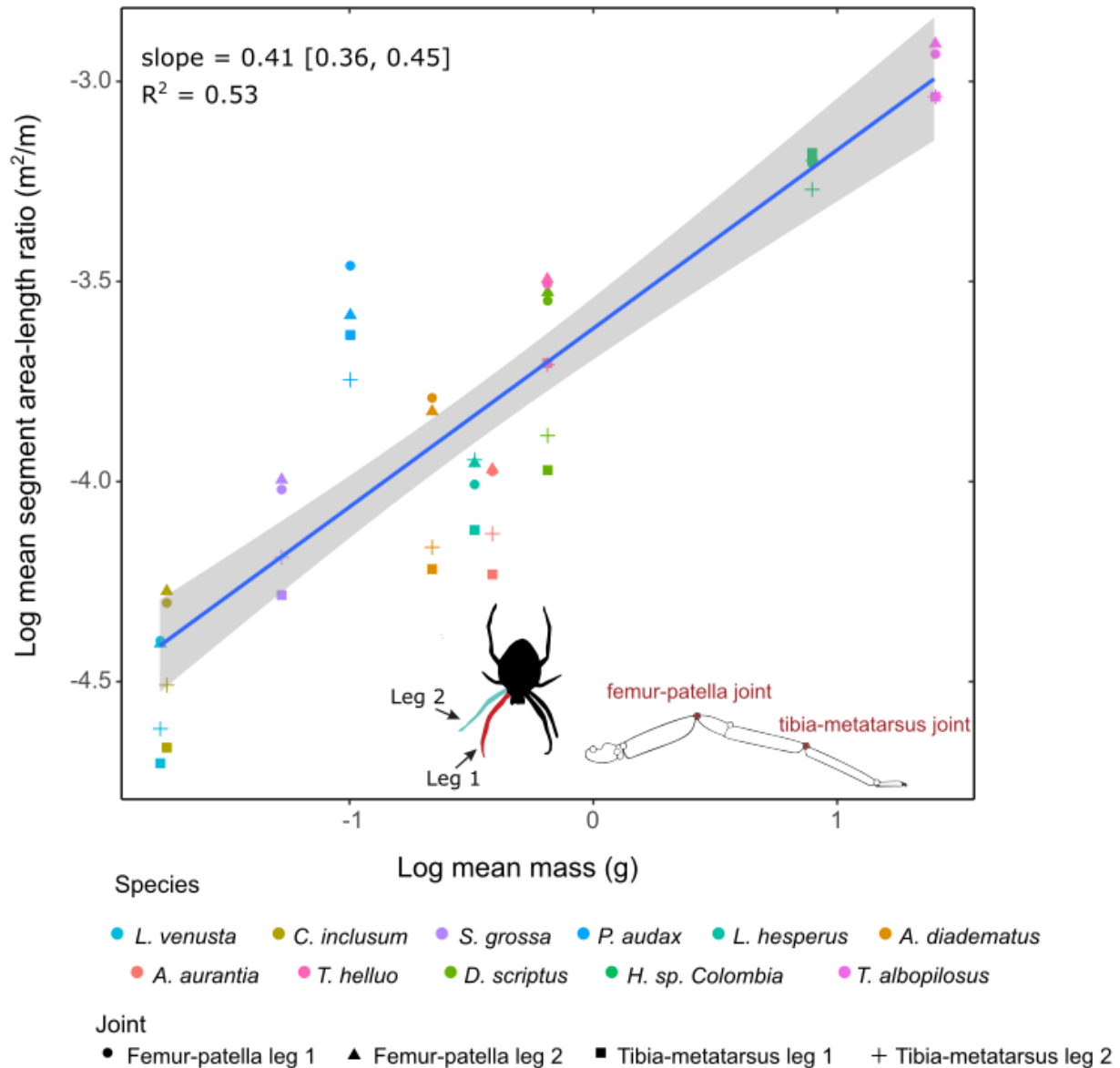


**Figure 2.3** Spider leg segment area-length ratio increases with mass. Each colour represents a species, and the shape of the data point represents whether the femur-patella or tibia-metatarsus joint on leg one or two are being represented. Both axes are log<sub>10</sub> transformed.

### 2.3.2 Joint stiffness increases hypometrically and varies across joints and species

The measured stiffness of each joint type in each species is summarized in Table 2.3.

While area-length ratio increased with mass and joint rotational stiffness scaled with area-

length ratio, I found that stiffness could not be predicted by the area-length ratio of the proximal segment alone and that the species identity and joint type were both important to consider (Table 2.4 and Fig. 2.4).

**Table 2.3** Mean and standard deviation of calculated rotational joint stiffness of each joint type measured (§ = three measurements per joint from eight individuals per species; \* = three measurements per joint from one individual). Spiders are ordered by increasing mass. Joint stiffnesses from both legs are pooled because I found no statistical evidence from mixed effects modeling distinguishing legs one and two from each other for either joint ( $P_{\text{femur-patella}} = 0.59$ ,  $P_{\text{tibia-metatarsus}} = 0.31$ ).

Species	Femur-patella (N·m/rad)	Tibia-metatarsus (N·m/rad)
<i>L. venusta</i> §	$3.26 \times 10^{-7} \pm 2.78 \times 10^{-7}$	$2.74 \times 10^{-7} \pm 3.16 \times 10^{-7}$
<i>C. inclusum</i> §	$3.11 \times 10^{-7} \pm 2.77 \times 10^{-7}$	$6.98 \times 10^{-8} \pm 6.99 \times 10^{-8}$
<i>S. grossa</i> §	$3.29 \times 10^{-6} \pm 2.44 \times 10^{-6}$	$1.00 \times 10^{-6} \pm 9.92 \times 10^{-7}$
<i>P. audax</i> §	$7.83 \times 10^{-6} \pm 6.91 \times 10^{-6}$	$1.01 \times 10^{-6} \pm 8.89 \times 10^{-7}$
<i>L. hesperus</i> §	$2.06 \times 10^{-5} \pm 1.16 \times 10^{-5}$	$4.27 \times 10^{-6} \pm 3.28 \times 10^{-6}$
<i>A. diadematus</i> §	$7.10 \times 10^{-6} \pm 2.96 \times 10^{-6}$	$1.83 \times 10^{-6} \pm 7.77 \times 10^{-7}$
<i>A. aurantia</i> §	$5.15 \times 10^{-6} \pm 3.25 \times 10^{-6}$	$1.91 \times 10^{-6} \pm 1.73 \times 10^{-6}$
<i>T. helluo</i> §	$2.57 \times 10^{-5} \pm 1.45 \times 10^{-5}$	$5.37 \times 10^{-6} \pm 6.24 \times 10^{-6}$
<i>D. scriptus</i> §	$3.53 \times 10^{-5} \pm 2.23 \times 10^{-5}$	$7.04 \times 10^{-6} \pm 6.21 \times 10^{-6}$
<i>H. sp. Colombia</i> *	$7.72 \times 10^{-4} \pm 4.24 \times 10^{-6}$	$2.31 \times 10^{-4} \pm 1.23 \times 10^{-4}$
<i>T. albopilosus</i> *	$4.49 \times 10^{-3} \pm 2.99 \times 10^{-3}$	$1.48 \times 10^{-3} \pm 3.74 \times 10^{-4}$

The first model of stiffness included segment area-length ratio, species identity, joint and leg identity, segment area-length ratio x species, and area-length ratio x joint identity as fixed effects and individual identity as a random effect (Table 2.4, Full Model). Following the approach outlined in section 2.2.4 to find the best model, I found no statistical evidence distinguishing legs one and two from each other for either joint ( $P_{\text{femur-patella}} = 0.59$ ,  $P_{\text{tibia-metatarsus}} = 0.31$ ) so, I re-ran the analysis with the leg identity removed, pooling the same joint types on different legs together. Pooling two legs of two sizes together increased the range of area-length ratios within

each species regression. This model with segment area-length ratio, species identity, joint identity and segment area-length ratio x joint identity showed that these factors had the greatest effect on the joint rotational stiffness, hereon referred to as the 'best model' ( $\Delta AIC = -7.1$ , Table 2.4, Model 1, Fig. 2.4).

**Table 2.4** A mixed effects model including segment area-length ratio, species identity, joint and leg identity, and size x joint identity best fits the joint stiffness data. The fixed effects included in each model are indicated by either a plus (+) or minus (-) sign, where '+' indicates the fixed effect is included in the model. Model fit comparisons were made using Akaike information criterion (AIC). If two models were within two AIC units, the simpler model was chosen. Each model was compared to the 'full model'. The  $\Delta$ AIC value indicates the difference in AIC units between the indicated model and full model. The model that best fit the data is indicated by an asterisk. Each model included individual identity as a random effect.

Fixed effects	Area-length ratio	Species identity	Joint and leg identity	Area-length ratio x species	Area-length ratio x joint
Full model AIC (216.8)	+	+	+	+	+
Model 1* $\Delta$ AIC (-7.1)	+	+	Only joint identity	-	+
Model 2 $\Delta$ AIC (-1.1)	+	+	+	-	+
Model 3 $\Delta$ AIC (5.4)	+	+	+	+	-
Model 4 $\Delta$ AIC (10.1)	+	+	+	-	-
Model 5 $\Delta$ AIC (85.7)	+	+	-	-	-
Model 6 $\Delta$ AIC (15.7)	-	+	+	-	-

The best model suggested that within a joint type, rotational stiffness scaled hypometrically with area-length ratio and each joint type had a distinct slope (Fig. 2.4, femur-patella  $\text{slope} = 0.73$ , 95% CI = [0.37, 1.10]; tibia-metatarsus  $\text{slope} = 0.33$ , 95% CI = [0.08, 0.65],  $P < 0.01$ ). Thus, each joint was distinct, and while spiders with greater mass had higher area-length ratios (relatively shorter, wider legs), area-length ratio did not generate the expected linear increase in joint stiffness. However, the model showed that each species, which also differ in mass (Table 2.1), have different intercepts (Fig. 2.4, Table 2.5). In the next analysis, I consider the effects of mass on baseline stiffness.

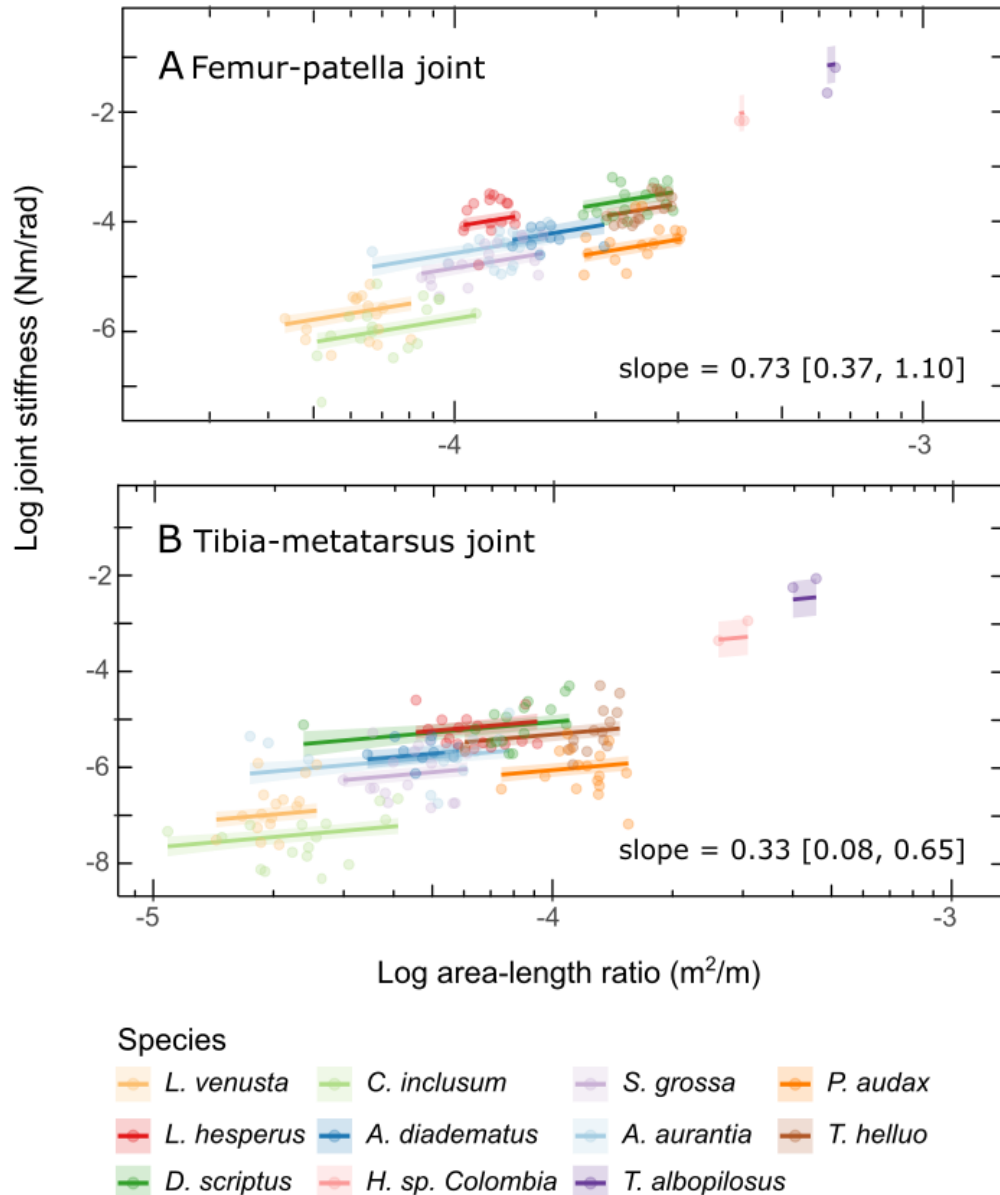


**Figure 2.4** Joint stiffness increased hypometrically with area-length ratio and was influenced by joint and species identity. The rotational stiffness (N·m/rad) of the (A) femur-patella and (B) tibia-metatarsus joints of each species is plotted against the segment area-length ratio ( $m^2/m$ ). Both axes are  $\log_{10}$  transformed. Lines indicate the relationship between joint stiffness and area-length ratio predicted by the best model. Species is indicated by the line colour and the shaded area indicates 95% confidence intervals. The dots indicate the mean measurement for each individual with one measurement each from leg one and two.

**Table 2.5** Values for the intercepts for each species predicted by the best model, both  $\log_{10}$  transformed and untransformed. The predicted intercepts are proportional to the effective elastic modulus of the tissues in the leg (N·m/rad) which I call the baseline stiffness. Data in brackets show the 95% confidence interval. Species are ordered by increasing mass.

Species	Log <sub>10</sub> transformed	Untransformed	Log <sub>10</sub> transformed	Untransformed
	femur-patella intercept [95% CI]	femur-patella intercept [95% CI] $\times 10^{-3}$	tibia-metatarsus intercept [95% CI]	tibia-metatarsus intercept [95% CI] $\times 10^{-5}$
<i>L. venusta</i>	-3.22 [-3.46, -2.97]	0.60 [0.34, 1.07]	-5.34 [-5.61, -5.08]	0.45 [0.24, 0.82]
<i>C. inclusum</i>	-3.60 [-3.82, -3.37]	0.24 [0.15, 0.42]	-5.72 [-5.97, -5.47]	0.19 [0.10, 0.33]
<i>S. grossa</i>	-2.65 [-2.85, -2.46]	2.20 [1.39, 3.44]	-4.77 [-4.99, -4.55]	1.67 [1.0, 2.7]
<i>P. audax</i>	-2.71 [-2.96, -2.46]	1.92 [1.08, 3.42]	-4.83 [-5.1, -4.57]	1.48 [0.79, 2.6]
<i>L. hesperus</i>	-1.92 [-2.12, -1.72]	12.0 [7.59, 19.1]	-4.04 [-4.25, -3.82]	9.12 [5.5, 15.1]
<i>A. diadematus</i>	-2.32 [-2.40, -2.10]	4.76 [3.94, 7.91]	-4.44 [-4.54, -4.20]	3.61 [2.87, 6.28]
<i>A. aurantia</i>	-2.39 [-3.65, -0.87]	4.07 [0.22, 135]	-4.51 [-5.88, -3.15]	3.09 [0.13, 70.4]
<i>T. helluo</i>	-2.08 [-2.33, -1.84]	8.17 [4.59, 14.4]	-4.21 [-4.48, -3.94]	6.17 [3.31, 11.5]
<i>D. scriptus</i>	-1.9 [-2.13, -1.68]	12.6 [7.41, 20.9]	-4.02 [-4.26, -3.78]	9.55 [5.50, 16.6]
<i>H. sp. Colombia</i>	-0.62 [-1.12, -0.11]	240 [75.9, 776]	-2.74 [-3.28, -2.19]	182 [52.5, 646]
<i>T. albopilosus</i>	0.02 [-0.53, 0.57]	1050 [295, 3720]	-2.1 [-2.68, -1.5]	794 [209, 3160]

### 2.3.3 Baseline stiffness increases isometrically with mass

As shown in equation (2.5), the baseline stiffness is the intercept of the mixed effects model regression and is proportional to the  $\log_{10}$ -transform of the effective elastic modulus of the tissues in the leg for each species. My previous results suggest that joint stiffness increases hypometrically with leg segment size and may be insufficient to support higher masses. However, each species also had a different baseline stiffness which may compensate for a possible insufficiently stiff joint. Since the sample size of each species was not equal, in particular the tarantulas, I used a weighted regression, where weighting was based on sample size, to test the effect of mass on baseline stiffness. I found that the baseline stiffness of the leg joints, could be explained by a model with mass and joint identity as explanatory variables (Fig. 2.5,  $\Delta AIC = -2.9$ ,  $R^2 = 0.96$ ). This final regression model suggests that the baseline stiffness increases isometrically with mass.

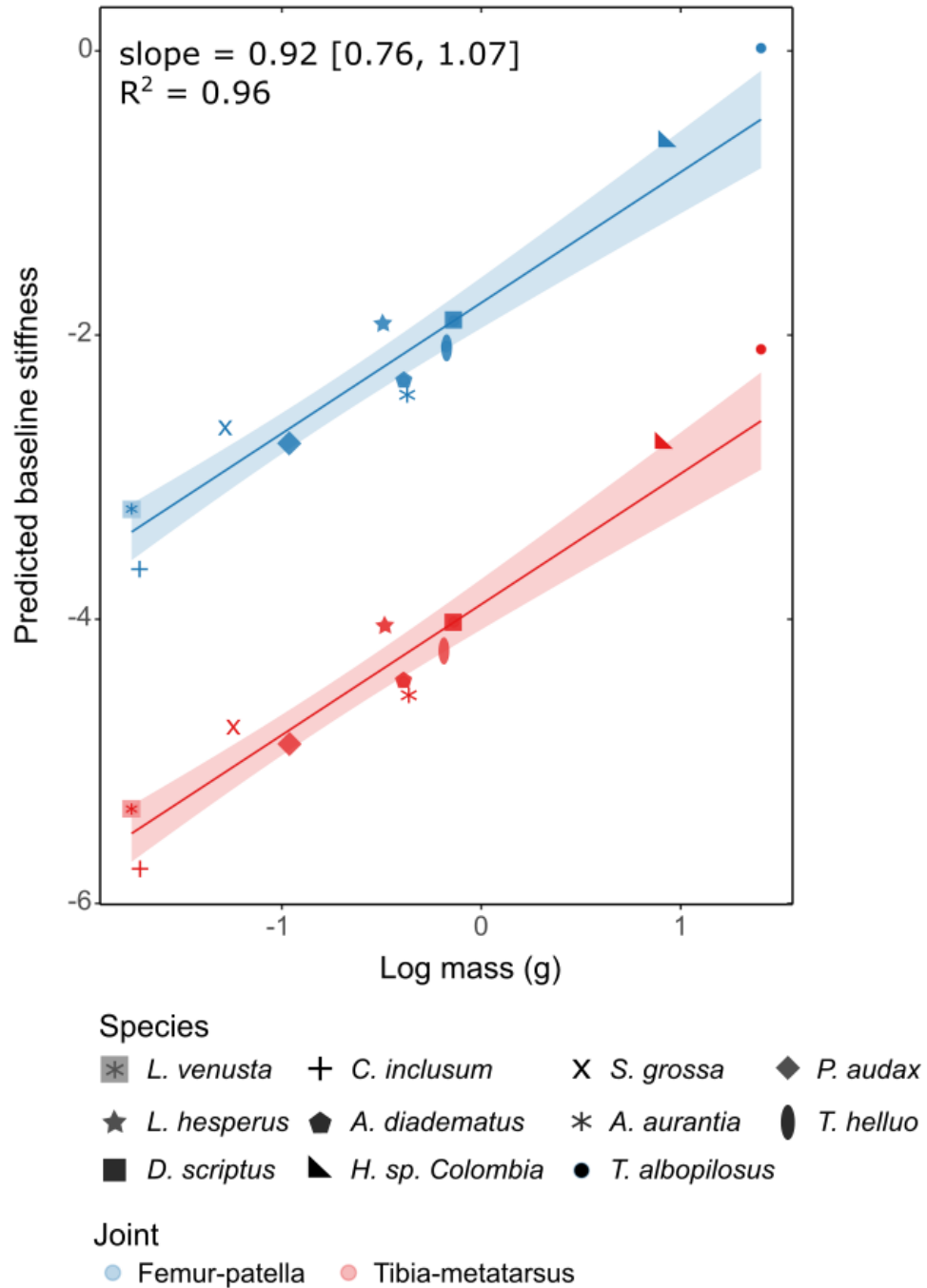


**Figure 2.5** Baseline stiffness increases with mass. A weighted regression between spider mass (g) and baseline stiffness predicted by the best fitting mixed effects model. The regression shows that the predicted intercepts, i.e., the baseline stiffness of a spider joint, increases with mass. Joint type is indicated by line colour. Each species is shown by a different shape. Each data

point represents the average mass for each species. The regression weights were calculated using sample size. The slope with the 95% confidence interval and the  $R^2$  value are indicated.

## 2.4 Discussion

As spiders increased in size, I expected that they would require stiffer joints to support their mass and that they would achieve this by having shorter and thicker legs. However, it was also possible that muscle architecture and the material properties of the tissues within the leg segment could differ across species and alter joint stiffness. My data showed that heavier spiders did have segments with higher area-length ratios (Fig. 2.3), however, joint stiffness did not increase linearly with area-length ratio (Fig. 2.4). In fact, I found I could not predict a joint's rotational stiffness from segment area-length ratio alone, but that species and joint identity must be considered. Different joint types had different stiffnesses and different scaling relationships. Most interestingly, I also found that different species had different baseline stiffnesses, which scaled isometrically with mass. Thus, I think that as spiders increase in mass, they use two strategies to stiffen their joints; they have shorter and thicker legs, but more important they also have stiffened their joints by perhaps using muscle activity, using stiffer materials or making morphological changes.

### 2.4.1 Comparisons with known active and passive joint stiffnesses

Muscle-driven dynamic variation in joint stiffness has been observed in the large tiger wandering spider *Cupiennius salei* (4 g, Trechaleidae family), where the tibia-metatarsus joint has variable joint stiffness during flexion and extension (Blickhan, 1986) and muscle force production is known to change over this range of joint angles (Siebert et al., 2010). Blickhan

(1986), measured the stiffness of the tibia-metatarsus joint of a live tarantula, however, he did not state which species he measured from in the paper. He did not calculate rotational joint stiffness as I have, so I have calculated rotational stiffness based on experimental details in his paper (Blickhan, 1986). Based on his data presented in Fig. 8, for a starting angle of about  $3^\circ$ , when about 0.05 N of force was applied to the leg segment, it caused the joint to rotate about  $21^\circ$  (0.37 rad) (Blickhan, 1986). From this I can calculate that the rotational stiffness of the tibia-metatarsus joint is about 0.0022 N·m/rad. From the same dataset, for starting leg angles of  $100\text{--}140^\circ$ , about 0.01 N of force causes the joint to rotate about  $2.1^\circ$  (0.037 rad), meaning the rotational stiffness is about 0.004 N·m/rad (Blickhan, 1986). This measure of active stiffness from a live, tethered tarantula is similar to the stiffnesses that I observe in my data for the tarantulas (for the femur-patella: about 0.0007 N·m/rad for *H. sp.* Colombia and 0.004 N·m/rad for *T. albopilosus*; for the tibia-metatarsus: about 0.0002 N·m/rad for *H. sp.* Colombia and 0.001 N·m/rad for *T. albopilosus* (Table 2.3)).

Passive measures of joint stiffness without muscular activity in tarantulas are lower. In the tarantula *Phrixotrichus roseus* (17 g), the passive stiffness of the femur-patella joint was  $3.7 \times 10^{-5}$  N·m/rad (Zentner, 2013). My measured stiffnesses from similarly sized species *H. sp.* Colombia (7 g) were 20 times stiffer and in *T. albopilosus* (25 g) were two orders of magnitude stiffer (Table 2.3). The passive stiffness of the femur-patella and tibia metatarsus joints of another tarantula *Aphonopelma seemani* (16 g) were about  $1.6 \times 10^{-4}$  N·m/rad and  $3.8 \times 10^{-5}$  N·m/rad respectively (Sensenig and Shultz, 2003). My measured stiffnesses of the femur-patella joint of *H. sp.* Colombia were 5 times stiffer and 28 times stiffer for *T. albopilosus*. For the tibia-metatarsus joint, my measured stiffness of *H. sp.* Colombia was 6 times stiffer and 38 times

stiffer for *T. albopilosus* (Table 2.3). This suggests that muscular activity adds considerable resistance and hence stiffness to joints. However, the force production capacity of muscles increases with volume (Biewener and Patek, 2018) and this effect will likely be largest in large spiders such as tarantulas. The fact that I did not include muscle activity and its scaling in my analysis could explain why I did not observe the predicted isometry between area-length ratio and joint stiffness. Since my measurements do not separate passive and active stiffness, future work could measure the passive and active stiffness independently. This would allow us to determine how much of the joint stiffness arose from passive and active stiffness, and how passive and active stiffness each scale with muscle cross-sectional area and length. This could explain how spiders of different sizes support their mass.

#### 2.4.2 Changing baseline stiffness across species and joints

Most of the variation in joint stiffness across species is observed in the baseline stiffness. Baseline stiffness as defined here is a combination of the passive elasticity and muscle activity. Given the large contribution of muscle activity observed in tarantulas (Blickhan, 1986; Sensenig and Shultz, 2003; Zentner, 2013) and the inability of area-length ratio to explain this variation, I expect that muscle activation is the major contributor to baseline stiffness.

A smaller contribution may be made from passive mechanisms. Several elastic proteins that could increase passive stiffness have been found in invertebrate muscle, such as connectin and projectin in striated muscle and kettin in insect flight and leg muscles (Lakey et al., 1993; Maruyama, 1994; Saide, 1981). Passive stiffness would also increase with more non-muscular connective tissue within the leg, such as collagen and tracheolated membranes connecting

muscle fibers into bundles, the structure of the fiber sarcolemma, or the tendon that attaches the muscle to the apodeme (Biewener and Patek, 2018; Chapman et al., 2013).

### 2.4.3 Differences in joint stiffness between joint types

Within a species, I found that joint rotational stiffness increases with different hypometric slopes for both joint types and the femur-patella was stiffer than the tibia-metatarsus (Fig. 2.4 and Fig. 2.5). Since my measurement does not separate the active and passive components of muscle stiffness, it is difficult to comment on the specific drivers of these differences.

These two joints are comparable because they are kinematically similar. During locomotion, the femur-patella and tibia-metatarsus joints show the greatest range of motion compared to other spider leg joints, with the femur-patella range being larger than the tibia-metatarsus, about  $150^\circ$  and  $120^\circ$  respectively (Foelix, 2011; Hao et al., 2019; Reußenzahn, 2010). Both are 'knee-like' joints, are held flexed at about  $100^\circ$  during standing posture and are two of the three main joints that exhibit large angular changes during locomotion (Boehm et al., 2021; Weihmann et al., 2010; Weihmann et al., 2012). Both extend using hydraulic pressure from the hemolymph of the open circulatory system and hydraulic lacunae found between muscles (Blickhan and Barth, 1985; Ellis, 1944; Kropf, 2013).

To understand why these two joints have different baseline stiffnesses and scaling relationships, I would have to measure several things both within and across species. First, I would need to know if there were systematic differences in the morphology of the muscle and other stiffening components in the two segments. Most studies have focused on the tibia-

metatarsus joint, and in the tiger wandering spider *C. salei*, the tibia was be nearly completely filled with muscle with very little space occupied by hydraulic lacunae (Blickhan and Barth, 1985). Unfortunately, there are no equivalent data for the femur of this species. I would also need to know how passive and active contributions to stiffness scale at different spider sizes and whether there are significant differences in muscle properties across species.

#### 2.4.4 Assumptions and limitations

A limitation with my approach to measuring joint stiffness in this chapter is that I cannot distinguish between the passive and active contributions of the muscle. Active stiffness is the largest contributor to stiffness in tarantulas (Blickhan, 1986; Sensenig and Shultz, 2003; Zentner, 2013), and the contribution of the active stiffness to the total stiffness may decrease with size, but this needs to be measured. Active stiffness could be measured in the future by experimentally contracting the muscle and measuring the force produced at different levels of muscle activation for species of different sizes (Blickhan, 1986; Siebert et al., 2010). To determine the passive contribution, passive stiffness could be measured by fatiguing the muscle before the measurement, by removing the muscle from the leg, removing the leg from the spider or measuring from a dead spider (Sensenig and Shultz, 2003; Zentner, 2013).

In this chapter, I used the diameter and the length of the leg segment as a proxy for the dimensions of the muscle. Since the tibia of *C. salei* was found to be nearly filled with muscle (Blickhan and Barth, 1985), I assumed that the dimensions of the muscle were proportional to that of the leg segment. One limitation of this assumption is that I may have overestimated the size of the muscle which may affect the resulting relationship between area-length ratio and

joint stiffness. A spider's leg muscles are typically restricted in length to the segment preceding the joint they act on (Blickhan and Barth, 1985; Parry, 1957; Ruhland and Rathmayer, 1978), therefore it is unlikely that I greatly underestimated the length of the muscle. Nonetheless, if the true length of the muscle was half of the length of the segment but the cross-sectional area was the same as the segment, then the true area-length ratio would be double what I calculated. Similarly, if the true cross-sectional area was half of the segment's but the length was the same as the segment, then the true area-length ratio would be half of what I calculated. However, since I am using a ratio, individual differences in cross-sectional area and length may have modulating effects. For example, if the length was half the segment's length and the cross-sectional area of the muscle was half of the segment's, then the effects of both would cancel and the ratio would remain the same as what I have calculated. Measuring the muscle's true dimensions would show how proportional muscle area and length change within the segment and whether these changes explain the differences between the scaling relationships I found and those I expected.

#### 2.4.5 Conclusions

In summary, in Chapter Two I show that joint mechanics differ across different joint types and species in spiders. The joint rotational stiffness scales hypometrically with segment area-length ratio, and baseline stiffness increases isometrically with mass. From this, I think as spiders increase in mass, they stiffen their joints by having shorter and thicker legs, using muscle activity, using stiffer materials or making morphological changes to the muscle.

# Chapter Three: modeling mechanical filtering by a spider's body

## 3.1 Introduction

Spiders use vibrations to communicate and obtain information about the world around them. Common sources of vibrations are prey trapped in a spider's web, male courtship vibrations, and environmental noise such as wind. To sense these vibrations, spiders use lyriform organs that are located near leg joints (Barth, 2004; Barth and Geethabali, 1982; Barth and Pickelmann, 1975). Lyriform organs are stimulated by cuticular strains generated by joint bending during vibration transmission through the body (Barth, 1971; Barth, 1985b; French et al., 2002). Spiders may distinguish between different sources of vibrations by using the frequency content of the vibrations being produced (Barth et al., 1988; Hergenröder and Barth, 1983; Klärner and Barth, 1982; Landolfa and Barth, 1996; Masters, 1984a; Masters, 1984b).

As a vibration travels to a spider, its frequency content may be changed or 'filtered' through many different processes. A process that filters signals effectively changes the relative amplitude of frequencies in the signal; the amplitude of frequencies that are 'filtered out' are decreased and *vice versa* for those that are 'filtered in' (Miller and Mortimer, 2020; Mortimer, 2017; Mortimer, 2019). Signal filtering can occur at multiple levels: in the web, in the body or in the nervous system. Filtering in the web (Landolfa and Barth, 1996; Masters and Markl, 1981; Naftilan, 1999; Singer et al., 2000; Vibert et al., 2016), the peripheral nervous system (Barth and Geethabali, 1982; Juusola and French, 1995) and the central nervous system of spiders (Speck-

Hergenr and Barth, 1986) have been studied in the past, however, fewer studies have addressed the mechanical processes within the body that can also filter signals.

Mechanical filtering by spider bodies has been qualitatively predicted using the principles of mechanical resonance. Using a simplified spring-mass-damper system as an inspiration, a spider's abdomen was predicted to be resonant, i.e., vibrate most, at low frequencies due to its higher mass whereas the lighter legs were predicted to resonate at higher frequencies (Masters, 1984b). Modes of vibration are one way to assess mechanical filtering because modal frequencies depend on the resonant frequencies of a spider's body, where the body undergoes highest amplitude motions relative to other frequencies. Previous work on *L. hesperus* has found two modes of vibration (Mhatre et al., 2018). In the first mode, the abdomen exhibits high amplitude vibrations, and the distal ends of the legs are relatively motionless. In the second, the legs exhibit high amplitude vibrations, and the abdomen is relatively motionless.

Using the effect of mass on resonant frequency, one would predict that larger spiders would resonate at lower frequencies than smaller spiders. However, mass is not the only determinant of resonant frequency. In mass-spring damper systems, resonant frequency also increases with increasing spring stiffness. Data presented in Chapter Two (section 2.3.3) shows that joint stiffness increases with increasing mass. It is unknown how changes in mass and stiffness interact to determine the resonant frequencies of spider bodies.

It is difficult to study the properties of body-based mechanical filtering because these depend on complex interactions between many aspects of the body's mechanics, such as

details of leg joint mechanics, leg segment and body masses, geometry, and spider posture (Mhatre et al., 2018; Miller and Mortimer, 2020). Quantitative techniques, such as multi-body modeling can, to an extent, simplify and integrate these interactions, even allowing quantitative predictions (Mhatre et al., 2018; Schiehlen, 1997; Wu et al., 2023; Zentner, 2013).

Multi-body modeling uses classical mechanics defined by the Newton-Euler equations to describe how rigid bodies change in position over time in response to external forces and the resulting internal force distribution (Schiehlen, 1997). In such a model, we assume rigid bodies, i.e., a solid object that does not deform when an external force is applied to it, and softer joint which do deform. While this is an approximation, it is reasonable in the case of arthropods where stiffness of body segments are much higher than those of joints (Göttler et al., 2021; McConney et al., 2007). The technique then develops a model of an object as a mechanical assembly, where each rigid body has a defined geometry and density, and all bodies are connected to one another, to fixed points or the 'ground', by joints. The mechanics of each joint are defined by stiffness and damping parameters. Stiffness is the resistance of an object to deformation, such as a joint to rotation (Ennos, 2012). Damping is the dissipation of energy during oscillation, such as energy dissipated as heat due to friction during joint bending (Rossing and Fletcher, 1995). Multi-body modeling has been used to study biomechanics in various contexts such as human locomotion (Chaffin, 1969; Gao et al., 2015; Huston and Passerello, 1971), locomotion of extinct species (Lautenschlager, 2020; Sellers et al., 2017), and even the falling cat phenomenon (Kane and Scher, 1969). Additionally, multi-body modeling has recently been used to study spider biomechanics (Mhatre et al., 2018; Wu et al., 2023).

In the western black widow, multi-body modeling was used to replicate empirical measurements of vibration transmission through a spider's body (Mhatre et al., 2018). However, in this model, the values of the joint parameters were unknown. Joint stiffness and damping parameters were estimated by using data from one spider as a starting point (Zentner, 2013), and then refined by comparing the model output of vibration transmission to the empirical measurements and adjusting parameter values until the output sufficiently matched the measurements. Resonant frequencies of the spider body were sensitive to changes in joint stiffness (Mhatre et al., 2018). However, the true value and level of variation of this parameter for black widow spiders was not known.

There are, however, several other sources of variation that can influence mechanical filtering within and across spider species, some of which were uncovered by Mhatre et al. (Mhatre et al., 2018). Within a species, individuals can vary in posture. They can vary in mass either naturally or due to feeding status. Even joint stiffness can vary depending on the level of muscle activation applied by a spider (Dorfmann et al., 2007; Ettema and Huijing, 1994; Johnson et al., 2011; Mhatre et al., 2018). Finally, web-dwelling spiders may also differ in orientation in the web or even in web type (Bradley, 2013). To make multi-body models as generalizable as possible, this variation among individuals needs to be incorporated into our models. Such generalized models would be more powerful because they can make more robust predictions and describe more scenarios than precise models based on a single idealized individual (Levins, 1966).

My first objective in this study was to parameterize and improve the existing multi-body model of mechanical filtering in a spider's body using the data collected in Chapter Two. My

second objective was to test if this modeling approach could capture the natural variation observed across different individuals from a species. To meet these objectives, I constructed multi-body models of three species of web-dwelling spider that differed in size and orientation: the European garden spider (*Araneus diadematus*), the western black widow (*Latrodectus hesperus*) and the long-bodied cellar spider (*Pholcus phalangioides*). In these models, I used data from Chapter Two to estimate the joint stiffness distribution. To assess each model's ability to predict mechanical filtering, I compared using *t*-tests the frequencies at which modes of vibration were predicted by each model to empirical measurements made using laser Doppler vibrometry. I also determined how frequencies from 10-150 Hz were transmitted through a single spider leg in the models and the data from real animals. I used probability density heatmaps made from multiple model runs to compare each model's prediction of vibration transmission to empirical measurements.

## 3.2 Methods

### 3.2.1 Web-dwelling species used in Chapter Three

I used three species of web-dwelling spiders: *A. diadematus*, *L. hesperus* and *P. phalangioides* (Fig. 3.1). I chose *L. hesperus* to continue past work and because a lab colony was readily available. I chose *A. diadematus* and *P. phalangioides* as they are locally available, are different in body size, and construct webs in different orientations (Table 3.1).

**Table 3.1** Table of species used in Chapter Three. Below I present each species, family, mean and standard deviation of body mass (mg), type of web constructed and web orientation. Eight adult females were used for each species.

<b>Family</b>	<b>Species</b>	<b>Mass (mg)</b>	<b>Web type and orientation</b>
Araneidae	<i>A. diadematus</i>	410 ± 54	Orb web, vertical
Theridiidae	<i>L. hesperus</i>	327 ± 33	Cobweb, horizontal
Pholcidae	<i>P. phalangioides</i>	10 ± 3	Cobweb, horizontal

For empirical measurements (i.e., morphological measurements and vibrometry measurements), I collected *A. diadematus* from unused aviaries at the Environmental Sciences Western Field Station, Ilderton, Ontario. I collected *P. phalangioides* from buildings on the University of Western Ontario campus and my home. I used eight adult females from each species for the empirical measurements. I used vibrometry data from *L. hesperus* previously reported by Mhatre et al. (2018).

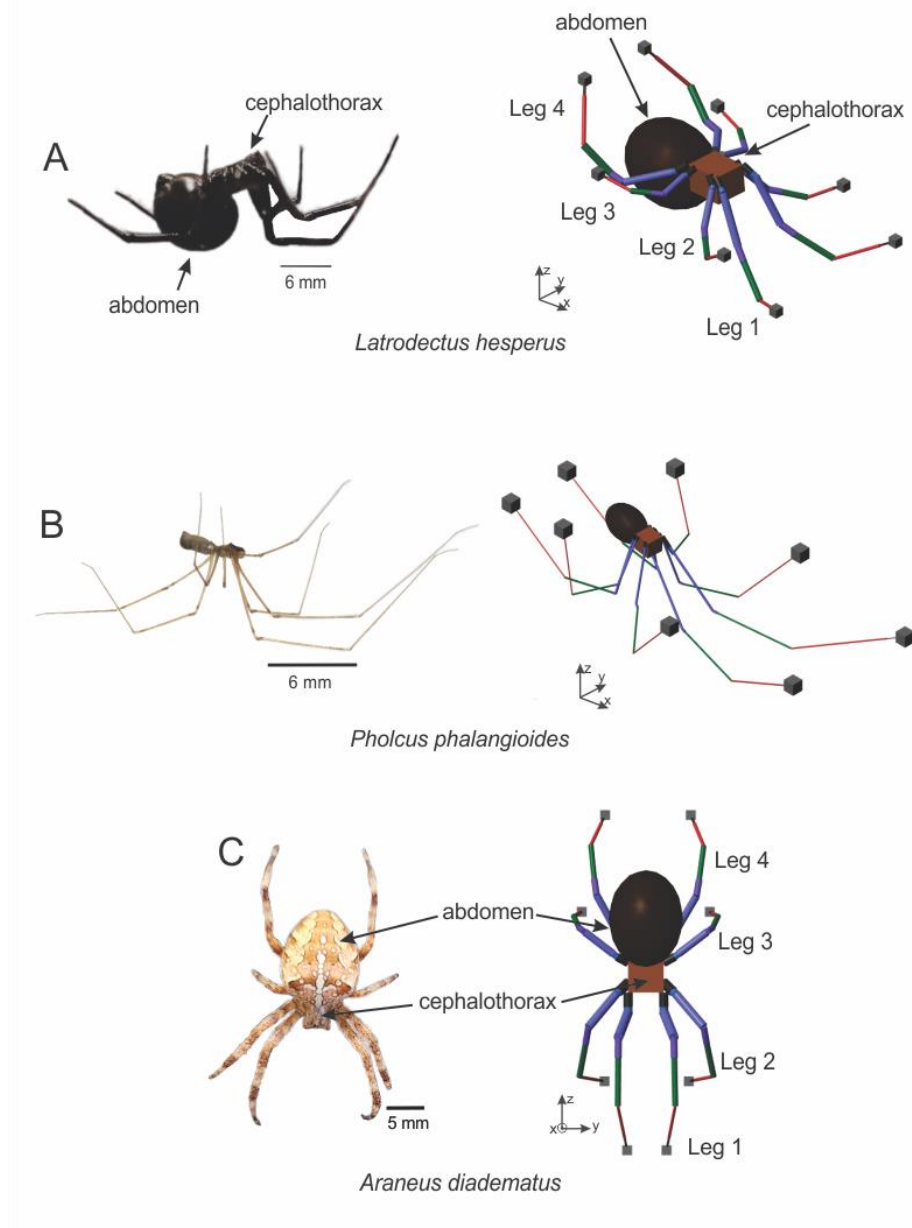


**Figure 3.1** Spider species studied in Chapter Three and the corresponding multi-body models. Scale bars indicate the size of each species. The multi-body models simulate a spider as a collection of rigid bodies connected by joints. Different leg segments are differentiated by colour. The dimensions of the rigid bodies are determined from empirical measurements of the body segments (Appendix 6). A spider's posture and orientation are reflected in the multi-body model, with gravity in the negative z-direction. The grey cubes on the tips of the legs are massless rigid bodies that represent the leg-web connection.

### 3.2.2 Vibrometry measurement

I made measurements from real spiders using laser Doppler vibrometry to capture the natural variation in the mechanical response of these species to vibrations in their webs. I used previous measurements of vibration velocity along the leg and body of *L. hesperus* (Mhatre et al., 2018) and collected new data for *A. diadematus* and *P. phalangioides*.

**3.2.2.1 Experimental setup:** Adult female *A. diadematus* and *P. phalangioides* individuals were allowed one week to build a web in a frame. *A. diadematus* built vertical orb webs in 20 cm x 20 cm x 6 cm (length x width x depth) shadow box picture frames. *P. phalangioides* built horizontal cobwebs on 9 cm x 9 cm x 8 cm frames constructed of bamboo skewers. Measurements were made from immobile spiders positioned in a central position in the web, while standing in a neutral posture. Occasionally, the spiders sat at the edge of the web in what is called a retreat. If the spider was in the retreat at any point during the measurement, I coaxed the spider out to the center of the web using a paintbrush. I waited for the spider to adopt a neutral resting posture and to stop moving before making a measurement. I measured eight mature females for each species.

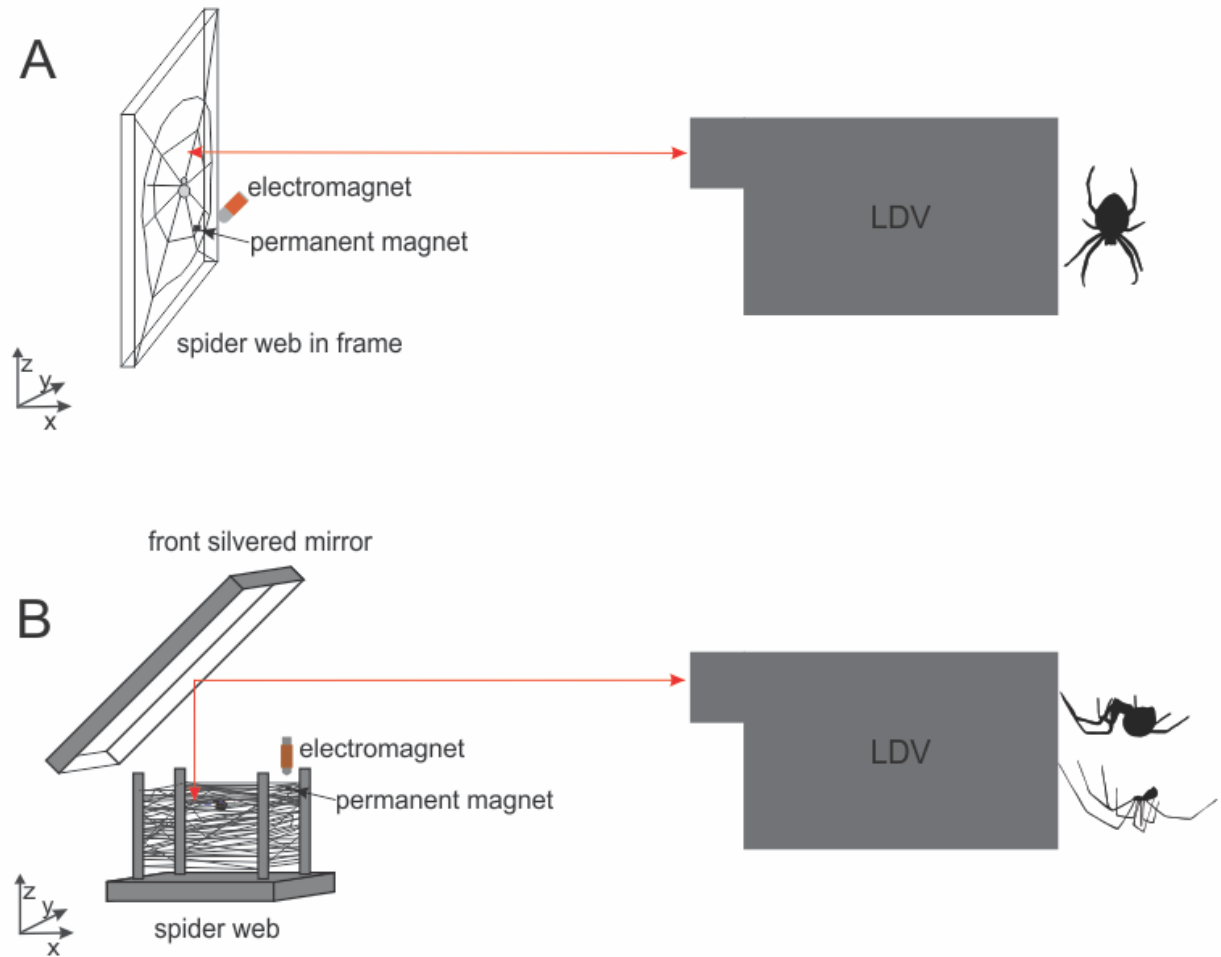


**Figure 3.2** Vibrometry setup for the vertically oriented *A. diadematus* (A) and horizontally oriented *L. hesperus* and *P. phalangioides* (B). Each individual created a web in a frame. A permanent magnet was hung in the web. I used an electromagnet to generate vibrations in the web by attracting and repelling the hanging permanent magnet. The laser Doppler vibrometer (LDV) measured the vibration velocity over time in the  $z$ -direction for the cobweb spiders and the  $x$ -direction for *A. diadematus* of the ventral side of the abdomen, cephalothorax, and leg segments of the spider in the web. Since *L. hesperus* and *P. phalangioides* hang horizontally in their webs, a front silvered mirror was used to reflect the laser down. (B) from Mhatre et al. (2018).

To generate vibrations in the web, I mounted a small neodymium disc magnet (3 x 0.5 mm cylinder, Super Magnet Man, Alabama, USA) on a small strip of Velcro (about 3 mm x 3 mm) and suspended it on the web at a selected position within 6 cm of the spider (Fig. 3.2). I made an electromagnet which received a 25 ms burst of voltage from the laser Doppler vibrometer system amplified by a power amplifier (Marantz Integrated Amplifier PM6007, California, USA). The burst of voltage was generated with a burst chirp pulse using the Polytec Vibrometer software (version 9.5, Polytec, Baden-Württemberg, Germany). The burst chirp pulse generates a broadband signal with energy from 0-200 Hz. This brief voltage generated a transient magnetic field which attracted and released the permanent magnet to generate vibrations in the web. The electromagnet was held 1-3 cm away from the permanent magnet, a distance that was close enough to attract the permanent magnet but far enough that the magnet did not contact the electromagnet. The signal was amplified until a peak velocity of about 15 mm/s was reached to ensure that the signal amplitude was large enough to reach and vibrate the spider (Mhatre et al., 2018).

**3.2.2.2 Measuring body vibrations:** I measured the vibration velocity of the ventral side of each visible leg segment, the cephalothorax, and the abdomen of the unrestrained spider in its web, and the permanent magnet which was used to vibrate the web as a reference using a scanning laser Doppler vibrometer (LDV; Polytec PSV-500, PSV-I-500 scanning head, Baden-Württemberg, Germany). The LDV uses the Doppler effect to measure the vibration velocity of a sample in one direction. The measurement beam is reflected by the sample and received by the vibrometer (Halliwell, 1979). If the sample is moving, the reflected light will be shifted in

frequency due to the Doppler effect. The frequency shift of the reflected light is used to calculate the vibration velocity of the sample in the measured direction (Halliwell, 1979).

The measurements of the vibration velocity of the spider's body using the Polytec Vibrometer software (version 9.1.1, Polytec, Baden-Württemberg, Germany) for *L. hesperus* were made at a sampling rate of 25.6 kHz. Vibration velocity was measured for 2.56 seconds and the magnet was vibrated at 0.64 seconds. For *A. diadematus* and *P. phalangioides*, I measured the vibration velocity of the spider's body using the Polytec Vibrometer software (version 9.5, Polytec, Baden-Württemberg, Germany) at a sampling rate of 25 kHz. Vibration velocity was measured for 2 seconds and the magnet was vibrated at 0.198 seconds. Ten measurements were made at every scan point and were averaged. Accurate placement of the laser points on the actual spider body were confirmed visually before recording. While data were collected, signal quality was monitored (Fig. 3.3).

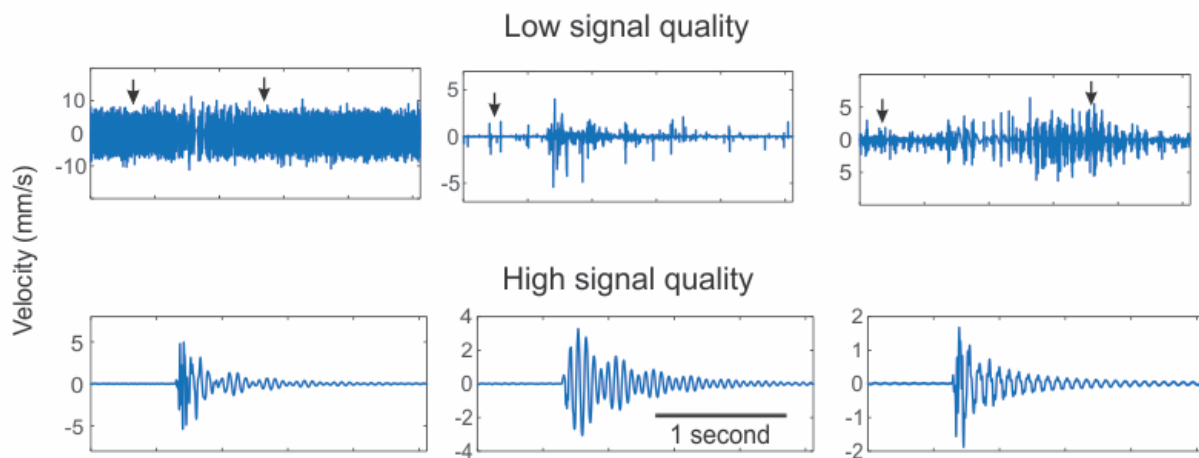


**Figure 3.3** Data point quality during vibrometry measurements was monitored using the measured vibration velocity of the scan point over time. Each plot shows the vibration amplitude of a leg segment measured from the spider. The spider cuticle may have low

reflectivity, especially for darker spiders, and therefore it is crucial to monitor signal quality. Monitoring the signal over time allowed the signal quality to be assessed quickly. Dense spikes in the data (examples shown by arrows) before the stimulation by the magnet indicate poor quality. These spikes usually persist after the stimulation by the magnet. Low quality signals appear to be dominated by noise whereas in high quality signals, the trace is easily seen. If a point was low quality, I did not use it in the analysis. From Mhatre et al. (2018).

### 3.2.3 Quantifying mechanical filtering

3.2.3.1 Minimizing the influence of the web on vibration analysis: To isolate the motion of the body and minimize the influence of the motion of the web in the empirical measurements, I used a transfer function analysis. A transfer function takes two signals collected over time, performs a Fast Fourier transform (FFT) to transform the time signals into the frequency domain, and calculates the amplitude of one signal relative to the other at each frequency. I calculated the transfer function using the Matlab (version R2020A, MathWorks, Massachusetts, USA) function *tfestimate* by taking the velocity of the abdomen and each leg segment and calculating the transfer function relative to the tarsus, which was where vibrations entered a spider's body. Aside from minimizing the motion of the web, the transfer function allowed me to see how different frequencies are transmitted through a spider's body independent from the magnitude of the force applied, i.e., this analysis allowed me to see how a spider body filters vibrations regardless of the vibration amplitude at different frequencies. I computed the transfer function for both the empirical data and the model output of the vibration velocity of each leg segment. I used the transfer function data to compare the model predictions of mechanical filtering to the empirical measurements made from the real spiders. This method

can only take data from a single point as the reference against which the transfer function is calculated however, vibrations impinge on the spider from other leg tips and can also transmit through silk from the spinnerets connected to the web. Thus, this method is imperfect and works better when vibrations reaching all these points of entry are more similar to each other.

I use the velocity of the segment motion instead of displacement for two reasons. The first is that the vibrometer measures vibration velocity, and the second is that it allows me to make inferences about the kinetic energy in each leg segment. A decrease in velocity as a vibration travels through the body indicates an absorption and dissipation of energy. Kinetic energy is related to velocity as follows:

$$E_k = \frac{m \cdot v^2}{2}$$

(3.1)

Where  $E_k$  is kinetic energy (J),  $m$  is mass (kg), and  $v$  is velocity (m/s).

I do not use displacement because to calculate displacement I would have to integrate the velocity measurements. To integrate a digital signal, I would have to perform numerical rather than analytical integration which can introduce additional errors. In digitized signals from the vibrometer, there is an error associated with each data point's time and instantaneous velocity. To integrate I would have to use two data points and use the trapezoid rule to calculate the area under the curve. The trapezoid rule is a simplification for dealing with digitized signals and uses a straight line to join the two data points. Thus, there are now four errors associated with the new data, two from each data point. In addition, there is an error

introduced by using the trapezoid rule because the real signal may vary more subtly within the integrated time period. Working with the measured velocity avoids these numerical errors and therefore, I used vibration velocity.

**3.2.3.2 Modes of vibration:** The first analysis I used to quantify mechanical filtering was to identify modes of vibration. Previous work on *L. hesperus* has found two modes of vibration (Mhatre et al., 2018). In the first mode, the abdomen exhibits high amplitude vibrations, and the distal ends of the legs are relatively motionless. In the second, the legs exhibit high amplitude vibrations, and the abdomen is relatively motionless. I looked for modes of vibration in the three species included in this chapter that were similar to those found previously in *L. hesperus* (Mhatre et al., 2018).

To identify the modes of vibration in the empirical data, I used a transfer function in Matlab (*tfestimate*) to make the velocity of each data point relative to one of the leg tips. For consistency, I used a high-quality data point from the tarsus of either the left or right foreleg. Data point quality was determined by the signal in the time domain (Fig. 3.3).

When the amplitude of the transfer function is plotted with frequency on the horizontal axis, a peak indicates that the spider body moves at a higher velocity at that frequency i.e., a peak indicates a possible mode of vibration (Fig. 3.4). To determine the frequency for the abdomen mode, I looked for peaks in the transfer function of the abdomen velocity data. If there were multiple candidate frequencies where the motion of the body resembled the abdomen mode, the frequency with the highest velocity magnitude was chosen. The real modal resonance may artificially be split into multiple peaks because the force applied to the system is

not the same at all frequencies (see section 3.2.5.5). By choosing the highest peak, I expect that I am able to pick a frequency closest to the real modal resonance. I repeated the process for the leg mode, using the transfer function of the leg segment velocity data.

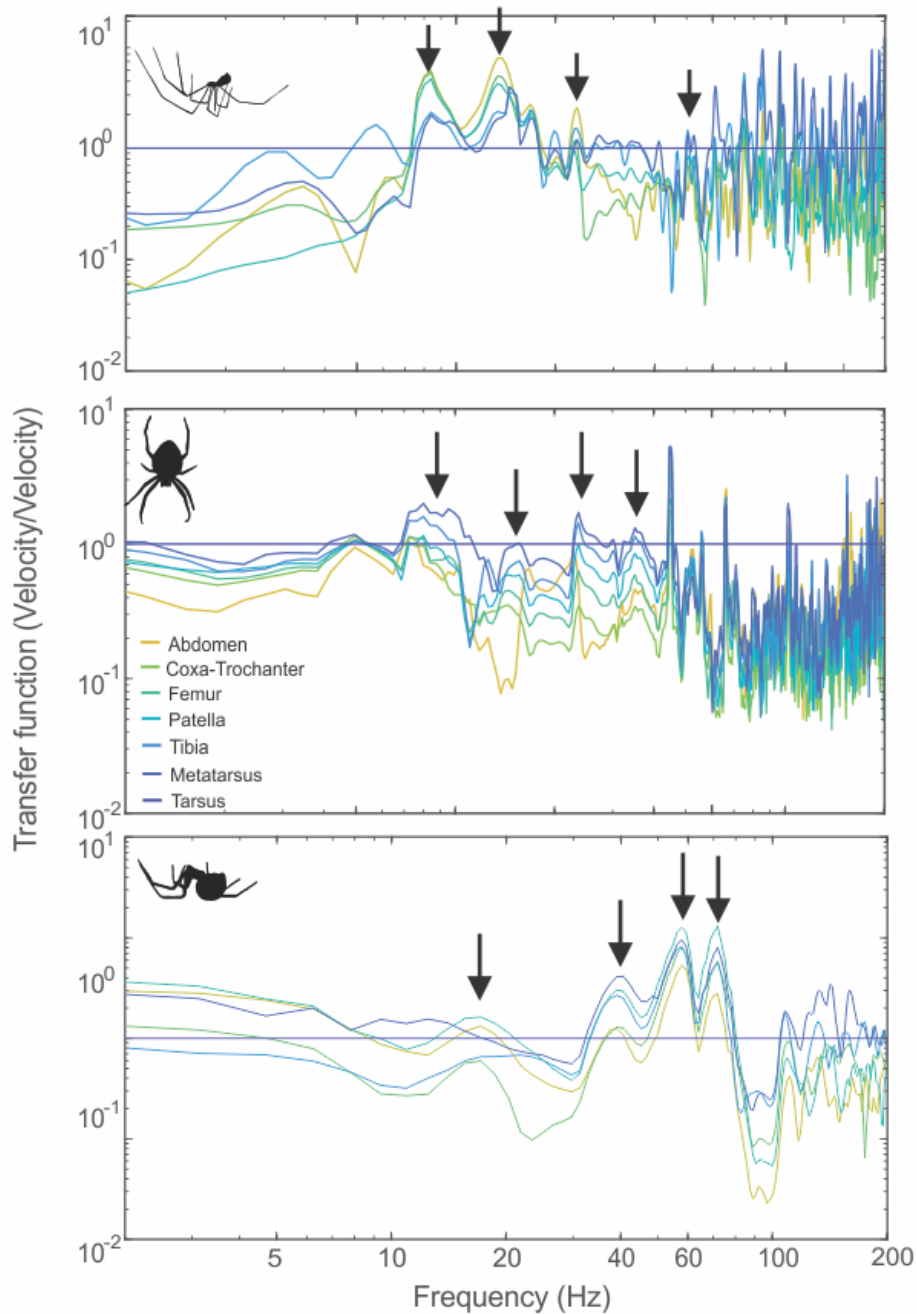


**Figure 3.4** Example data of the vibration velocity of the spider leg segments and abdomen showing peaks in the amplitude of the transfer function at each frequency for each species. The transfer function was calculated with respect to the tarsus. Each line indicates the motion of the measured leg segments and abdomen at each frequency. Arrows indicate peaks at candidate frequencies of potential modes of vibration. Species identity is shown by the silhouettes. If the same pattern of movement was seen at multiple frequencies, the one where the velocity magnitude was highest was taken as the mode frequency.

### 3.2.4 Building the multi-body models

3.2.4.1 Modelling platform: I used Simscape Multibody package (version 10.1) in Matlab

(version R2020A, MathWorks, Massachusetts, USA) to build multi-body models of each species.

Simscape Multibody is a multi-body simulation program which solves the equations of motion of the rigid bodies and joints in the assembly when an external force is applied. A single simulation of a model would be when one calculates the response of the underlying model, i.e., the multibody system, to an arbitrary applied force. The simulation can be varied from one run to another by changing the parameters of the underlying model. The model used in my thesis and its underlying parameters are described below and all parameter values are listed in Appendix 6.

3.2.4.2 Rigid bodies: I based all shape generalizations for rigid bodies on previous work (Mhatre

et al., 2018). A spider leg is composed of seven segments, listed from the most proximal to most distal segment: coxa, trochanter, femur, patella, tibia, metatarsus, and tarsus (see

Chapter One, Fig. 1.2A). I modeled each leg segment as a cylinder. The length and radius of each cylinder was taken from the morphological measurements outlined in Chapter Two

(section 2.2.2, Appendix 6). The abdomen was modeled as an ellipsoid and the cephalothorax

as a rectangular prism (Fig. 3.5A). Using the method outlined in section 2.2.2, I measured the length, width, and height of the abdomen and cephalothorax for each individual spider of all three species in ImageJ (version 1.53k (Schneider et al., 2012)). I averaged each measurement to determine the three radii of the ellipsoid that represented the abdomen and the length, width, and height of the rectangular prism that represented the cephalothorax (Appendix 6). The density of each rigid body was defined as  $1060 \text{ kg/m}^3$ , which is the density of the cuticle of most arthropods (Mhatre et al., 2018; Vincent and Wegst, 2004). This is close to the density of pure water ( $1000 \text{ kg/m}^3$ ) and to the density of most 'wet', non-mineralized biological tissues (Wegst and Ashby, 2004). For instance, arthropod tissue lies between approximately 1060 and  $1200 \text{ kg/m}^3$  (Vincent and Wegst, 2004). Changes in abdominal density from 20% - 150% had negligible effects on *L. hesperus* model output as tested by a sensitivity analysis (Mhatre et al., 2018). Similarly, shape parameters of the rigid bodies are used to calculate the masses of these parts and the moments and torques that develop around them during a simulation. Changes in body size from 75% - 125% had negligible effects on *L. hesperus* model output (Mhatre et al., 2018).

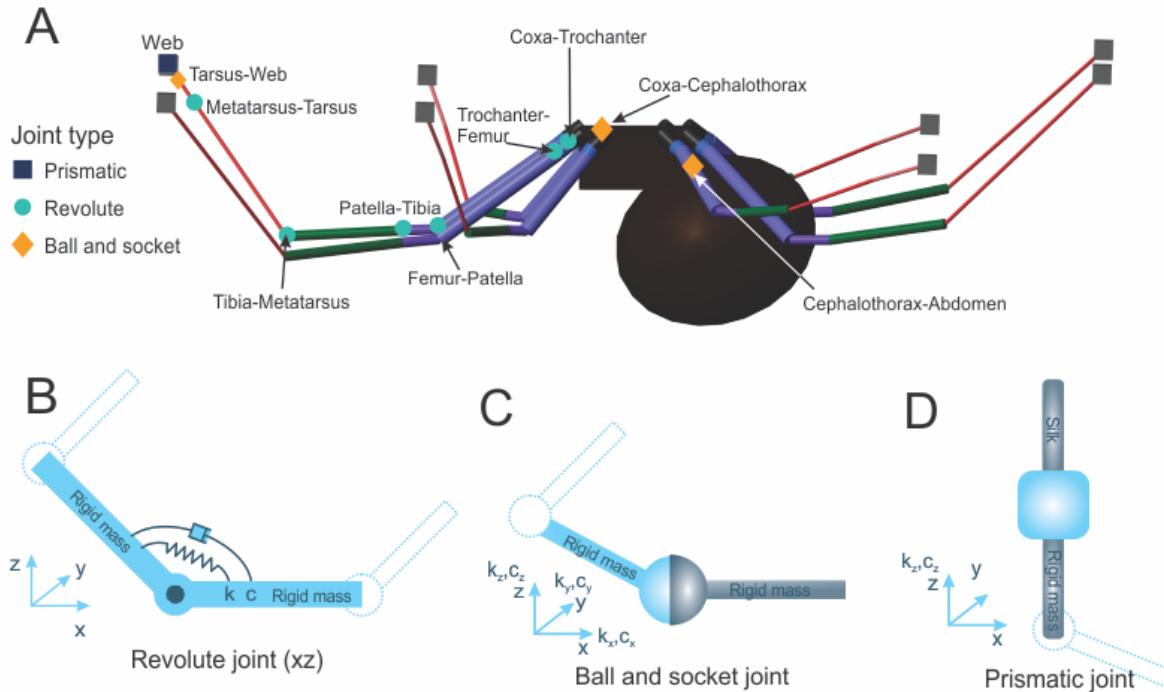


**Figure 3.5** The multi-body modeling process. Each spider body part was modeled as a rigid body. (A) The leg segments were modeled as cylinders, the cephalothorax a rectangular box, and the abdomen as an ellipsoid. Leg segments are differentiated by colour. Apart from their geometry, the input parameter for the rigid bodies was a density parameter that determined their effective mass. (B-D) Three joint types are used in the model and are based on the range of motion observed in live spiders. (B) A revolute joint moves in one plane and was used to connect all the segments within the leg. (C) A ball and socket joint moves in three axes ( $x$ ,  $y$ , and  $z$ ) and was used to connect the leg to the cephalothorax via the coxa, the tarsus to the silk, and the cephalothorax to the abdomen. (D) A prismatic joint moves in the  $z$ -axis and modeled the motion of the web during vibration transmission. The mechanics of each joint were determined by two input parameters, a stiffness ( $k$ ) and a damping parameter ( $c$ ).

3.2.4.3 Joints: Each rigid body is connected to the adjacent one by a joint. I based my choice of joint type on previous work and the observed range of motion of the joints in live spiders (Ellis, 1944; Mhatre et al., 2018; Sensenig and Shultz, 2003; Zentner, 2013). I treated the coxa-

cephalothorax, cephalothorax-abdomen and the silk-tarsus connections as ball and socket joints which allow rotational motion in the  $x$ - $y$ - $z$  planes (Fig. 3.5A and C). The ball and socket joint of the tarsus reflects a spider's ability to adjust where the tarsal claws connect to the web. I treated the coxa-trochanter, trochanter-femur, femur-patella, patella-tibia, tibia-metatarsus, and metatarsus-tarsus joints as revolute joints, which only allow rotational motion in the  $x$ - $z$  plane (Fig. 3.5A and B). For each joint, the spring and damper components, which determine the stiffness and damping of each joint, were assumed to be in parallel. When initializing the model, the model settles into a stable position in which all the forces on the bodies and joints are equilibrated. This equilibrium position is in part determined by the joint mechanics, outlined below, and the equilibrium position of the joint which is defined by an angle (see section 3.2.4.4, Appendix 6 and 7).

In the model, joint mechanics are defined by two parameters: joint stiffness and damping. For the revolute joints, there is a stiffness and damping in a single axis, whereas for the ball and socket joints there is a stiffness and damping parameter in each of the three axes of motion. For each species, the stiffness was assumed to be the same in each axis for the ball and socket joints. For *L. hesperus* and *A. diadematus*, I estimated the stiffness of the leg joints using the species-specific distributions of stiffness defined by all measurements from the four joints types measured in Chapter Two (Appendix 6). I combined the measured stiffnesses of all joints for a particular species together to define the stiffness distribution because when I varied the stiffness of different joints individually, it did not change the predicted transmission in the leg (Appendix 8). The stiffness of *P. phalangoides* joints were not measured in Chapter Two. The legs of this spider species are very thin and delicate and this species also readily

autotomizes legs when injured or entangled, making joint stiffness measurements with my method not feasible (Maughan, 1978). Instead, I used the joint stiffness distribution of *L. venusta*, the species that was the most similar to *P. phalangioides* in terms of leg dimensions and mass.

The value of the joint damping parameter was varied by the surface area of the joint since I expect frictional damping from parts of the joint's structure being in contact during rotation to be the main source of energy dissipation in these joints. The overall damping of each joint was calculated as a multiple of the base value  $1 \mu\text{N}\cdot\text{m}/(\text{rad}/\text{s})$  and the radius of the proximal leg segment (Appendix 6). This estimate of the joint damping was found to be reasonable in previous work by comparing the model output to empirical measurements of the vibration amplitude of each leg segment (Mhatre et al., 2018).

**3.2.4.4 Posture and orientation:** I wanted to capture how each species sat in their web at rest and then add postural variation in the model. As mentioned previously, the three species naturally sit in different orientations relative to the ground. *P. phalangioides* and *L. hesperus* construct horizontal webs whereas *A. diadematus* constructs vertical webs. I accounted for these differences in orientation relative to the ground in the model. Gravity was defined in the downward z-direction, and each spider model was oriented appropriately (Fig. 3.1).

In addition to their orientation in the web, each species sits in slightly different postures. I determined each model's posture by using the empirically observed joint angles between two adjacent leg segments and where the leg connects to the web (Appendix 6 and 7). The femur-patella and tibia-metatarsus joints have the greatest range of motion and thus are the main

joints that determine a spider's posture (Ellis, 1944). I took photos of the spider at rest in the web perpendicular to the lateral view of the spider to minimize any distortion in measured angles, however, some perspective error might be included. After determining the angles of the resting posture, I added variation to the model posture (see section 3.2.5.3) to capture small postural variations seen across real individuals.

**3.2.4.5 The web:** In the model, the full web was not included but its behaviour was captured using a prismatic joint (Fig. 3.5A and D). A prismatic joint only moves in one direction, as the web primarily would due to the weight of a spider suspended in it. I set the stiffness parameter of the prismatic joint for each species to 0.3 N/m which was determined by previous measurements of the stiffness of *L. hesperus* webs (Mhatre et al., 2018). A sensitivity analysis on silk stiffness suggested that silk stiffness did not have a significant effect on *L. hesperus* model output (Mhatre et al., 2018). This may not apply to all species, especially *A. diadematus* which is an orb web spider. I used a transfer function analysis to calculate the movement of each body segment relative to the most distal leg segment so that the model output was comparable to the real animal data (see section 3.2.3.1).

### 3.2.5 Model parameter variation and simulation

Running the model only once would simulate a single spider defined by a single parameter set. In reality, individual spiders will be different from each other, and an 'ideal' spider does not exist. In addition to inter-individual variability, even individual spiders can show morphological and physiological variation over time. Spider abdomen mass can double after a meal (Johnson et al., 2011), joint stiffness can be changed by muscle activation, posture might vary due to the web's structure, and in some cases, a spider may have a silk-line connected to

the web. Finally, because webs are not perfectly stereotyped, even the vibrations evoked in a spider's web can vary in the frequency and amplitude components. Given the wide range of possible variation in real animals, instead of running a single idealised model, I developed an ensemble of models where these parameters are varied independently of each other. To achieve this, I incorporated variation in each of these parameters and ran each spider model 200 times. This generates a range of predicted outcomes, and if I have a reasonable model and have incorporated all the possible sources of variation, I expect that all real animals will fit within this distribution of predictions. I found that it was necessary to include all these sources of variation to generate a distribution of model outputs that encompassed the variation in the data from real animals.

3.2.5.1 Variation in abdomen volume: The volume of a spider's abdomen varies based on the size of its last meal and how recent the meal was. A spider that has recently eaten a large meal will have a larger abdominal volume than a starved spider (Blackledge and Zevenbergen, 2007; Johnson et al., 2011). The reported range of masses for *L. hesperus* is from 122 – 515 mg (Johnson et al., 2011). Assuming the abdomen contributes the most to the female's mass, I calculated the range of abdomen dimensions using equation (3.2) and (3.3) (Appendix 6).

$$V = \frac{m}{d}$$

(3.2)

$$V = \frac{4}{3} \cdot \pi \cdot (xyz)$$

(3.3)

Where  $V$  is the volume of the ellipsoid abdomen ( $m^3$ ),  $m$  is the mass (kg),  $d$  is the density ( $kg/m^3$ , assumed to be  $1060 kg/m^3$  (Vincent and Wegst, 2004)), and  $x$ ,  $y$  and  $z$  are the radii of the abdomen (m). From this range, I used a random number generator (Matlab function *rand*) to choose a single value for the  $x$  and  $y$  dimensions from a uniform distribution. A different value for the  $z$  dimension was chosen so that it was greater than the  $x$  and  $y$  dimensions and the ellipsoid shape was conserved. The ranges of these parameters are given in Appendix 6. This gave me a mass range of 118 – 503 mg for *L. hesperus* (Fig. 3.6A).

For *A. diadematus* and *P. phalangioides*, I assumed the average mass of my measured individuals was a typical individual's mass. However, all my sample animals were fed weekly and would not show natural variation. I determined the mass range for *A. diadematus* and *P. phalangioides* using the percent variation in body mass reported from *L. hesperus* and determined the  $x$ ,  $y$  and  $z$  radii ranges using equations (3.2) and (3.3). This gave me a mass range of 261 – 421 mg for *A. diadematus* and 3.4 – 17.4 mg for *P. phalangioides*. The ranges of the three radii are given in Appendix 6.

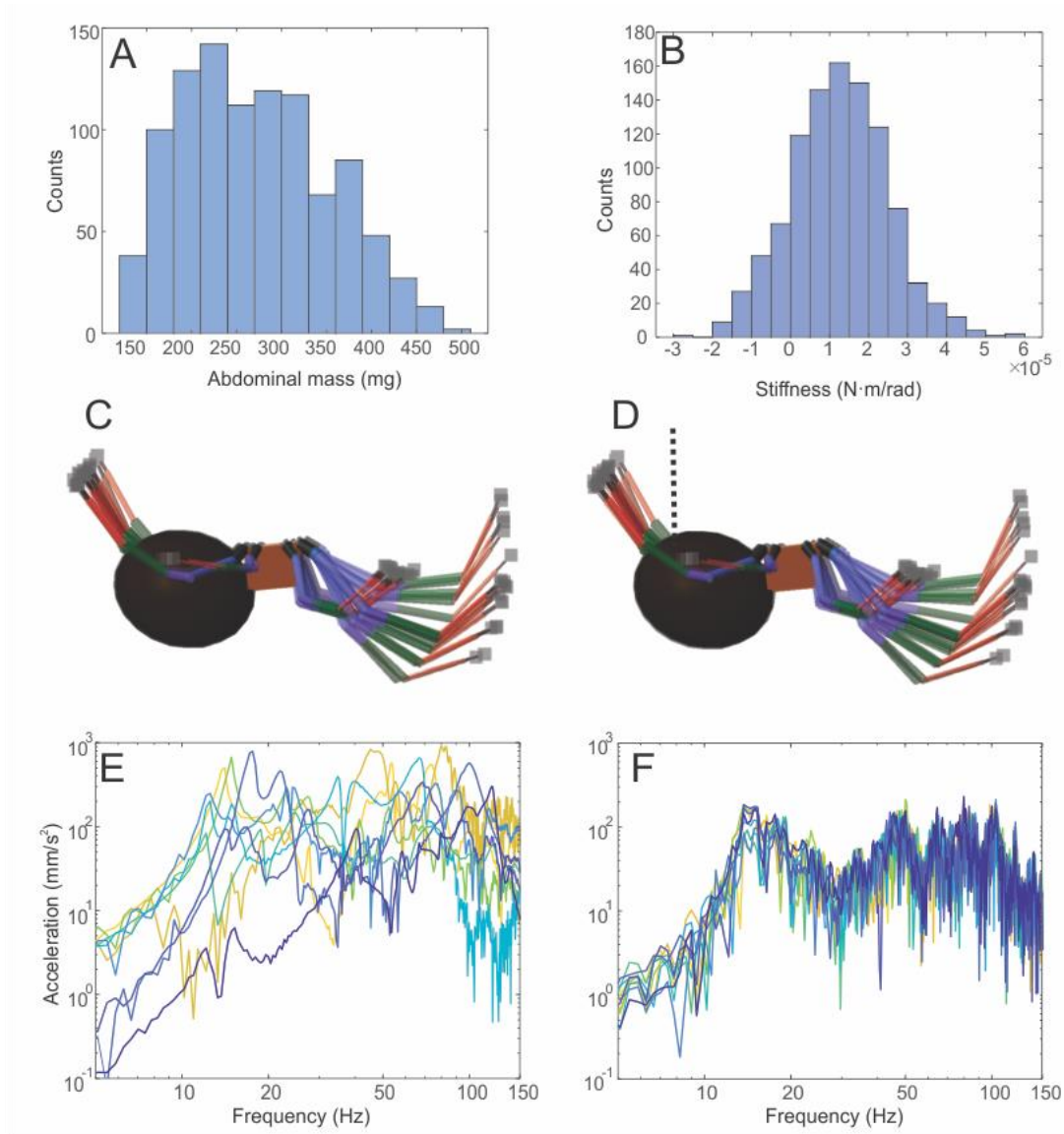


**Figure 3.6** Model parameter variation, using *L. hesperus* as an example. The process was identical for the other two modeled species. (A) The distribution of abdominal mass (mg) to capture variation in spider mass. (B) I chose joint stiffness parameter values from  $2.5 \times 10^{-7} - 6 \times 10^{-5}$  N·m/rad based on the species-specific joint stiffness distribution measured in Chapter Two. (C) The posture and whether the abdomen was connected to the web by a strand of silk (D) was also varied for each model run. (E) To generate forces for the models, I started with the spectra of the acceleration of the tarsus ( $\text{mm/s}^2$ ) from empirical measurements of eight animals. I used these measurements to make acceleration traces which were used to vary the acceleration applied to the tarsus in each model run. Each line is the acceleration of the tarsus from one

animal. (F) A sample of ten generated acceleration spectra which reflect peaks at similar frequencies as the original acceleration spectra. For each species, I generated 200 acceleration traces and used one for each model run.

3.2.5.2 *Variation in joint stiffness*: I varied the joint stiffness parameter value using data from Chapter Two. For each run, the stiffness parameter value was chosen using a random number generator (Matlab function *normrnd*) from a normal distribution defined by the mean and standard deviation of all measurements from the four joint types measured in Chapter Two (Fig. 3.6B and Appendix 6 for distribution parameters). As mentioned previously, I used the mean and standard deviation of the *L. venusta* data for the *P. phalangioides* model. I used the species-specific data measured in Chapter Two for *L. hesperus* and *A. diadematus*. I assigned each leg joint in the model the same stiffness value. I tested a model where these four joints were given stiffnesses from their specific joint stiffness distribution, and the other joints were given stiffnesses from the average joint stiffness distribution across all four of these joints. I found that this did not significantly alter predicted outcomes suggesting that if the stiffness values were in the overall range for this spider, the specific value of joint stiffness did not significantly alter the prediction distribution (Appendix 8).

3.2.5.3 *Variation in posture*: To generate small variations in posture, I varied the leg tip placement by generating a number within a defined range using a random number generator and adding it to the original distance between the leg tip and the cephalothorax. The range was defined by changing the distribution parameters until visually realistic changes in model

posture were achieved (Appendix 7). The original distance was determined from the spider at rest (see Appendix 7). These differences can be observed in the model geometry (Fig. 3.6C).

**3.2.5.4 Variation in web connection:** Spiders can occasionally connect their abdomen to the web via a strand of silk from their spinnerets (Fig. 3.6D). To incorporate the impact of this connection on the abdomen movement when vibrated, I made another model of each species with the web connection present. Similar to the leg-web connections, I used a prismatic joint with the same silk stiffness parameter (0.3 N/m) to model the abdomen-web connection. I ran the models with and without the web connection 100 consecutive times each. Each model run included the parameter variations discussed previously. I concatenated the two datasets to form one large dataset which therefore consists of 200 runs for each species.

**3.2.5.5 Variation in applied force:** At the beginning of the model run, the spider model settles into a stable position where the forces on the bodies are equilibrated. The equilibrium position is influenced by the spider posture, the force of gravity acting on each rigid body, and the joint mechanics. Only after reaching equilibrium is the force administered to the leg tips, causing the modeled spider to vibrate. Each model run is carried out for six seconds, at which point all evoked vibrations have been dissipated.

The stimulation applied is effectively a downward, broadband acceleration applied to the tarsus of each leg (Fig. 3.6E and F). Instead of energy being concentrated in a particular frequency band, the broadband signal I use contains a wide range of frequencies which were based on those experienced by real spiders and allowed me to stimulate the model in the most realistic way possible. I generated acceleration signals to mimic those observed in the empirical

vibrometry measurements (Appendix 9; see section 3.2.2 for details of the vibrometry method). A new signal was generated for each model run of each species (Fig 3.6E and F).

### 3.2.6 Comparing model output to empirical measurements

3.2.6.1 Model-predicted modes of vibration: The ability of each species' model to predict mechanical filtering was assessed by comparing the modes of vibration predicted by the model to those observed in the empirical data (see section 3.2.3). The predicted modes of vibration were identified using the same method as the empirical data described above (section 3.2.3.2). As with the empirical data, the mode frequencies where the velocity amplitudes were greatest were chosen if the same patterns of movement were seen at several frequencies. To determine the variation in frequency of each mode, I ran the models sixteen times with all parameter variations (eight times with the web-abdominal connection and eight times without the connection) and repeated the mode identification process. I compared the modal frequencies predicted by the model and those empirically observed using two-sample *t*-tests.

3.2.6.2 Vibration transmission through the leg: The second way I quantified mechanical filtering was by assessing how vibrations are transmitted through a single spider leg. To compare model predictions to empirical data, I computed the transfer function at each segment along the leg for each of the 200 model simulations. I generated probability density heatmaps using these transfer function spectra from the 200 model simulations. To generate this heatmap, I calculated the probability density function (pdf) of the velocity amplitudes of the 200 run model data at each frequency and at each leg segment. To estimate this pdf, I fit a Kernel distribution to the segment amplitudes using the Matlab functions *fitdist* and *pdf*. I chose a Kernel distribution because the model output exhibited a bimodal shape due to the differences in the

web-connection. I concatenated the pdfs at each frequency into 2D matrices for each leg segment. I generated a 2D heatmap of the probability densities at each frequency for each leg segment with the colour of the heatmap indicating the value of the pdf. I overlaid the empirical data on each heatmap in white for visual contrast (Appendix 10).

To quantitatively assess the model fit to the empirical data, I calculated the 1<sup>st</sup> and 99<sup>th</sup> percentile of the amplitudes predicted by the 200 model runs at each frequency using the Matlab function *prctile* for each leg segment. To quantify the model fit, I calculated what percentage of the empirical data lay within the 1<sup>st</sup> and 99<sup>th</sup> percentiles at each frequency from 10-150 Hz for each segment. I chose an upper limit of 150 Hz for all species (Fig. 3.7) because in cobwebs (*L. hesperus*) and orb webs (*Nuctenea sclopetaria*, *Nephila clavipes*, and *Cyclosa turbinata*) the frequencies of vibrations in the web typically decay to a very low level above 100 Hz (Landolfa and Barth, 1996; Masters, 1984a; Suter, 1978; Vibert et al., 2014). I chose a frequency that is 50 Hz higher so that I could observe whether this decay was also present within the body mechanics.

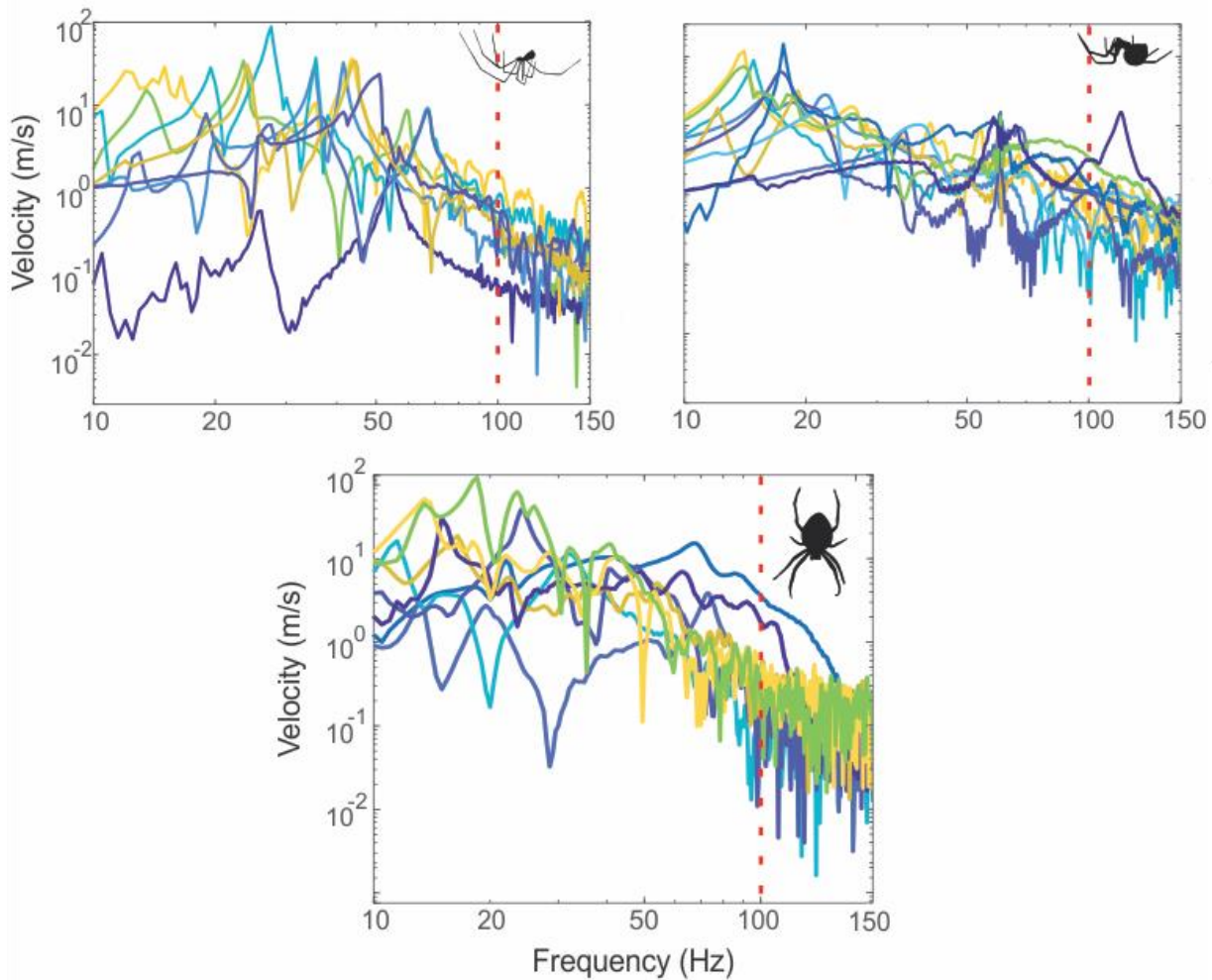


**Figure 3.7** Frequency range cutoff for model and empirical data comparison based on the empirical data. Species identity is shown with silhouettes. Each line colour indicates the vibration velocity spectrum of the magnet measured with the LDV for one trial. I chose an upper limit of 150 Hz for all species. Vibrations in the web typically decay to a very low level above 100 Hz, indicated in red. I chose a limit 50 Hz above to observe if this decay is present in the spider's mechanics.

### 3.3 Results

#### 3.3.1 Empirically measured modes differed with spider orientation

For both horizontally oriented spiders, *L. hesperus* and *P. phalangioides*, I found two modes of vibration in the empirical vibrometry measurements (Figs. 3.8 and 3.9, see Appendix

11 and 12 for data from all individuals). In the first mode, the abdomen moved at a higher amplitude than the leg tips (abdomen mode). In the second mode, the leg tips moved at a higher amplitude than the abdomen (leg mode). For both species, the leg mode occurred at a higher frequency than the abdomen mode. This is consistent with what has previously been observed in *L. hesperus* (Mhatre et al., 2018). For *L. hesperus*, the abdomen mode occurred at  $14.6 \pm 5.0$  Hz and the leg mode occurred at  $47.2 \pm 8.6$  Hz ( $n=8$ , mean  $\pm$  SD). For *P. phalangioides*, the abdomen mode occurred at  $13.0 \pm 1.3$  Hz and the leg mode occurred at  $57.7 \pm 25.4$  Hz ( $n=8$ , mean  $\pm$  SD).

As mentioned previously, in simple systems, resonant frequency decreases with increasing mass (Rossing and Fletcher, 1995). Therefore, it is not unexpected that the abdomen mode occurred at a lower frequency than the leg mode. What is unexpected is that the modes occur at similar frequencies in *L. hesperus* and *P. phalangioides* ( $t_8 = 0.82$ ,  $P_{abd} = 0.43$ ;  $t_9 = -1.03$ ,  $P_{leg} = 0.32$ ) despite *P. phalangioides* having a much lower mass (10 mg compared to 330 mg for *L. hesperus*). Thus, based on spider mass, one would initially expect that the modes of vibration of *P. phalangioides* would occur at higher frequencies in comparison to *L. hesperus*.

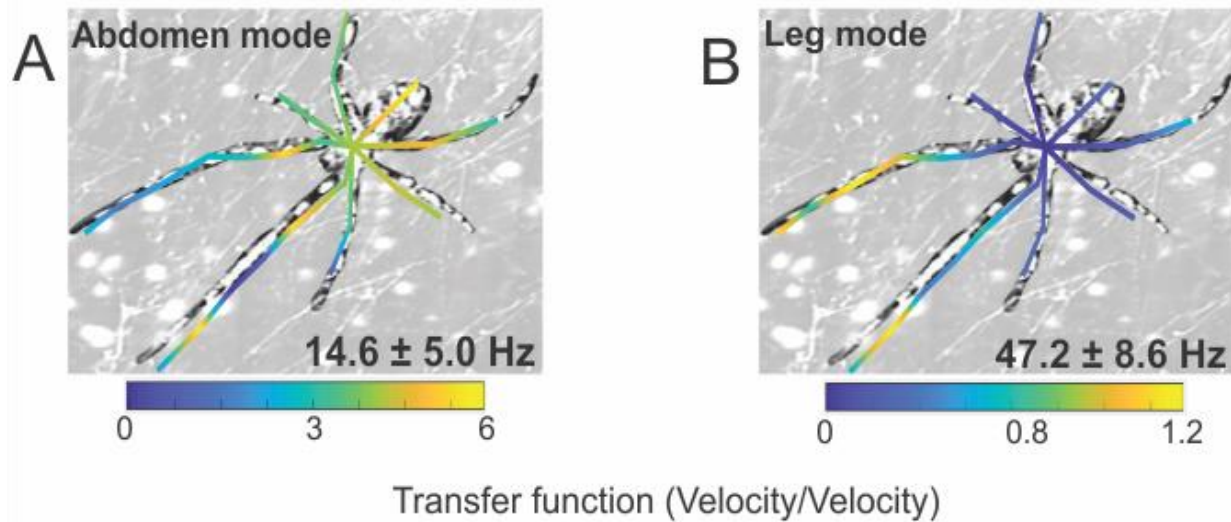


**Figure 3.8** Two modes of vibration were observed from the vibrometry measurements of *L. hesperus* ( $n = 8$ , see Appendix 11 for data from all individuals). (A) In the first mode (abdomen mode), the abdomen moved more and the legs were relatively motionless. (B) In the second mode (leg mode), the legs exhibited high amplitude movement, and the abdomen was relatively motionless. The mean and standard deviation of the frequencies at which the modes occurred are indicated. The lines overlaid on the spider photo indicate the pattern of movement of the spider body at the modal frequency. The line colour indicates the magnitude of the body's motion, as shown by the colour bar. The background is made partially transparent to make the spider more visible. Please note that the locations of the line may not correspond to the silhouette perfectly due to parallax depending on the sample depth, i.e., the variation in the actual height within the spider body. To correct for different depths within the sample, the position of the laser coordinates on the 2D projection do not fully correspond to the silhouette.

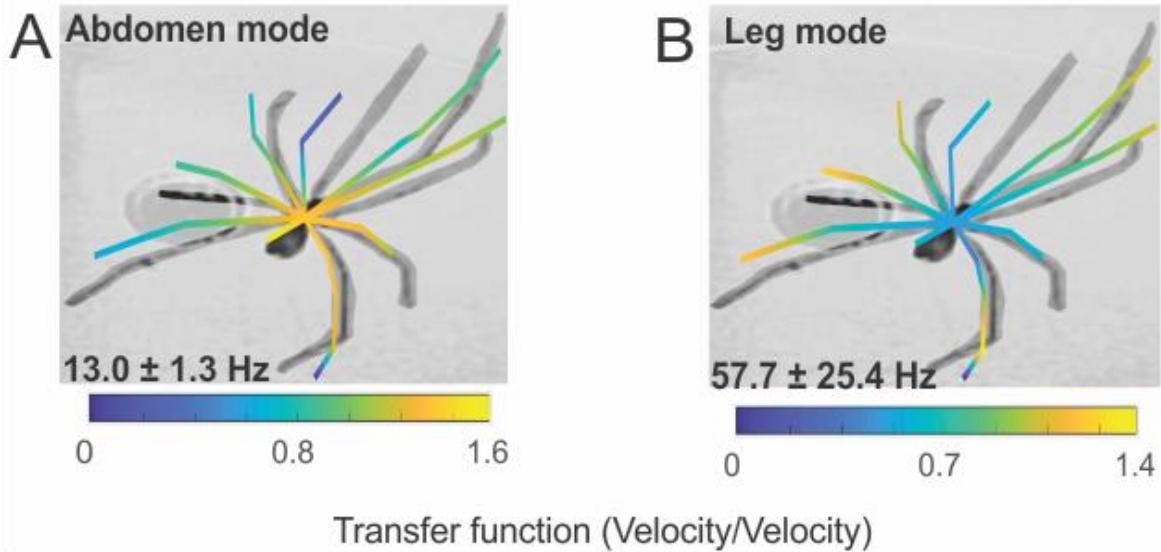


**Figure 3.9** Two modes of vibration were observed from the vibrometry measurements of *P. phalangioides* ( $n = 8$ , see Appendix 12 for data from all individuals). (A) Similar to *L. hesperus*, the first mode is the abdomen mode, and the second (B) is the leg mode. The mean and standard deviation of the frequencies at which the modes occurred are indicated. The lines overlaid on the spider photo indicate the pattern of movement of the spider body at the mode frequency. The line colour indicates the magnitude of the body's motion, as shown by the colour bar. The background is made partially transparent to make the spider more visible.

For the vertically oriented spider *A. diadematus*, I found only a leg mode (Fig. 3.10, see Appendix 13 for data from all individuals). The leg mode occurred at  $32.4 \pm 9.0$  Hz ( $n=8$ , mean  $\pm$  SD). In only two of eight individuals, did I find a mode that resembled the abdomen mode that I observed in the other two species (Appendix 13). Differences in the modes of the three species may be due to differences in orientation and is discussed in section 3.4.1.

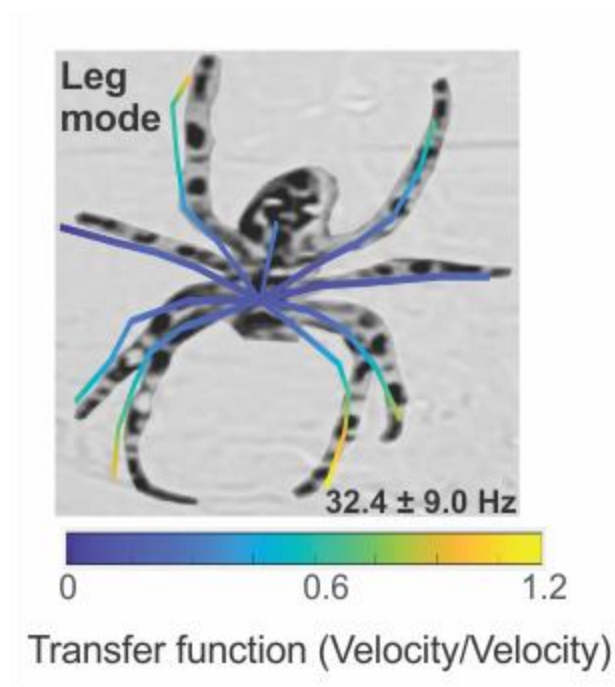


**Figure 3.10** One mode of vibration was observed from the vibrometry measurements of *A. diadematus* ( $n = 8$ , see Appendix 13 for data from all individuals). Only the leg mode was found in most individuals, where the legs exhibited high amplitude motion and the abdomen was relatively motionless. The mean and standard deviation of the frequency at which the mode occurred is indicated. The lines overlaid on the spider photo indicate the pattern of movement of the spider body at the mode frequency. The line colour indicates the magnitude of the body's motion as shown by the colourbar. The background is made partially transparent for contrast against the spider image.

### 3.3.2 Models predict similar modes of vibration

The multi-body models of each species predicted the same mode shapes in each species and at the same frequencies in *L. hesperus* and *P. phalangioides* as those empirically observed. For *L. hesperus*, the same two modes of vibration were found in the model; the abdomen mode (Fig. 3.11A and B) and the leg mode (Fig. 3.11C and D). The modes predicted by the 16 model runs occurred at similar frequencies to those empirically observed ( $t_9 = 0.71$   $P_{abd} = 0.49$ ;  $t_{10} = 0.2$ ,  $P_{leg} = 0.84$ ). For *P. phalangioides*, the abdomen mode (Fig. 3.12A and B) and the leg mode

(Fig. 3.12C and D) were also predicted by the model. The predicted modes also occurred at similar frequencies to those empirically observed ( $t_{11} = 2.1$ ,  $P_{abd} = 0.06$ ;  $t_9 = 1.1$ ;  $P_{leg} = 0.26$ ).

The models also showed similar levels of variation in the predicted modal frequencies to those observed in empirical data (Fig. 3.11E and F, Fig. 3.12E and F). The multiple model runs predicted similar variation in the predicted abdomen mode frequencies of both species (Fig. 3.11F for *L. hesperus* and Fig. 3.12F for *P. phalangioides*), but less so in the leg mode of *P. phalangioides* (Fig. 3.12F). Interestingly, when the web connection was present, the abdomen mode was not observed in the *P. phalangioides* model. In the empirical data, the abdomen mode of F11 was less clear in comparison to other individuals (Appendix 12). It is possible that the abdomen was connected to the web via a strand of silk during the trial and thus, reduced the presence of the abdomen mode. The influence of the web connection on the presence of the abdomen mode may be greater in *P. phalangioides* than *L. hesperus* due to their differences in mass.

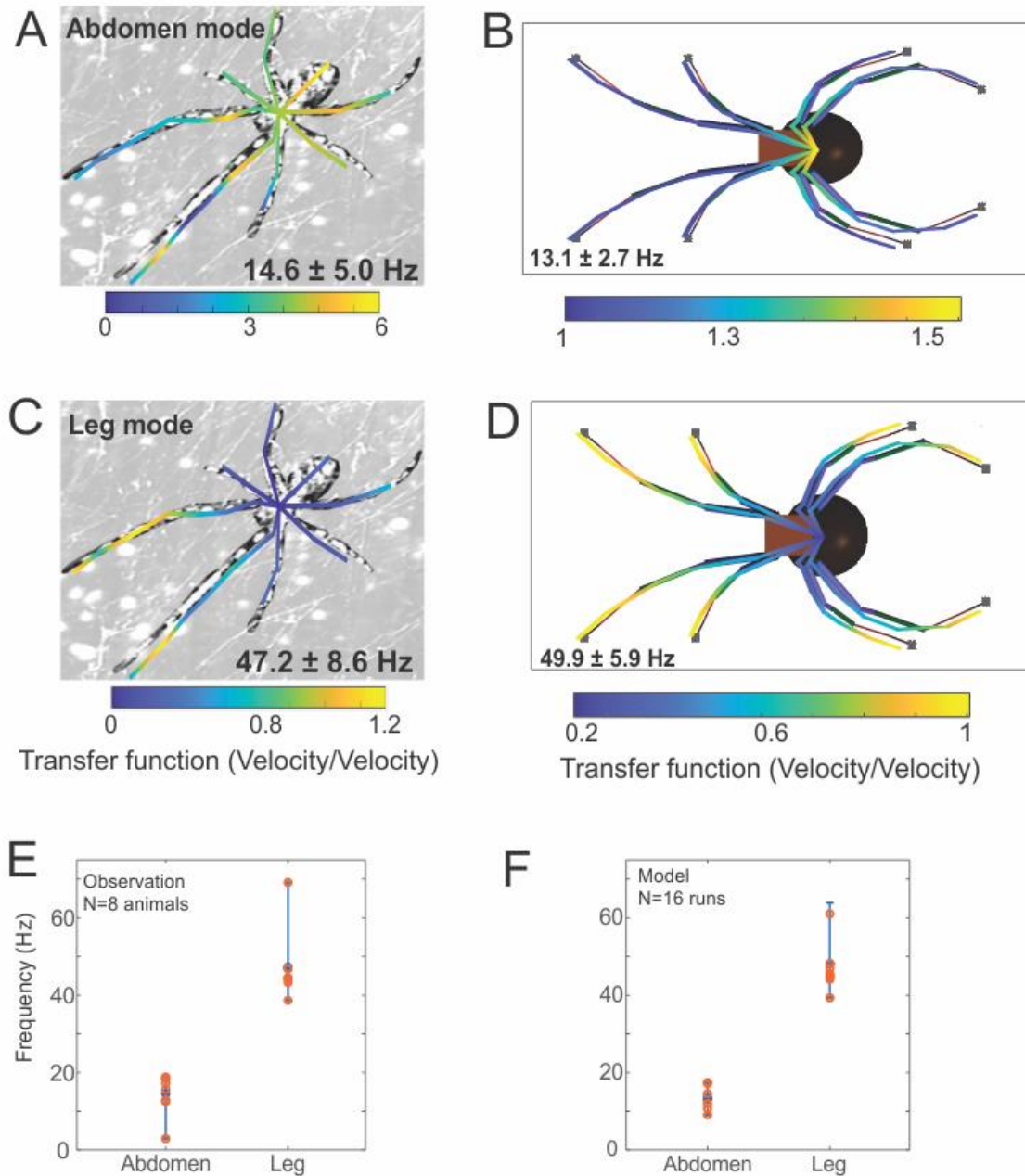


**Figure 3.11** The *L. hesperus* model predicted the same modes of vibration at similar frequencies to empirically observed modes. (A and B) In the first mode, the abdomen moved at a high amplitude and the legs were relatively motionless. (C and D) In the second mode, this relationship was reversed. In each mode shape plot, the lines indicate the pattern of the body movement, and the colour indicates the magnitude of the motion as per the scale bar. (E and F) Varying the joint stiffness parameter, the abdomen size, the posture and the presence of the

abdomen-web connection in the model created similar levels of variation in the mode frequencies to what is empirically observed. Orange points indicate the mode frequencies observed from the empirical data or the output of the multiple model runs, and the blue bars show the range of modal frequencies. (n=8 observations, n=16 model runs).

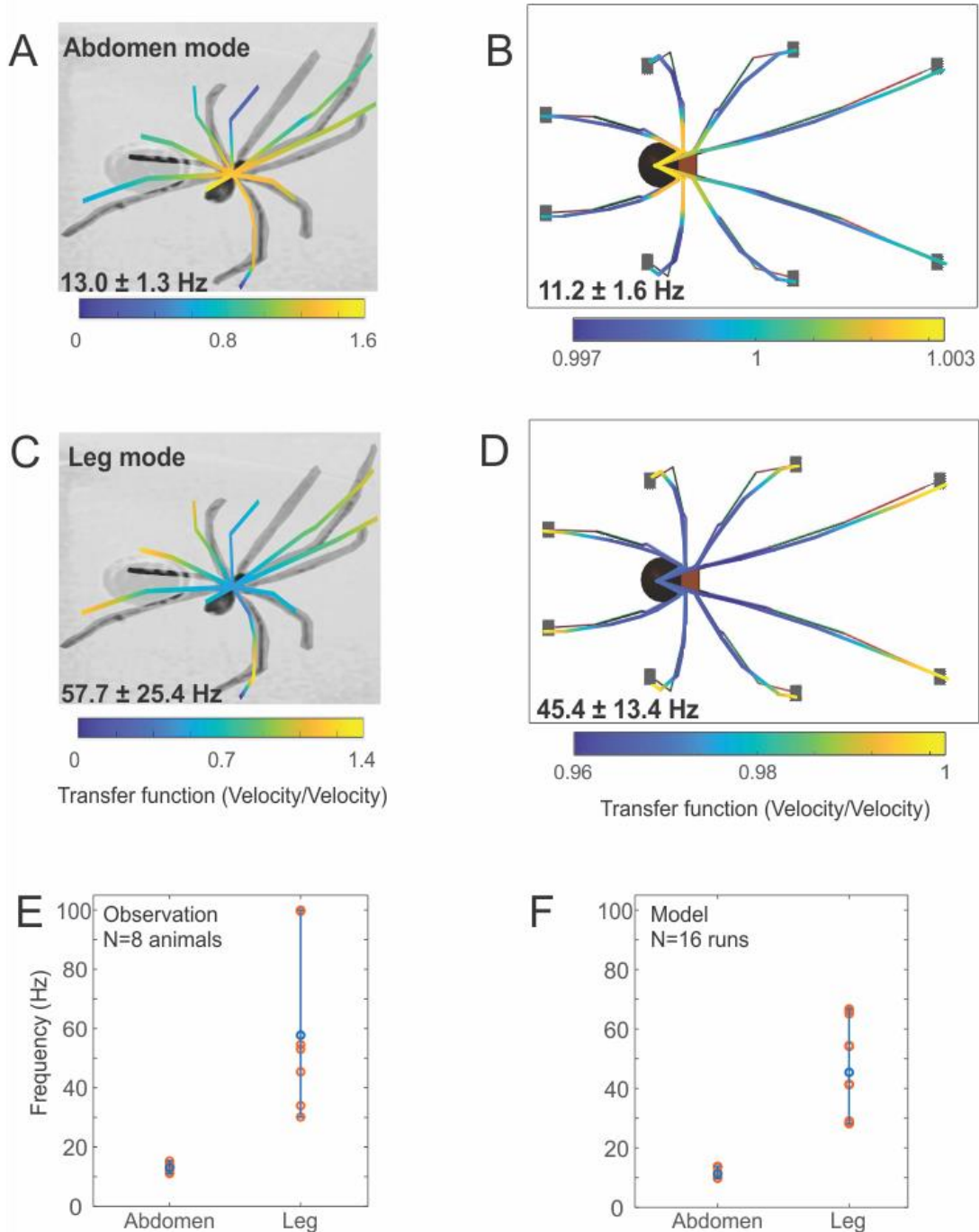


**Figure 3.12** The *P. phalangioides* model predicted the same modes of vibration at similar frequencies to those observed in real animals. (A and B) show the abdomen mode and (B and C) show the leg mode. Similar to the *L. hesperus* plots, the lines indicate the pattern of the body motion and the colour indicates the magnitude of the segment motion relative to the leg tips. (E and F) Varying the model parameters created a similar level of variation in the abdomen

mode frequencies to what is empirically observed. Variation in the leg mode frequency is likely due to variation in leg posture or perhaps joint stiffness between measured individuals. Orange points indicate the mode frequencies observed from the empirical data or the output of the multiple model runs, and the blue bars show the range of modal frequencies. The leg mode in the model has lower frequency variation. However, the model does capture the fact that there is more frequency variation in the leg mode than in the abdomen mode. (n=8 observations, n=16 model runs).

Similar to the empirical measurements, the *A. diadematus* model only predicted the presence of the leg mode (Fig 3.13A and B). However, the model predicted the leg mode to occur at lower frequencies than what was empirically observed ( $t_7 = 3.0$ ,  $P_{leg} = 0.01$ ). The model predicted that the most proximal segment, the coxa, was relatively motionless in the leg mode, as indicated by the purple lines. In the mode observed empirically, the vibrations were transmitted further through the leg, indicated by the increased amplitude motion of the femur and coxa. Data from the 16 model runs predicted lower variation in the modal frequencies compared to that observed (Fig 3.13D).

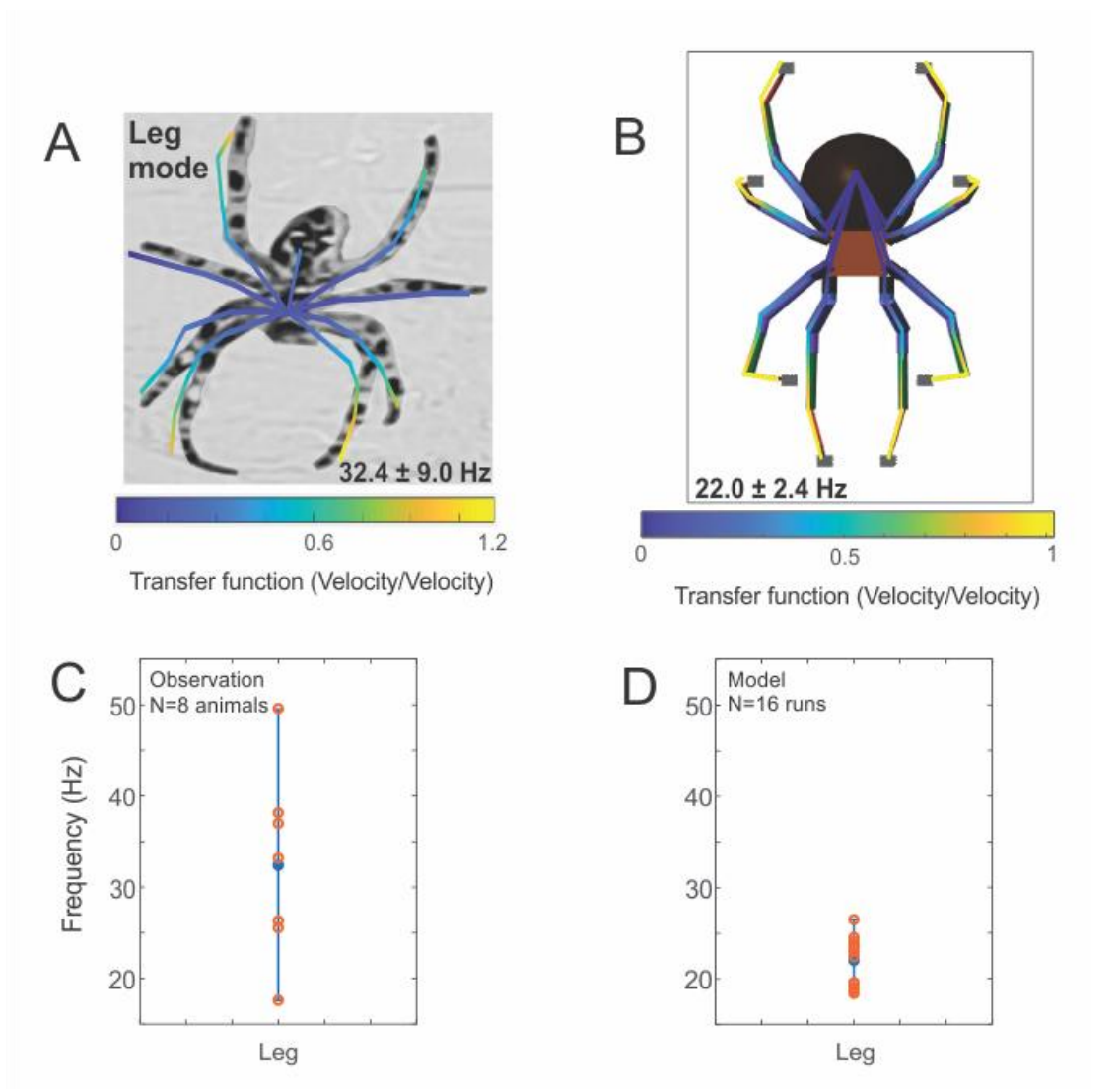


**Figure 3.13** The modeled and empirically observed mode of vibration in *A. diadematus*. (A and B) Similar to the empirical measurements, the model only predicted the leg mode. In each mode shape plot, the lines indicate the pattern of the body's movement and the colourbar indicates the magnitude of the movement. (C and D) Orange points indicate the modal frequencies observed from the empirical data or the output of the multiple model runs, and the blue bars show the range of modal frequencies. Varying the joint stiffness parameter, the abdomen size, the posture, and the presence of the abdomen-web connection created some variation in the modal frequency predicted by the model. More variation was seen in the empirical measurements as indicated by the wider range in frequency.

### 3.3.3 Model predictions of vibration transmission through a single leg

The predictions of the multi-body models of *L. hesperus* and *P. phalangioides* were reasonably successful at capturing the observed vibration transmission through a single leg. The model of *A. diadematus* did not successfully capture the empirical data. I assessed the ability of each model to predict vibration transmission through a single leg by asking whether the empirical data fell within the range of possible outcomes predicted by the 200 model runs which accounted for natural variation in model parameters. For each species, each heatmap shows data for a single leg segment of the front leg and captures the probability density of all possible velocity transfer functions as predicted by 200 model runs (Figs. 3.14, 3.15 and 3.16). In each heatmap, the transfer functions measured from real animals are overlaid in white, showing where they lie relative to model predictions. Red lines indicate the 1<sup>st</sup> and 99<sup>th</sup> percentiles of the distributions predicted by 200 model transfer functions.

It must be noted that the heatmaps show probability density, which is a different measure than probability, and hence the heatmap data can exceed one. For continuous variables, the probability is calculated by the area under the probability density function (Evans and Rosenthal, 2010). Therefore, the area under the probability density function must integrate to one, however, the values of the probability density function itself can be greater than one. Probability density indicates how dense the probability of the occurrence of the empirical data is based on the model output. A higher probability density means the model predicts that more of the empirical data will occur at a particular magnitude near a particular frequency.

Importantly, if more of the empirical data from real animals is found in areas of high probability density, it suggests that the model is well parametrized and captures the natural

range of vibration transmission through the single leg. As mentioned previously, I quantified the model fit to the empirical data by calculating the percentage of empirical data between the 1<sup>st</sup> and 99<sup>th</sup> percentiles at each frequency. I considered a fit of 70% or higher to be a good model fit, indicated by the red-dashed line in the model fit plots for each species (Figure 3.14, 3.15 and 3.16 Model fit subplots).

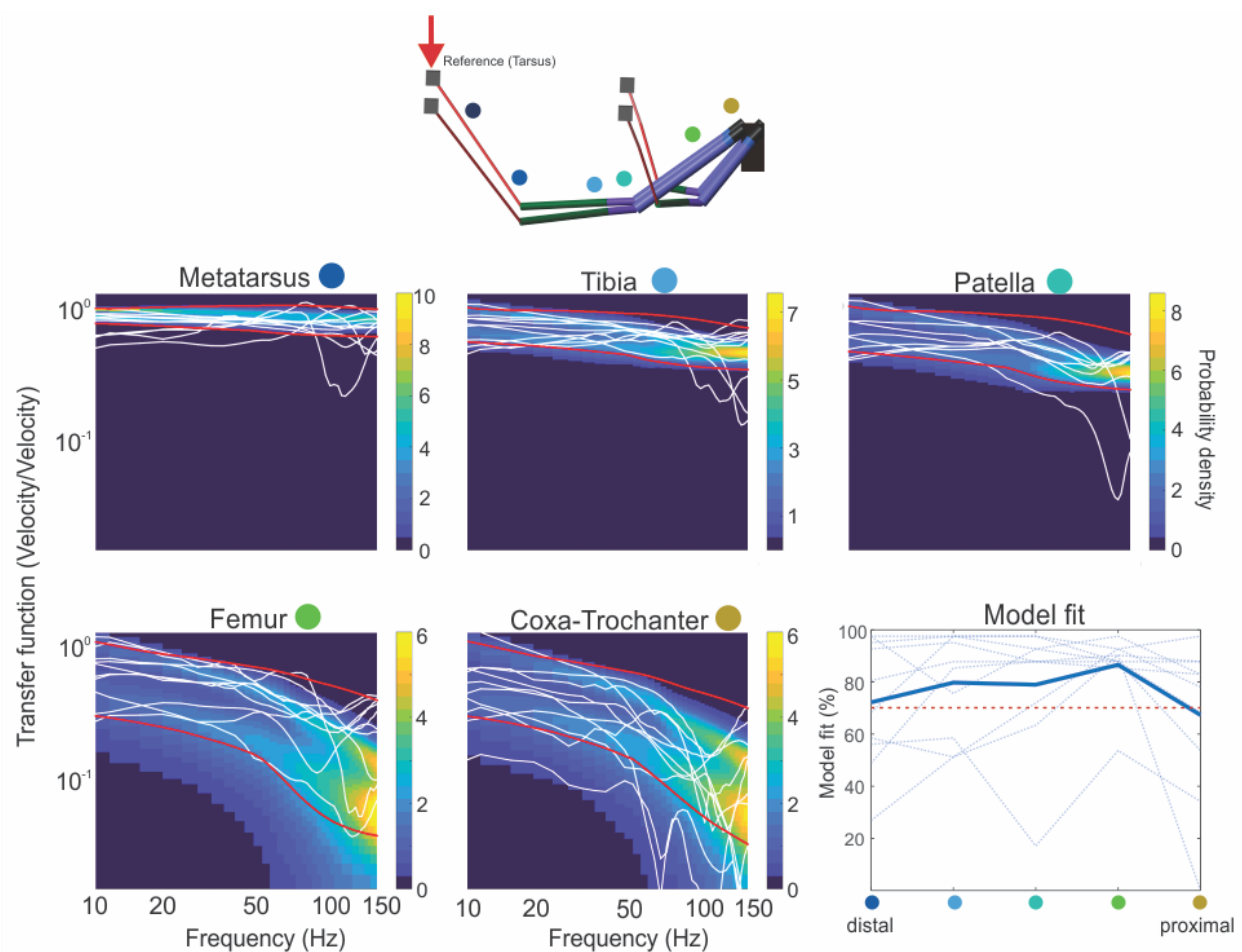


**Figure 3.14** Probability density heatmaps of *L. hesperus* model predictions of vibration transmission in a single leg with overlaid data from real animals. I ran the model 200 times varying the joint stiffness, the posture, the abdomen size, the force applied, and the web-abdomen connection. Each heatmap shows data for the vibration of a single leg segment of the

front leg and captures the probability density of all possible velocity transfer functions as predicted by multiple model runs. The probability density was calculated from the 200 model transfer functions against the tarsus and indicates how dense the probability of the occurrence of the empirical data is based on the model output. A colourbar maps the colour to the corresponding probability density. The red lines indicate the 1<sup>st</sup> and 99<sup>th</sup> percentiles of the amplitudes predicted by the model transfer functions at each frequency. The white lines represent empirical measurements from *L. hesperus* (n=8). The model fit plot indicates what percentage of the empirical measurements lie within the 1<sup>st</sup> and 99<sup>th</sup> percentile lines. The blue-dotted lines indicate the fit for each individual, showing the variability in measurement quality. The red-dashed line indicates the 70% threshold used to assess model fit. The identity of leg segments are indicated in each plot by coloured circles.

In the heatmaps based on model predictions for *L. hesperus*, I observed a decrease in the vibration transmission in frequencies above about 75 Hz in the femur and coxa-trochanter, i.e., motion of the segments decreased in the proximal segments (Fig. 3.14). The same trend was also seen in the empirical data from real animals which are overlaid on the model data. Overall, I observed that most of the empirical data lie within regions of high probability density. In a few cases, a few traces lay outside this zone, particularly in the coxa and metatarsus segments.

I assessed the model's ability to predict vibration transmission quantitatively by calculating model fit as a percentage of the empirical transfer functions within the 98-percentile zone (Fig. 3.14 Model fit plot). For all segments, the *L. hesperus* model fit was higher than 70%. For frequencies between 75-150 Hz, model fit declined significantly as shown by more of the empirical data being outside the 98 percentile zone. This decline in fit was driven by about

three measurements, in a frequency range where the amplitude of the force, i.e., the magnet's acceleration, has declined significantly. There is considerable individual variation in the model fit, particularly in the metatarsus, patella and coxa-trochanter. This variation may be real and not captured by my model or it may be due to measurement quality. Measurement quality is affected by how well the laser is reflected and also by whether the reflection is truly from the animal rather than from the web. Indeed, model fit was highest in the tibia and femur and less variation is seen in the femur. The tibia and femur are larger segments that are held more perpendicular to the laser and therefore likely have the best quality measurements due to better laser reflection.

The probability density heatmaps comparing the predicted vibration transmission to empirical measurements for *P. phalangioides* are shown in Fig. 3.15. The patella was not included in the *P. phalangioides* heatmaps because measurements of this leg segment were not feasible due to its small size in this species. Overall, most of the real data lies in areas of high probability density however, the model did not capture the decrease in transmission of frequencies above about 50 Hz seen in the empirical data of three individuals. The model predicted that the amplitude of the segment motion stays relatively constant across all frequencies in each leg segment, as indicated by the flat percentiles. The empirical data shows a decrease in the segment amplitude above 50 Hz in three individuals, starting in the tibia. In the coxa, all traces showed a decrease in vibration transmission above 50 Hz.

Similar to *L. hesperus*, the *P. phalangioides* multi-body model fit was highest in the lower frequencies (10-50 Hz) and decreased at higher frequencies (50-150 Hz) (Fig. 3.15). However, the model fit was poorer overall and did not exceed 70% in any leg segments.

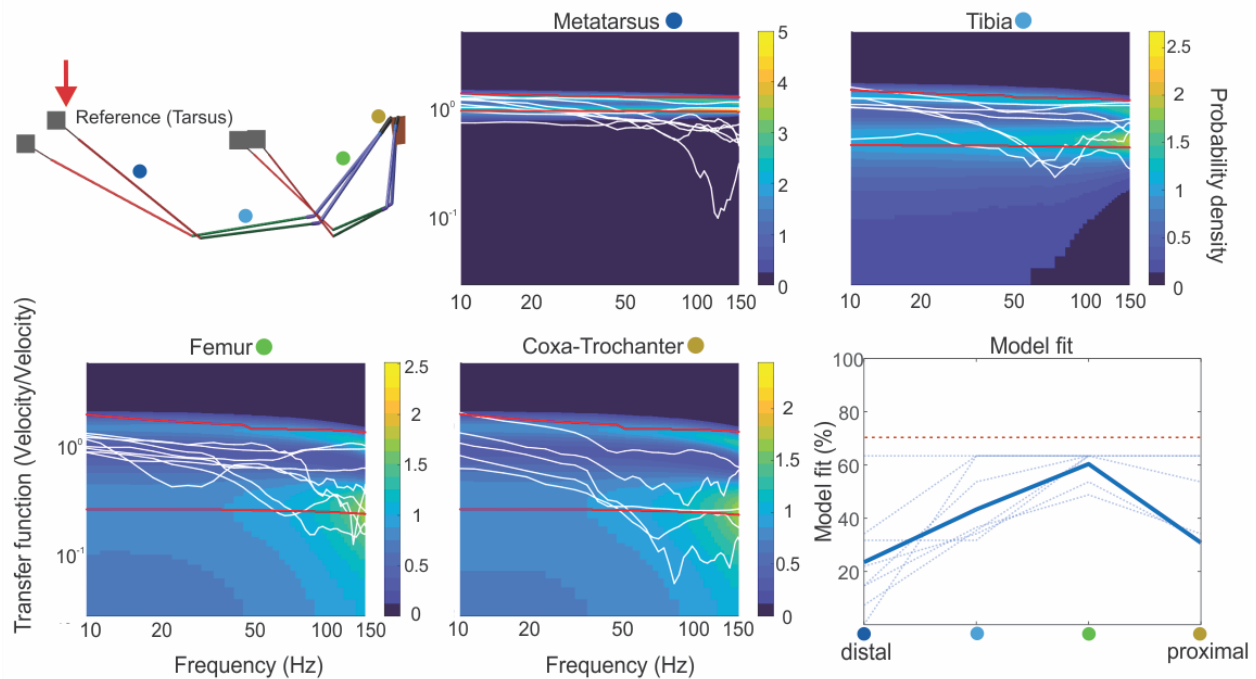


**Figure 3.15** Probability density heatmaps of *P. phalangioides* model predictions of vibration transmission in a single leg with overlaid data from real animals. I ran the model 200 times varying the joint stiffness, the posture, the abdomen size, the force applied and the web connection. Each heatmap shows the data for how vibrations transmit through a single leg segment from the front leg and captures the probability density of all possible velocity transfer functions predicted by the model. The colourbar maps the colour to the corresponding probability density. The red lines are the 1<sup>st</sup> and 99<sup>th</sup> percentiles of the model transfer functions, and the white lines are the empirical measurements (n=8). The model fit plot indicates what percentage of the empirical measurements lie within the 98-percentile for each segment. The blue-dotted lines indicate the fit for each individual, showing the variability in measurement quality. The red-dashed line indicates the 70% threshold used to assess model fit. The identity of the leg segments are indicated in each plot by coloured circles.

The probability density heatmaps comparing the predicted vibration transmission through a single leg to empirical measurements for *A. diadematus* are shown in Fig. 3.16. For

this species, the model fit is poorer and none of the empirical data is in the areas of the high probability density, except for the metatarsus of four individuals. For the metatarsus, the model fit for each individual never exceeded 70%.

The *A. diadematus* model captured the overall transmission levels in the metatarsus, tibia, and patella well, i.e., the model output and empirical data were both flat across all frequencies, indicating that most frequencies were transmitted through these segments. However, the model predicted that the amplitude of segment motion was much lower than what was empirically observed, and, in each segment, the amplitude of the motion progressively decreased as the vibration moved towards the coxa-trochanter. For the coxa-trochanter and femur, the predicted amplitude of the segment motion was at least an order of magnitude lower than what was measured from the real animals. In the femur and coxa-trochanter, the model predicted that higher frequencies above about 50 Hz were transmitted better than lower frequencies, indicated by the upward curve. The empirical data does not reflect this trend.

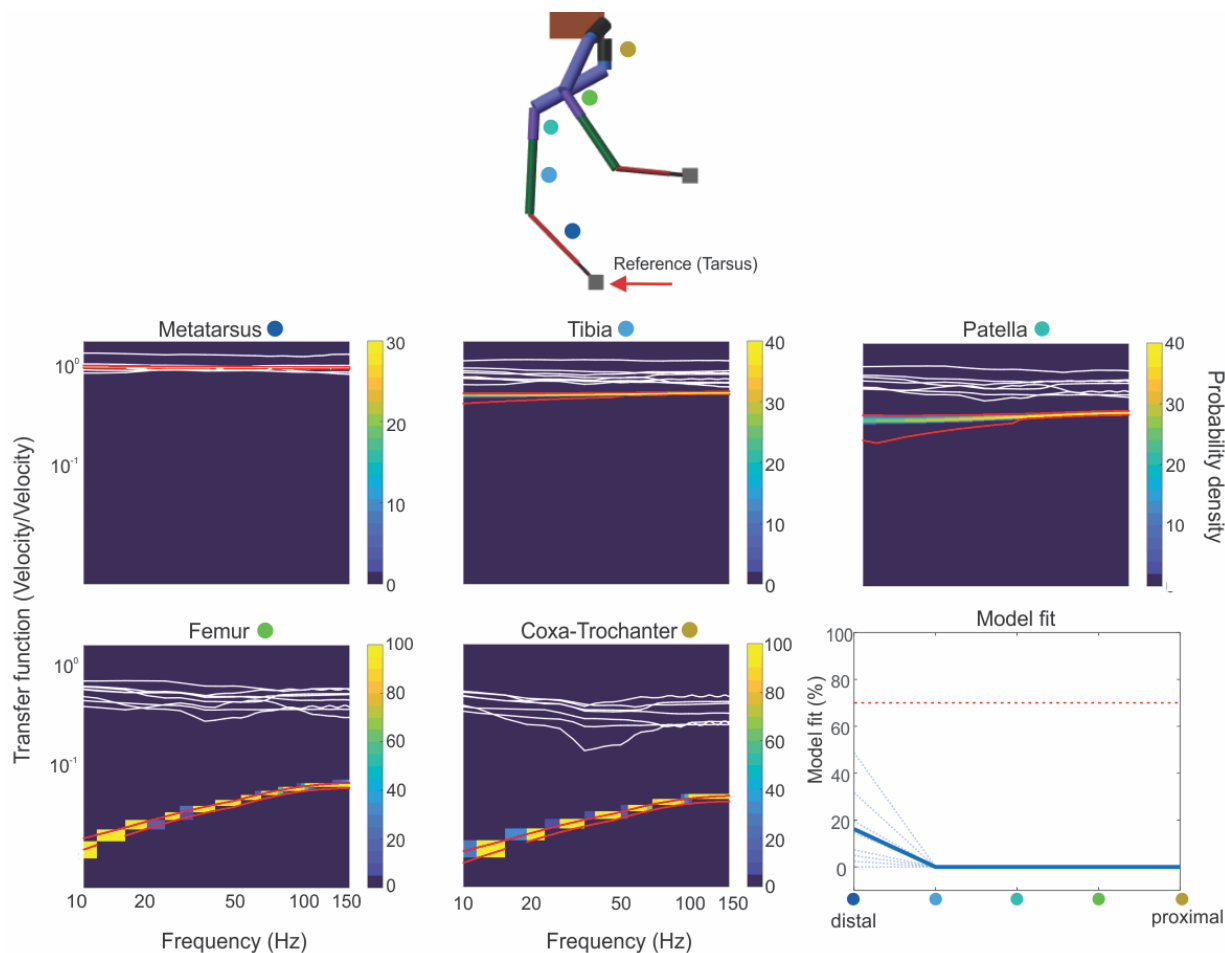


**Figure 3.16** Probability density heatmaps of *A. diadematus* model predictions of vibration transmission through a single leg with overlaid data from real animals. I ran the model 200 times varying the joint stiffness, the posture, the abdomen size, the force applied and the presence of the abdomen-web connection. Each heatmap shows data for vibration transmission through a single leg segment from the front leg and captures the probability density of all possible velocity transfer functions. The colourbar maps the corresponding probability density. The red lines are the 1<sup>st</sup> and 99<sup>th</sup> percentiles of the model transfer functions. The white lines are the empirical measurements (n=8). The model fit plot indicates what percentage of the empirical measurements lie within the 98-percentile lines. The blue-dotted lines indicate the fit for each individual, showing the variability in measurement quality. The red-dashed line indicates the 70% threshold used to assess model fit. The identity of the leg segments are indicated in each plot by coloured circles.

The 98-percentile range of the model output was very narrow in comparison to the other two modeled species. The narrow percentile range suggested that the model may not be well parameterized or variation in the model parameters during the 200 runs may not have captured the variation present in the empirical data. Increasing parameter variation in the model, however, would cause an unsolvable model, i.e., the model could not equilibrate likely due to an unnatural posture, the abdomen being too large or the stiffness being too low.

### 3.4 Discussion

My objectives in this chapter were to parameterize and improve the existing multi-body model of mechanical filtering in a spider's body using the data collected in Chapter Two and to test if this modeling approach could capture the natural variation observed across different individuals from a species. By incorporating variation in several model parameters, I successfully made an ensemble of multi-body models which could account for individuals in different postures, of abdomen sizes, and with different joint stiffnesses. This ensemble modeling technique successfully predicted the modes of vibration and vibration transmission in *L. hesperus*. In *P. phalangioides*, it was successful at predicting modes but was less so at predicting vibration transmission through the leg. The technique did not predict the mode frequency or vibration transmission in *A. diadematus*, which may be a failure of the modeling technique or the vibrometric measurements on a highly resonant and mobile orb-web.

#### 3.4.1 Possible reasons for the lack of congruency between the *Araneus diadematus* model and real data

I found that the vertically oriented spider *A. diadematus* only had the leg mode of vibration at 32.4 Hz. This is within the expected frequency range of prey vibrations (Barth et al.,

1988; Hergenröder and Barth, 1983; Landolfa and Barth, 1996; Masters, 1984a) and similar in frequency to the leg mode of *L. hesperus* and *P. phalangioides*. The model predicted the same leg mode at a lower frequency but could not capture the vibration transmission through a single leg. Therefore, the model appears partially correct but difficult to validate.

The lack of an abdomen mode in *A. diadematus* could be due to the vertical orientation of this species. Vibrations are often generated in the web in the x-direction (Fig. 3.1C), and the forces acting on the abdomen are likely quite low in magnitude because they have to transmit through the legs to reach the abdomen. The magnitude of the force of gravity in the z-direction is likely much greater than the web vibrations, which may further reduce the motion of the abdomen in the mode. Preliminary data predicts that *A. diadematus* in the horizontal orientation does have an abdomen mode (Gartly, 2021). Unlike my work in this chapter, this preliminary modeling did not incorporate the natural posture of the species or the parameter variations I did here. Future modeling could confirm this explanation and explore the extent of the impact that orientation may have on the modes of vibration. The abdomen mode is driven by bending in proximal leg joints and the abdomen-cephalothorax joint. Errors in joint stiffness parameters or in joint type assumptions in the model could strongly affect mode predictions. Future modeling could change the underlying model, for example changing the joint type to a Hill-type joint that has the spring and damper components in series and parallel to test if joint type impacts model predictions.

An interesting explanation for the lack of an abdomen mode may be this spider's web location. *A. diadematus* webs are generally found between trees and bushes, oriented to catch flying prey (Foelix, 2011). Due to their location, the orb webs may be subjected to more wind,

rain or anthropogenic noise (Tew and Hesselberg, 2017; Wu and Elias, 2014). In contrast, *L. hesperus* and *P. phalangioides* webs are found in crevices under rocks or branches (Bradley, 2013) and may be more protected from the elements. Additionally, cobwebs with their complicated three-dimensional structure with several connections in many directions are likely to dampen vibrations much more than highly resonant orb-webs which are built to dissipate energy through large amplitude movements (Challita et al., 2021; Sensenig et al., 2012; Sensenig et al., 2013). Vibrations due to environmental noise are typically 10 Hz and below (Barth et al., 1988; Masters, 1984a), which is relatively close to the abdomen frequency of *L. hesperus* and *P. phalangioides* and may make the webs of *A. diadematus* vibrate more. Perhaps *A. diadematus* lacks an abdomen mode to filter out environmental noise more effectively.

The *A. diadematus* model could not predict vibration transmission through a single leg as observed in empirical measurements (Fig. 3.16) which I believe may be due to the influence of the web. In Fig. 3.16, all segments in the leg appear to move at similar amplitudes which may suggest that the measured segment motion is actually the combined motion of the segment and the web, with the motion of the web dominating. Indeed, in the vibrometry measurements, the whole body of F1 and F6 appear to be moving at similar amplitudes which may be due to the high amplitude motion of the web (Appendix 13). Therefore, the transfer function analysis I used may be insufficient to minimize the effect of the web movement for this species. The web structure of *A. diadematus* is more two-dimensional in comparison to the cobwebs of *L. hesperus* and *P. phalangioides* and the *A. diadematus* web can move as a plane in response to airborne sound and vibrations (Challita et al., 2021; Sensenig et al., 2012; Zhou et

al., 2022). The web likely moves in a similar way in response to the vibrations generated in the web in this chapter.

In the model, I try to reduce the web to a single parameter which is the silk stiffness at each leg. This treatment of the web works for three-dimensional cobwebs that are prevented from having high amplitude movements by a dense network of silk strands but may not work for highly resonant orb webs. This may impact how the vibration is initially transmitted to the *A. diadematus* model legs and subsequently, the vibration that is transmitted through the body. Using a different model type or including the entire web structure in the model could improve these predictions for orb weaving spiders.

#### 3.4.2 Poorer model fit for *Pholcus phalangioides* compared to *Latrodectus hesperus*

The overall fit of the *P. phalangioides* model was poorer in comparison to *L. hesperus*. One reason for the poorer fit is poorer measurement quality of *P. phalangioides* than of *L. hesperus* (Fig. 3.15 Model fit subplot). Vibrometry measurement quality depends in part on how reflective the sample is. The fit was poorest for the coxa-trochanter and metatarsus segments which, due to the spider's posture, were often held at an angle to the laser during measurement. The laser may have been more dispersed on these segments and more poorly reflected. To contrast, the fit was higher in the femur and tibia which are held at a smaller angle and may have had better laser reflectance. The *P. phalangioides* legs are very small and thin and as a result, it was difficult to get a strong laser reflection off the legs. *L. hesperus* is almost entirely black however, reflectivity was improved by using white paint or retroreflective beads (Mhatre et al., 2018). Even with improved reflectivity, the quality of the *L. hesperus* empirical data varied greatly among individuals and between leg segments within an individual (Fig. 3.14

Model fit subplot). For *P. phalangioides*, the additional mass from adding paint or beads would likely alter the mechanics of the whole spider because the legs are very thin and light. Adding other materials to enhance reflectivity but not alter the leg mechanics, such as pieces of thin gold foil, may help improve the quality of future vibrometry measurements.

Another possibility is that the model does not capture some crucial mechanical feature which drives the vibrational behaviour of *P. phalangioides*. This species is an exceptionally small spider and represents an extreme morphology in terms of its very thin legs. Given their unusual size, it is possible that they violate the rigid body assumption and within segment bending may come into play. Some other possible changes to the model could be changing joint types to non-linear joints where the stiffness could vary during rotation or changing to Hill-model joints, which are often used to model muscle and have the spring and damper components in series and in parallel (Winters, 1990).

### 3.4.3 Assumptions and limitations: measuring spider mechanics

There are some limitations with the vibrometry measurements. One limitation is that it is impossible to make a stimulus which has a flat frequency spectrum, which would be preferable and is the norm in acoustic measurements (Erbe and Thomas, 2022). Due to uncontrolled differences in web structure, the applied stimulus evolves differently in each web (Eberhard, 2019; Nakata, 2012). However, this is a compromise that allows me to study and make inferences about freely suspended animals in naturalistic postures. An improvement could be to measure each species in an artificial web that is the same in each measurement which would result in a more stereotyped stimulus.

Another limitation with the vibrometry method is that the measurements itself takes about 15 – 20 minutes, depending on the number of scan points (e.g. 2 seconds x 10 averages per scan point x 50 scan points). During this time, despite the initial visual inspection the spider may move after the recording has begun or silk strands may move position due to the spider's weight shifting. To help reduce this limitation, I monitored the signal quality and measured the spiders in webs that had a relatively lower density of silk strands.

A final limitation is that only the motion in one of three possible axes can be measured. I measured from the ventral side of the spider and oriented the spider so that this axis had the greatest motion when vibrating, however possible movements in other directions were missed. One advantage of the multi-body models is the model can be tested on the available data but can then output the leg segment motion in any axis. It can also make predictions of joint bending that cannot be measured with this method. Therefore, we can make stronger predictions of lyriform organ stimulation using models that are validated by empirical data.

#### 3.4.4 Assumptions and limitations: modeling spider mechanics

As with all modeling, I made several assumptions and simplifications, many of which were made based on previous modeling work (Mhatre et al., 2018). The modeling in this chapter generates a distribution of possible outcomes and the effect of the modeling assumptions relating to parameter values, is mainly to change the width and shape of distributions in predicted outcomes, which are often complex and not unimodal.

3.4.4.1 Geometry assumptions: I based the shape approximations for all rigid bodies on previous work (Mhatre et al., 2018) and to reflect true spider anatomy as closely as possible. The true shape of a spider's segments may differ slightly because a spider's leg segments are

often tapered at the distal ends from the body and therefore are not a symmetric cylinder. However, the rigid body shape mainly contributes to its mass in this type of model. I took the difference in cross-section into account by using the average of three measures of segment diameter, therefore I believe that the shape approximations reflect the mass and its distribution over space well.

**3.4.4.2 Density assumptions:** In addition to the geometry approximations, I assumed the density of each rigid body was the density of insect cuticle (Mhatre et al., 2018; Vincent and Wegst, 2004). As mentioned previously (section 3.2.4.2), arthropod tissue lies between approximately 1060 and 1200 kg/m<sup>3</sup> (Vincent and Wegst, 2004) which is close to the density of most 'wet', non mineralized biological tissue (about 1000 kg/m<sup>3</sup>) (Wegst and Ashby, 2004). Small variations in density were also found to have a negligible effect on model output (Mhatre et al., 2018).

**3.4.4.3 Abdominal mass:** This parameter is effectively set by abdomen density and geometry which can be highly variable (Johnson et al., 2011). I assumed that the mass ranges for *A. diadematus* and *P. phalangioides* were equivalent to that of *L. hesperus*. These mass ranges created realistic changes in the abdomen size during model runs that I could visually assess. Therefore, I believe the assumption of the mass range based on *L. hesperus* data is appropriate for *P. phalangioides*. Due to the lack of congruency between model predictions and empirical data, this assumption may not have been appropriate for *A. diadematus*.

**3.4.4.4 Joint mechanics:** As mentioned previously (section 3.2.4.3), the value of the joint stiffness parameter was chosen from a distribution defined by the Chapter Two data and each joint had the same stiffness parameter value. I ran the *L. hesperus* model with different stiffness

parameters chosen for the femur-patella and tibia-metatarsus joints than the other leg joints and compared the output to the model output where all leg joints had the same stiffness parameter. I found very small difference in vibration transmission through the leg (Appendix 8). The *L. hesperus* and *P. phalangioides* models accounted for the majority of individual variation when each joint was assigned the same stiffness parameter value, suggesting that differences in joint stiffness within the leg may not impact mechanical filtering greatly.

The other key joint mechanics parameter is joint damping. As mentioned previously (section 3.2.4.3), I assumed this parameter had a baseline value that varied with the surface area of the joint. This assumption was sufficient in previous work and was sufficient for the *L. hesperus* and *P. phalangioides* models. However, in the *A. diadematus* heatmap, the vibration amplitude in the model decreases notably as the vibration transmits from the metatarsus to the patella, which suggests that the joint damping parameter in the model may be too high. I did a preliminary assessment of changing the joint damping parameter baseline value in the *A. diadematus* model however, this did not change the vibration transmission predicted by the model. Nonetheless, the exact value of joint damping in spider joints is unknown, and quantifying the damping of each joint would improve this parameter estimate and perhaps the model fit.

**3.4.4.5 Web contribution:** Another limitation of the models is that I did not model the web itself. For the empirical measurements, the spider was in its web to measure mechanical filtering in a naturalistic setting. A transfer function analysis was effective for *L. hesperus* and *P. phalangioides*, but not for *A. diadematus*. Thus, modeling the web with a prismatic joint may be sufficient for species that construct cobwebs but not orb webs. Future work in developing a

method that vibrates the spider directly or including the web in the model of orb weaving spiders could mitigate this limitation.

### 3.4.5 Conclusions

To conclude, using vibrometry measurements I found that in species of different sizes and orientations, a spider's abdomen resonates at low frequencies and the legs resonate at high frequencies. This finding is consistent with previous qualitative predictions that at lower frequencies the body moves as a rigid object but at higher frequencies the legs move more (Masters, 1984b). The metatarsal lyriform organ is very sensitive and can respond to segment displacements of as little as 100  $\mu\text{m}$  (Barth and Geethabali, 1982). I found that the amplitude of the leg and abdomen mode were similar which may indicate that this lyriform organ may be stimulated in both modes. Perhaps different patterns of other lyriform organ stimulation within the leg due to joint bending allows spiders to differentiate between low and high frequencies. Low frequencies cause more bending in joints more proximal to the body and high frequencies cause more bending of distal joints. Therefore, spiders may mechanically filter low and high frequencies differently in the body. In addition, spider orientation impacts the presence of the abdomen mode which may be advantageous and help filter out low frequency environmental noise.

Similar results were also predicted by multi-body models of each species. Multi-body models successfully predicted the shape of the modes of vibration in *A. diadematus*, *L. hesperus* and *P. phalangoides* and vibration transmission through a single leg in *L. hesperus* and *P. phalangoides*. However, in *A. diadematus*, the movement of the web in the vibrometry measurements could not be removed from the movement of the body. As a result, I cannot

compare the model output to empirical data and the ability of this model to predict vibration transmission in *A. diadematus* remains unknown.

# Chapter Four: Conclusions

## 4.1 Mass independent resonant frequencies of spider bodies

In my thesis, I investigated how size and joint stiffness influence the mechanical filtering of a spider's body. In Chapter Two, I found that the baseline stiffness increased isometrically with spider mass. Spider joints are multi-functional. Leg joints must support a spider's mass during locomotion but are also involved in vibration sensing. Increasing baseline stiffness with mass will support the increasing mass but it will also affect whether a particular frequency will cause joint bending. If the forces generated during joint bending cause cuticular strain through changes in hemolymph pressure, the lyriform organs near the leg joints may be stimulated (Barth and Pickelmann, 1975; Blickhan and Barth, 1985; Hergenröder and Barth, 1983; Schaber et al., 2012; Seyfarth and Barth, 1972). Whether the forces generated during joint bending cause sufficient cuticular strain will be influenced in part by the stiffness of a particular joint. Therefore, joint stiffness is likely important for both locomotion and vibration perception in spiders.

In a simple oscillatory system, such as a mass suspended by a spring, the resonant frequency of the system is determined by equation (4.1).

$$2\pi (f) = \sqrt{\frac{k}{m}} \tag{4.1}$$

Where  $f$  is the resonant frequency (Hz),  $k$  is the spring constant, or stiffness of the spring (N/m), and  $m$  is the mass of the hanging mass (kg). The mechanics of a complete spider body are more

complex as shown by previous work (Mhatre et al., 2018) and my thesis. That said, if one were to simplify the spider body to a simple hanging mass and the legs as springs,  $k$  would be the stiffness of the leg spring. If the mass and the stiffness were to covary in the simple system, as I found with the baseline stiffness and mass (Fig. 2.5), then I speculate that this would result in a relatively static resonant frequency across masses. If a spider's body and leg segments move more at its resonant frequencies, then there is likely more joint bending. If two leg segments are moving at different magnitudes, then the joint between them is likely bending. Joint bending will likely lead to internal strain on the muscles connected to the joint and changes in hemolymph pressure. These internal strains can lead to cuticular strain which can lead to more lyriform organs stimulation at a spider body's resonant frequencies. Therefore, if the resonant frequencies are relatively static, then the vibration frequencies that excite joint bending may be mass independent in spiders.

In Chapter Three, I found that the modes of vibration in *L. hesperus* and *P. phalangoides* occurred at the same frequencies, supporting my prediction that the resonant frequencies of spider bodies may be mass independent. I found two modes of vibration: the abdomen mode where the abdomen and proximal leg segments move more at lower frequencies, and the leg mode where the leg tips move more at higher frequencies. Modes effectively describe the spatial patterns of vibration and show how a spider body moves at its resonant frequencies. From these spatial patterns, we can infer which lyriform organs are most likely being stimulated. We know that displacing a leg segment above the threshold displacement at different frequencies can elicit an action potential in the dendrites of the slit sensillae neurons (Barth and Geethabali, 1982; Bohnenberger, 1981). Since the leg segment has a rigid

exoskeleton, when the segment is displaced, it will rotate around the joint it is connected to. Joint rotation can cause strains on internal tissues such as muscles and changes in hemolymph pressure (Blickhan and Barth, 1985; Schaber et al., 2012). Forces caused by these internal changes can cause minute cuticular strains which will concentrate at the slits in lyriform organs (Höböl et al., 2007; Höböl et al., 2009; Schaber et al., 2012), and if the cuticular strain is great enough, result in an action potential. By looking at the patterns of leg segment movement in the modes of vibration, we can make predictions about what lyriform organs may be stimulated and therefore, what the spider may be perceiving. At lower frequencies, the segments more proximal to the body move more and therefore lyriform organs found near the proximal segments are more likely being stimulated. Likewise, at higher frequencies, segments more distal to the body move more and the lyriform organs found near the distal segments are more likely being stimulated. Spiders may use these potential differences in the pattern of lyriform organ stimulation to differentiate between low and high frequencies. This could be used to differentiate between large and small prey, since small prey generate higher frequency vibrations (Barth et al., 1988; Hergenröder and Barth, 1983; Landolfa and Barth, 1996; Masters, 1984a). Additionally, since these modes of vibration occur at the same frequencies in *L. hesperus* and *P. phalangioides*, these two species with very different morphologies are likely sensing the same frequencies and may be perceiving the world in the same ways.

Interestingly, the vibrations that may be of biological interest to spiders of different sizes occur at relatively similar frequencies. As mentioned previously, small prey like flies generate higher frequency vibrations in comparison to larger prey like crickets. However, the frequency range of vibrations generated by prey is relatively narrow, from 20-100 Hz (Barth et

al., 1988; Hergenröder and Barth, 1983; Landolfa and Barth, 1996; Masters, 1984a). The modes of vibration found in Chapter Three are within this range. If spiders of different sizes are resonating at similar frequencies, the patterns of joint bending and lyriform organ stimulation are likely similar at frequencies commonly made by prey. Therefore, spiders of different sizes may be perceiving prey vibrations in similar ways.

As mentioned previously, males generate courtship vibrations by vibrating their abdomen, drumming their legs or pedipalps on the substrate or by plucking a female's web (Baurecht and Barth, 1992; Elias et al., 2003; Sivalinghem and Mason, 2021; Vibert et al., 2014; Wignall and Herberstein, 2021). This happens both in spider webs and on substrates such as leaves, soil and water (Baurecht and Barth, 1992; Bleckmann and Barth, 1984; Roland and Rovner, 1983; Uetz et al., 2013). What is very interesting is that the frequencies of male courtship vibrations occur within a frequency band of 10-500 Hz whether we look at tiny ground dwelling jumping spiders (*Phiddipus clarus* or *Habronattus dossensus*) (Elias et al., 2003; Elias et al., 2010), small cobweb making hobo spiders (*Eratigena agrestis*) (Vibert et al., 2014), or medium sized western black widow spiders (*Latrodectus hesperus*) (Mhatre et al., 2018; Sivalinghem and Mason, 2021; Vibert et al., 2014), or large spiders like wolf spiders (Elias et al., 2006; Rosenthal et al., 2021) or the tiger wandering spider (*Cupiennius salei*) (Baurecht and Barth, 1992). The conservation of male courtship vibration frequencies may be a consequence of the possible mass independent resonant frequencies of spider bodies.

Since the mechanical filtering by a spider's body may be mass independent, spiders may be filtering vibrational information using other mechanisms which are in their control. It has been found that the mechanical filtering by the body changes with spider posture. The western

black widow in a defensive crouch posture resonates at higher frequencies than in a neutral posture, therefore filtering out frequencies below about 50 Hz (Mhatre et al., 2018). Web-dwelling spiders can also alter properties of the web to change its filtering (Mortimer, 2019). The resonance of the web will influence the frequencies that it vibrates more at, and therefore the frequencies that the web transmits to the spider (Mortimer, 2017). If we think of the silk as a spring, increasing the silk stiffness will increase its resonant frequency (equation 4.1) likely resulting in higher frequencies, such as those associated with prey, to be filtered-in and transmitted to the spider. Changing the web geometry can alter the silk stiffness by aligning silk proteins, where greater alignment leads to increased stiffness (Mortimer et al., 2014; Mortimer et al., 2016). Orb weaving spiders can also alter the stiffness of silk strands with spinning speed. Increasing spinning speed leads to silk with a higher stiffness due to greater alignment of silk proteins (Vollrath et al., 2001). Tensioning the web after spinning will also increase the silk stiffness (Guan et al., 2012). Under high humidity conditions, supercontraction can cause silk strands to contract up to 50% of their length and lead to a decrease in silk stiffness due to poorer alignment of silk proteins (Boutry and Blackledge, 2010; Pérez-Rigueiro et al., 2003). Increased silk stiffness can also increase the speed at which vibrations transmit through the web so that they may reach the spider sooner (Mortimer et al., 2014), but decreased stiffness can increase the amplitude of vibrations generated by prey so that they may cause more joint bending in the spider (Mortimer et al., 2016). Therefore, spiders may focus on particular frequencies by changing the mechanical filtering of the web rather than changing the mechanical filtering by their bodies.

## 4.2 Future research directions

In Chapter Two, I found that each species had a joint stiffness which increased with increasing mass, independent of morphology. I discussed that joint stiffness is likely dominated by active contributions from the muscle. Past work has primarily focused on identifying the number of leg muscles and their function in spider locomotion (Brown, 1939; Ellis, 1944; Parry, 1957; Ruhland and Rathmayer, 1978; Whitehead and Rempel, 1959). Fewer studies have focused on identifying muscle volume, morphology, or muscle fiber type and innervation in spiders (Maier et al., 1987; Ruhland and Rathmayer, 1978). Future work into each of the listed avenues and into muscle force production in spiders would provide insight not only into joint mechanics and mechanical filtering of spider bodies but also spider muscle anatomy and physiology.

As described in section 4.1, from my data in Chapter Two and Three, I predict that vibration sensitivity may be conserved across spider species. However, future studies that include more than two species are required to fully test this. In addition to testing the conservation of vibration sensitivity, future work can use a multi-body modeling approach to predict the amount of joint bending at different frequencies. Predictions of joint bending can be used to infer lyriform organ stimulation and by extension, spider vibration perception.

In Chapter Three, I modeled three species of web-dwelling spiders. Future work can also use multi-body modeling to model spiders of different ecologies, such as wandering spiders that do not build webs but still encounter vibrations through soil, leaves, and water (Baurecht and Barth, 1992; Bleckmann and Barth, 1984; Roland and Rovner, 1983; Uetz et al., 2013). Including

ground dwelling spiders would make the multi-body modeling approach more generalizable, and likely expand the kinds of questions that can be asked using these models. The power of making generalizable models is that these models can make predictions about vibration mechanics for species that we are unable to make empirical measurements from. For example, creating multi-body models using morphological measurements from spider fossils could be used to predict the mechanical filtering of extinct species and to study how mechanical filtering in spiders may have changed over evolutionary time.

Finally, vibration perception is not limited to spiders. Communication using vibrations is found throughout the animal kingdom, and is particularly diverse in insects (Hill, 2015). For example, carpenter ants drum their mandibles against tree trunks to communicate to other ants in the colony (Fuchs, 1976). Male crickets are well-known for their acoustic mating calls, but the Australian cricket, *Balamara gydia*, does not signal acoustically. Instead, both sexes generate vibrations by tapping their abdomens on vegetation to communicate (Huber et al., 1989). Females of the green stink bug, *Nezara viridula*, produce vibrations on plant stems to help searching males locate them (Čokl et al., 1999). Female katydids, *Conocephalus nigropleurum*, discriminate between small and large males using male-generated vibratory signals (De Luca and Morris, 1998). The multi-body modeling technique simplifies the system into a collection of rigid bodies that do not deform in response to external forces. Since insects also have rigid exoskeletons, this method could be applied to this group as well. Future research could use multi-body models to study the vibration mechanics of insects and compare how the mechanical filtering of insect bodies may differ from those of spiders.

# References

- Barth, F. G.** (1971). The sensory apparatus of the slit sense organs (*Cupiennius salei* Keys., Araneae). *Cell Tissue Res* **112**, 212–246.
- Barth, F. G.** (1985a). Neuroethology of the Spider Vibration Sense. In *Neurobiology of Arachnids* (ed. Barth, F. G.), pp. 203–229. Berlin, Heidelberg: Springer.
- Barth, F. G.** (1985b). Slit Sensilla and the Measurement of Cuticular Strains. In *Neurobiology of Arachnids* (ed. Barth, F. G.), pp. 162–188. Berlin, Heidelberg: Springer.
- Barth, F. G.** (2001). *A Spider's World: Senses and Behaviour*. Springer-Verlag Berlin Heidelberg.
- Barth, F. G.** (2002). Spider senses – technical perfection and biology. *Zoology* **105**, 271–285.
- Barth, F. G.** (2004). Spider mechanoreceptors. *Curr. Opin. Neurobiol.* **14**, 415–422.
- Barth, F. G.** (2012). Learning from animal sensors: the clever “design” of spider mechanoreceptors. In *Bioinspiration, Biomimetics, and Bioreplication 2012*, pp. 28–38. SPIE.
- Barth, F. G. and Bohnenberger, J.** (1978). Lyriform slit sense organ: Thresholds and stimulus amplitude ranges in a multi-unit mechanoreceptor. *J. Comp. Physiol.* **125**, 37–43.
- Barth, F. G. and Geethabali** (1982). Spider vibration receptors: Threshold curves of individual slits in the metatarsal lyriform organ. *J. Comp. Physiol.* **148**, 175–185.
- Barth, F. G. and Pickelmann, P.** (1975). Lyriform slit sense organs. *J. Comp. Physiol.* **103**, 39–54.
- Barth, F. G., Bleckmann, H., Bohnenberger, J. and Seyfarth, E.-A.** (1988). Spiders of the genus *Cupiennius* Simon 1891 (Araneae, Ctenidae). *Oecologia* **77**, 194–201.
- Baurecht, D. and Barth, F. G.** (1992). Vibratory communication in spiders. *J. Comp. Physiol. A* **171**, 231–243.
- Biewener, A. A. and Patek, S. N.** (2018). *Animal locomotion*. Second. United Kingdom: Oxford University Press.
- Blackledge, T. A. and Zevenbergen, J. M.** (2007). Condition-dependent spider web architecture in the western black widow, *Latrodectus hesperus*. *Anim. Behav.* **73**, 855–864.
- Bleckmann, H. and Barth, F. G.** (1984). Sensory ecology of a semi-aquatic spider (*Dolomedes triton*). *Behav. Ecol. Sociobiol.* **14**, 303–312.
- Blickhan, R.** (1986). Stiffness of an arthropod leg joint. *J. Biomech.* **19**, 375–384.
- Blickhan, R. and Barth, F. G.** (1985). Strains in the exoskeleton of spiders. *J. Comp. Physiol. A* **157**, 115–147.

- Boehm, C., Schultz, J. and Clemente, C.** (2021). Understanding the limits to the hydraulic leg mechanism: the effects of speed and size on limb kinematics in vagrant arachnids. *J. Comp. Physiol. A* **207**, 105–116.
- Bohnenberger, J.** (1981). Matched transfer characteristics of single units in a compound slit sense organ. *J. Comp. Physiol.* **142**, 391–402.
- Boutry, C. and Blackledge, T. A.** (2010). Evolution of supercontraction in spider silk: structure–function relationship from tarantulas to orb-weavers. *J. Exp. Biol.* **213**, 3505–3514.
- Bradley, R.** (2013). *Common spiders of North America*. Oakland, California: University of California Press.
- Brooks, M. E., Kristensen, K., van Benthem, K. J., Magnusson, A., Berg, C. W., Nielson, A., Skaug, H. J., Maechler, M. and Bolker, B. M.** (2017). {glmmTMB} Balances Speed and Flexibility Among Packaged for Zero-inflated Generalized Linear Mixed Modeling. *The R Journal* **9**, 378–400.
- Brown, R. B.** (1939). The musculature of *Agelena naevia*. *J. Morphol.* **64**, 115–166.
- Chaffin, D. B.** (1969). A computerized biomechanical model—Development of and use in studying gross body actions. *J. Biomech.* **2**, 429–441.
- Challita, E. J., Alexander, S., Han, S., Blackledge, T. A., Coddington, J. A., Jung, S. and Bhamla, M. S.** (2021). Slingshot spiders build tensed underdamped webs for ultrafast launches and speedy halts. *arXiv:2103.05756 [physics]*.
- Chapman, R. F., Simpson, S. J. and Douglas, A. E.** (2013). *The Insects: Structure and Function*. Fifth. New York: Cambridge University Press.
- Čokl, A., Virant-Doberlet, M. and McDowell, A.** (1999). Vibrational directionality in the southern green stink bug, *Nezara viridula* (L.), is mediated by female song. *Anim. Behav.* **58**, 1277–1283.
- De Luca, P. A. and Morris, G. K.** (1998). Courtship Communication in Meadow Katydid: Female Preference for Large Male Vibrations. *Behaviour* **135**, 777–794.
- Dimitrov, D. and Hormiga, G.** (2021). Spider Diversification Through Space and Time. *Annu. Rev. Entomol.* **66**, 225–241.
- Dorfmann, A., Trimmer, B. A. and Woods, W. A.** (2007). A constitutive model for muscle properties in a soft-bodied arthropod. *J. R. Soc. Interface* **4**, 257–269.
- Eberhard, W. G.** (2019). Adaptive flexibility in cues guiding spider web construction and its possible implications for spider cognition. *Behaviour* **156**, 331–362.
- Elias, D. O., Mason, A. C., Maddison, W. P. and Hoy, R. R.** (2003). Seismic signals in a courting male jumping spider (Araneae: Salticidae). *J. Exp. Biol.* **206**, 4029–4039.
- Elias, D. O., Lee, N., Hebets, E. A. and Mason, A. C.** (2006). Seismic signal production in a wolf spider: parallel versus serial multi-component signals. *J. Exp. Biol.* **209**, 1074–1084.

- Elias, D. O., Sivalinghem, S., Mason, A. C., Andrade, M. C. B. and Kasumovic, M. M.** (2010). Vibratory Communication in the Jumping Spider *Phidippus clarus*: Substrate-borne Courtship Signals are Important for Male Mating Success. *Ethology* **116**, 990–998.
- Ellis, C. H.** (1944). The mechanism of extension in the legs of spiders. *Biol. Bull.* **86**, 41–50.
- Ennos, R.** (2012). *Solid biomechanics*. Princeton University Press.
- Erbe, C. and Thomas, J. A.** (2022). *Exploring Animal Behavior Through Sound*. Springer.
- Erko, M., Younes-Metzler, O., Rack, A., Zaslansky, P., Young, S. L., Milliron, G., Chyasnovich, M., Barth, F. G., Fratzi, P., Tsukruk, V., et al.** (2015). Micro- and nano-structural details of a spider's filter for substrate vibrations: relevance for low-frequency signal transmission. *J. R. Soc. Interface* **12**, 20141111.
- Ettema, G. J. C. and Huijing, P. A.** (1994). Skeletal muscle stiffness in static and dynamic contractions. *J. Biomech.* **27**, 1361–1368.
- Evans, M. J. and Rosenthal, J. S.** (2010). *Probability and Statistics, The Science of Uncertainty*. Second. Macmillan Learning.
- Foelix, R. F.** (2011). *Biology of Spiders*. Third. Oxford University Press.
- Fratzi, P. and Barth, F. G.** (2009). Biomaterial systems for mechanosensing and actuation. *Nature* **462**, 442–448.
- French, A. S., Torkkeli, P. H. and Seyfarth, E.-A.** (2002). From stress and strain to spikes: mechanotransduction in spider slit sensilla. *J. Comp. Physiol.* **188**, 739–752.
- Fuchs, S.** (1976). The response to vibrations of the substrate and reactions to the specific drumming in colonies of carpenter ants (*Camponotus*, Formicidae, Hymenoptera). *Behav. Ecol. Sociobiol.* **1**, 155–184.
- Gao, Z., Gibson, I., Ding, C., Wang, J. and Wang, J.** (2015). Virtual Lumbar Spine of Multi-body Model Based on Simbody. *Procedia Technology* **20**, 26–31.
- Garrison, N. L., Rodriguez, J., Agnarsson, I., Coddington, J. A., Griswold, C. E., Hamilton, C. A., Hedin, M., Kocot, K. M., Ledford, J. M. and Bond, J. E.** (2016). Spider phylogenomics: untangling the Spider Tree of Life. *PeerJ* **4**, e1719.
- Gartly, R.** (2021). Modeling the effect of morphology on spider vibration perception.
- Göttler, C., Elflein, K., Siegwart, R. and Sitti, M.** (2021). Spider Origami: Folding Principle of Jumping Spider Leg Joints for Bioinspired Fluidic Actuators. *Adv. Sci.* **8**, 2003890.
- Guan, J., Porter, D. and Vollrath, F.** (2012). Silks cope with stress by tuning their mechanical properties under load. *Polymer* **53**, 2717–2726.

- Halliwell, N. A.** (1979). Laser-Doppler measurement of vibrating surfaces: A portable instrument. *JSV* **62**, 312–315.
- Hao, X., Ma, W., Liu, C., Li, Y., Qian, Z., Ren, L. and Ren, L.** (2019). Analysis of Spiders' Joint Kinematics and Driving Modes under Different Ground Conditions. *Appl. Bionics. Biomech.* **2019**, e4617212.
- Hergenröder, R. and Barth, F. G.** (1983). The release of attack and escape behavior by vibratory stimuli in a wandering spider (*Cupiennius salei* Keys.). *J. Comp. Physiol.* **152**, 347–359.
- Hill, P. S. M.** (2015). Vibration and Animal Communication: A Review. *Integr. Comp. Biol.* **41**, 1135–1142.
- Höfl, B., Böhm, H. J., Rammerstorfer, F. G. and Barth, F. G.** (2007). Finite element modeling of arachnid slit sensilla—I. The mechanical significance of different slit arrays. *J. Comp. Physiol. A* **193**, 445–459.
- Höfl, B., Böhm, H. J., Schaber, C. F., Rammerstorfer, F. G. and Barth, F. G.** (2009). Finite element modeling of arachnid slit sensilla: II. Actual lyriform organs and the face deformations of the individual slits. *J. Comp. Physiol. A* **195**, 881–894.
- Huber, F., Moore, T. E. and Loher, W.** (1989). *Cricket Behavior and Neurobiology*. Cornell University Press.
- Huston, R. L. and Passerello, C. E.** (1971). On the dynamics of a human body model. *J. Biomech.* **4**, 369–378.
- Johnson, J. C., Trubl, P., Blackmore, V. and Miles, L.** (2011). Male black widows court well-fed females more than starved females: silken cues indicate sexual cannibalism risk. *Anim. Behav.* **82**, 383–390.
- Johnson, J. A. G., Liu, H., Höger, U., Rogers, S. M., Sivapalan, K., French, A. S. and Torkkeli, P. H.** (2021). Mechanotransduction channel Piezo is widely expressed in the spider, *Cupiennius salei*, mechanosensory neurons and central nervous system. *Sci Rep* **11**, 7994.
- Juusola, M. and French, A. S.** (1995). Transduction and adaptation in spider slit sense organ mechanoreceptors. *J. Neurophysiol.* **74**, 2513–2523.
- Kane, T. R. and Scher, M. P.** (1969). A dynamical explanation of the falling cat phenomenon. *Int. J. Solids Structures* **5**, 663–670.
- King, G. C.** (2009). *Vibrations and Waves*. First. United Kingdom: Wiley & Sons.
- Klärner, D. and Barth, F. G.** (1982). Vibratory signals and prey capture in orb-weaving spiders (*Zygiella x-notata*, *Nephila clavipes*; Araneidae). *J. Comp. Physiol.* **148**, 445–455.
- Kropf, C.** (2013). Hydraulic System of Locomotion. In *Spider Ecophysiology* (ed. Nentwig, W.), pp. 43–56. Berlin, Heidelberg: Springer.
- Lakey, A., Labeit, S., Gautel, M., Ferguson, C., Barlow, D. p., Leonard, K. and Bullard, B.** (1993). Kettin, a large modular protein in the Z-disc of insect muscles. *The EMBO Journal* **12**, 2863–2871.

- Landkammer, S., Valek, R. and Hornfeck, R.** (2014). A novel bio-inspired fluidic actuator for robotic applications. In *ICAST2014*, p. The Hague, The Netherlands.
- Landkammer, S., Winter, F., Schneider, D. and Hornfeck, R.** (2016). Biomimetic Spider Leg Joints: A Review from Biomechanical Research to Compliant Robotic Actuators. *Robotics* **5**, 15.
- Landolf, M. A. and Barth, F. G.** (1996). Vibrations in the orb web of the spider *Nephila clavipes*: cues for discrimination and orientation. *J. Comp. Physiol. A* **176**, 493–508.
- Lautenschlager, S.** (2020). Multibody dynamics analysis (MDA) as a numerical modelling tool to reconstruct the function and palaeobiology of extinct organisms. *Palaeontology* **63**, 703–715.
- Levins, R.** (1966). The Strategy of Model Building in Population Biology. *American Scientist* **54**, 421–431.
- Liu, C., Chen, S., Sheng, C., Ding, P., Qian, Z. and Ren, L.** (2019). The art of a hydraulic joint in a spider's leg: modelling, computational fluid dynamics (CFD) simulation, and bio-inspired design. *J. Comp. Physiol. A* **205**, 491–504.
- Maier, L., Root, T. M. and Seyfarth, E.-A.** (1987). Heterogeneity of spider leg muscle: Histochemistry and electrophysiology of identified fibers in the claw levator. *J. Comp. Physiol. B* **157**, 285–294.
- Maruyama, K.** (1994). Connectin, an elastic protein of striated muscle. *Biophysical Chemistry* **50**, 73–85.
- Masters, W. M.** (1984a). Vibrations in the Orbwebs of *Nuctenea sclopetaria* (Araneidae): II. Prey and Wind Signals and the Spider's Response Threshold. *Behav. Ecol. Sociobiol.* **15**, 217–223.
- Masters, W. M.** (1984b). Vibrations in the orbwebs of *Nuctenea sclopetaria* (Araneidae). *Behav. Ecol. Sociobiol.* **15**, 207–215.
- Masters, W. M. and Markl, H.** (1981). Vibration Signal Transmission in Spider Orb Webs. *Science* **213**, 363–365.
- Maughan, O. E.** (1978). The Ecology and Behavior of *Pholcus muralicola*. *Am. Midl. Nat.* **100**, 483–487.
- McConney, M. E., Schaber, C. F., Julian, M. D., Barth, F. G. and Tsukruk, V. V.** (2007). Viscoelastic nanoscale properties of cuticle contribute to the high-pass properties of spider vibration receptor (*Cupiennius salei* Keys). *J. R. Soc. Interface* **4**, 1135–1143.
- Mhatre, N., Sivalingham, S. and Mason, A. C.** (2018). Posture controls mechanical tuning in the black widow spider mechanosensory system. *bioRxiv*.
- Miller, T. E. and Mortimer, B.** (2020). Control vs. Constraint: Understanding the Mechanisms of Vibration Transmission During Material-Bound Information Transfer. *Front. Ecol. Evol.* **8**, 460.
- Mitoyen, C., Quigley, C. and Fusani, L.** (2019). Evolution and function of multimodal courtship displays. *Ethology* **125**, 503–515.
- Montgomery, D. C., Peck, E. A. and Vining, G. G.** (2021). *Introduction to Linear Regression Analysis*. Hoboken, NJ, USA: Wiley & Sons.

- Morley, E. L., Sivalingham, S. and Mason, A. C.** (2016). Developmental morphology of a lyriform organ in the Western black widow (*Latrodectus hesperus*). *Zoomorphology* **135**, 433–440.
- Mortimer, B.** (2017). Biotremology: Do physical constraints limit the propagation of vibrational information? *Anim. Behav.* **130**, 165–174.
- Mortimer, B.** (2019). A Spider's Vibration Landscape: Adaptations to Promote Vibrational Information Transfer in Orb Webs. *Integr. Comp. Biol.* **59**, 1636–1645.
- Mortimer, B., Gordon, S. D., Holland, C., Siviour, C. R., Vollrath, F. and Windmill, J. F. C.** (2014). The Speed of Sound in Silk: Linking Material Performance to Biological Function. *Adv Mater* **26**, 5179–5183.
- Mortimer, B., Soler, A., Siviour, C. R., Zaera, R. and Vollrath, F.** (2016). Tuning the instrument: sonic properties in the spider's web. *J. R. Soc. Interface* **13**, 20160341.
- Moya-Laraño, J., Vinković, D., Mas, E. D., Corcobado, G. and Moreno, E.** (2008). Morphological Evolution of Spiders Predicted by Pendulum Mechanics. *PLOS ONE* **3**, e1841.
- Naftilan, S. A.** (1999). Transmission of vibrations in funnel and sheet spider webs. *Int. J. Biol. Macromol.* **24**, 289–293.
- Nakata, K.** (2012). Plasticity in an extended phenotype and reversed up-down asymmetry of spider orb webs. *Anim. Behav.* **83**, 821–826.
- Parry, D. A.** (1957). Spider Leg-muscles and the Autotomy Mechanism. *J. Cell. Sci.* **s3-98**, 331–340.
- Pérez-Rigueiro, J., Elices, M. and Guinea, G. V.** (2003). Controlled supercontraction tailors the tensile behaviour of spider silk. *Polymer* **44**, 3733–3736.
- R Core Team** (2022). R: A language and environment for statistical computing.
- Reußenzehn, S.** (2010). Mechanical design of the legs of *Dolomedes aquaticus*.
- Roland, C. and Rovner, J. S.** (1983). Chemical and Vibratory Communication in the Aquatic Pisaurid Spider *Dolomedes triton*. *J. Arachnol.* **11**, 77–85.
- Rosenthal, M. F., Hebets, E. A., McGinley, R., Raiza, C., Starrett, J., Yan, L. and Elias, D. O.** (2021). Exploring a novel substrate-borne vibratory signal in the wolf spider *Schizocosa floridana*. *Ethology* **127**, 135–144.
- Rossing, T. D. and Fletcher, N. H.** (1995). *Principles of Vibration and Sound*. Springer-Verlag New York.
- Ruhland, M. and Rathmayer, W.** (1978). Anatomy of the leg muscles and their innervation in the tarantula *Dugesia hentzi* (Ch.) (Araneae, Aviculariidae). *Zoomorphologie* **89**, 33–46.
- Saide, J. D.** (1981). Identification of a connecting filament protein in insect fibrillar flight muscle. *J. Mol. Biol.* **153**, 661–679.

- Schaber, C. F., Gorb, S. N. and Barth, F. G.** (2012). Force transformation in spider strain sensors: white light interferometry. *J. R. Soc. Interface* **9**, 1254–1264.
- Schiehlen, W.** (1997). Multibody System Dynamics: Roots and Perspectives | SpringerLink. *Multibody System Dynamics* **1**, 149–188.
- Schneider, C. A., Rasband, W. S. and Eliceiri, K. W.** (2012). NIH Image to ImageJ: 25 years of image analysis. *Nat Methods* **9**, 671–675.
- Sellers, W. I., Pond, S. B., Brassey, C. A., Manning, P. L. and Bates, K. T.** (2017). Investigating the running abilities of *Tyrannosaurus rex* using stress-constrained multibody dynamic analysis. *PeerJ* **5**, e3420.
- Sensenig, A. T. and Shultz, J. W.** (2003). Mechanics of cuticular elastic energy storage in leg joints lacking extensor muscles in arachnids. *J. Exp. Biol.* **206**, 771–784.
- Sensenig, A. T., Lorentz, K. A., Kelly, S. P. and Blackledge, T. A.** (2012). Spider orb webs rely on radial threads to absorb prey kinetic energy. *J. R. Soc. Interface* **9**, 1880–1891.
- Sensenig, A. T., Kelly, S. P., Lorentz, K. A., Leshner, B. and Blackledge, T. A.** (2013). Mechanical performance of spider orb webs is tuned for high-speed prey. *J. Exp. Biol.* **216**, 3388–3394.
- Seyfarth, E.-A. and Barth, F. G.** (1972). Compound slit sense organs on the spider leg: Mechanoreceptors involved in kinesthetic orientation. *J. Comp. Physiol.* **78**, 176–191.
- Seyfarth, E. A. and French, A. S.** (1994). Intracellular characterization of identified sensory cells in a new spider mechanoreceptor preparation. *J. Neurophysiol.* **71**, 1422–1427.
- Siebert, T., Weihmann, T., Rode, C. and Blickhan, R.** (2010). *Cupiennius salei*: biomechanical properties of the tibia–metatarsus joint and its flexing muscles. *J. Comp. Physiol. B* **180**, 199–209.
- Singer, F., Riechert, S., Xu, H., Morris, A., Becker, E., Hale, J. and Nouredine, M.** (2000). ANALYSIS OF COURTSHIP SUCCESS IN THE FUNNEL-WEB SPIDER *AGELENOPSIS APERTA*. *Behaviour* **137**, 93–117.
- Sivalinghem, S. and Mason, A. C.** (2021). Vibratory communication in a black widow spider (*Latrodectus hesperus*): signal structure and signalling mechanisms. *Anim. Behav.* **174**, 217–235.
- Speck-Hergenr, J. and Barth, F. G.** (1986). Tuning of vibration sensitive neurons in the central nervous system of a wandering spider, *Cupiennius salei* Keys. *J. Comp. Physiol.* **160**, 467–475.
- Strauß, J. and Stritih-Peljhan, N.** (2022). Vibration detection in arthropods: Signal transfer, biomechanics and sensory adaptations. *Arthropod Struct Dev* **68**.
- Suter, R. B.** (1978). *Cyclosa turbinata* (Araneae, Araneidae): Prey Discrimination via Web-Borne Vibrations. *Behav. Ecol. Sociobiol.* **3**, 283–296.
- Tew, N. and Hesselberg, T.** (2017). The Effect of Wind Exposure on the Web Characteristics of a Tetragnathid Orb Spider. *J. Insect. Behav.* **30**, 273–286.

- Uetz, G. W., Roberts, J. A., Clark, D. L., Gibson, J. S. and Gordon, S. D.** (2013). Multimodal signals increase active space of communication by wolf spiders in a complex litter environment. *Behav. Ecol. Sociobiol.* **67**, 1471–1482.
- Vibert, S., Scott, C. and Gries, G.** (2014). A meal or a male: the ‘whispers’ of black widow males do not trigger a predatory response in females. *Front. Zool.* **11**, 4.
- Vibert, S., Scott, C. and Gries, G.** (2016). Vibration transmission through sheet webs of hobo spiders (*Eratigena agrestis*) and tangle webs of western black widow spiders (*Latrodectus hesperus*). *J. Comp. Physiol. A* **202**, 749–758.
- Vincent, J. F. V. and Wegst, U. G. K.** (2004). Design and mechanical properties of insect cuticle. *Arthropod Struct Dev* **33**, 187–199.
- Vollrath, F., Madsen, B. and Shao, Z.** (2001). The effect of spinning conditions on the mechanics of a spider’s dragline silk. *Proc. Royal. Soc. B* **268**, 2339–2346.
- Wegst, U. G. K. and Ashby, M. F.** (2004). The mechanical efficiency of natural materials. *Phil. Mag.* **84**, 2167–2186.
- Weihmann, T., Karner, M., Full, R. J. and Blickhan, R.** (2010). Jumping kinematics in the wandering spider *Cupiennius salei*. *J Comp Physiol A* **196**, 421–438.
- Weihmann, T., Günther, M. and Blickhan, R.** (2012). Hydraulic leg extension is not necessarily the main drive in large spiders. *J. Exp. Biol.* **215**, 578–583.
- Wheeler, W. C., Coddington, J. A., Crowley, L. M., Dimitrov, D., Goloboff, P. A., Griswold, C. E., Hormiga, G., Prendini, L., Ramírez, M. J., Sierwald, P., et al.** (2017). The spider tree of life: phylogeny of Araneae based on target-gene analyses from an extensive taxon sampling. *Cladistics* **33**, 574–616.
- Whitehead, W. F. and Rempel, J. G.** (1959). A study of the musculature of the black widow spider, *Latrodectus mactans* (Fabr.). *Can. J. Zool.* **37**, 831–870.
- Wignall, A. E. and Herberstein, M. E.** (2013). The Influence of Vibratory Courtship on Female Mating Behaviour in Orb-Web Spiders (*Argiope keyserlingi*, Karsch 1878). *PLOS ONE* **8**, e53057.
- Wignall, A. E. and Herberstein, M. E.** (2021). Male courtship reduces the risk of female aggression in web-building spiders but varies in structure. *Behav. Ecol.* arab140.
- Winters, J. M.** (1990). Hill-Based Muscle Models: A Systems Engineering Perspective. In *Multiple Muscle Systems: Biomechanics and Movement Organization* (ed. Winters, J. M.) and Woo, S. L.-Y.), pp. 69–93. New York, NY: Springer.
- Wu, C.-H. and Elias, D. O.** (2014). Vibratory noise in anthropogenic habitats and its effect on prey detection in a web-building spider. *Anim. Behav.* **90**, 47–56.
- Wu, J., Miller, T. E., Cicirello, A. and Mortimer, B.** (2023). Spider dynamics under vertical vibration and its implications for biological vibration sensing. *J. R. Soc. Interface* **20**, 20230365.

- Young, S. L., Chyasnavichyus, M., Erko, M., Barth, F. G., Fratzi, P., Zlotnikov, I., Politi, Y. and Tsukruk, V. V.** (2014). A spider's biological vibration filter: Micromechanical characteristics of a biomaterial surface. *Acta Biomaterialia* **10**, 4832–4842.
- Zentner, L.** (2013). Modelling and Application of the Hydraulic Spider Leg Mechanism. In *Spider Ecophysiology* (ed. Nentwig, W.), pp. 451–462. Berlin, Heidelberg: Springer.
- Zhou, J., Lai, J., Menda, G., Stafstrom, J. A., Miles, C. I., Hoy, R. R. and Miles, R. N.** (2022). Outsourced hearing in an orb-weaving spider that uses its web as an auditory sensor.
- Zuur, A. F., Ieno, E. N., Walker, N. J., Saveliev, A. A. and Smith, G. M.** (2009). Mixed Effects Modelling for Nested Data. In *Mixed effects models and extensions in ecology with R* (ed. Zuur, A. F., Ieno, E. N., Walker, N.), Saveliev, A. A., and Smith, G. M.), pp. 101–142. New York, NY: Springer.

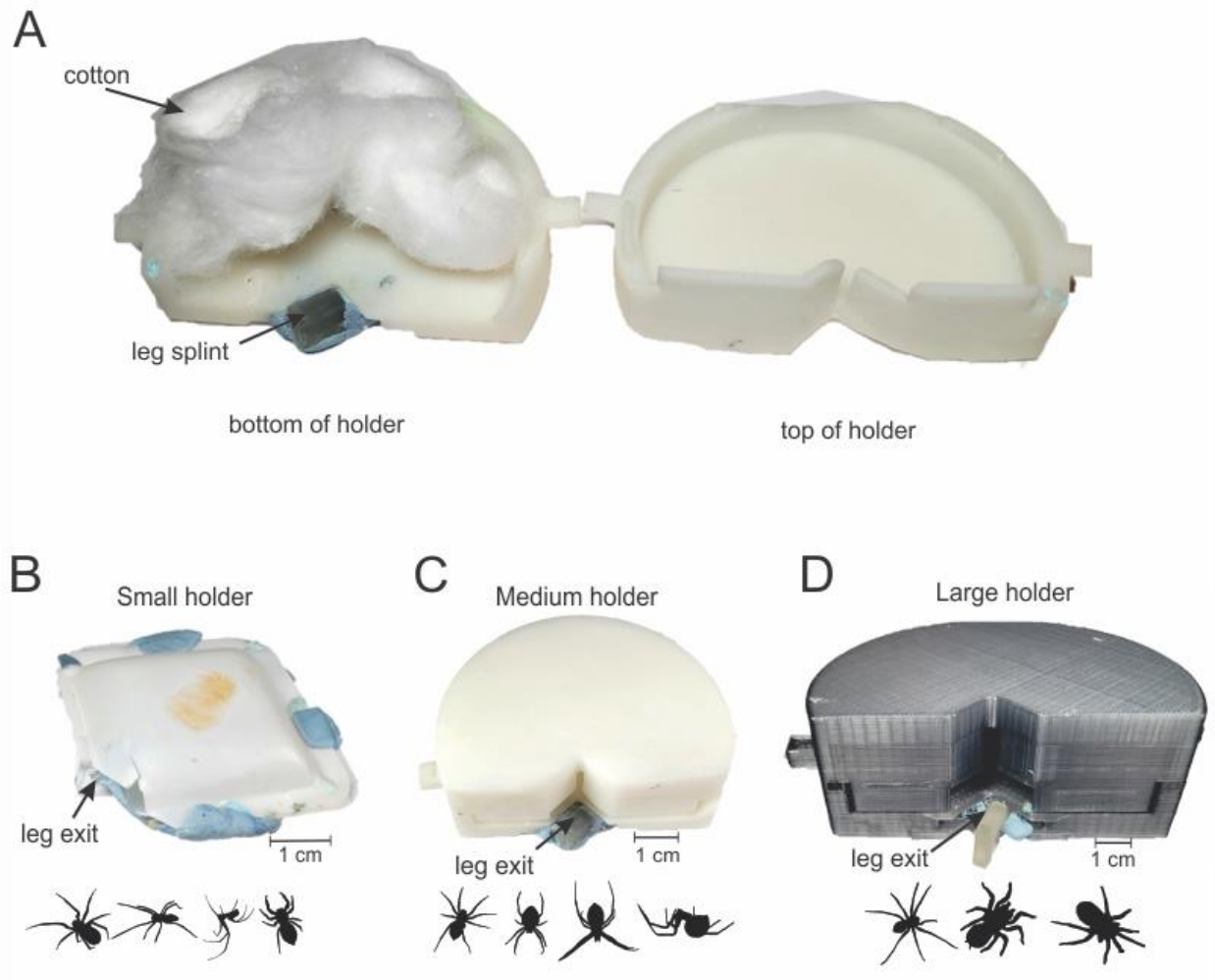
# Appendices

## Appendix 1. Permissions for select figures in Chapter One.

Figure	License Number	Publisher	Publication	Author
1.1	CCYP 2.0 DEED Attribution 2.0 Generic ( <a href="https://creativecommons.org/licenses/by/2.0/">https://creativecommons.org/licenses/by/2.0/</a> )	BioMed Central	Frontiers in Zoology	Samantha Vibert et al
1.2 B	5659480021395	Springer Nature	Journal of Comparative Physiology A: Neuroethology, Sensory, Neural, and Behavioral Physiology	Andrew S. French et al
1.2 C	5660840024802	Springer Nature	Zeitschrift für Zellforschung und Mikroskopische Anatomie	Friedrich G. Barth
1.2 C	5659480021395	Springer Nature	Journal of Comparative Physiology A: Neuroethology, Sensory, Neural, and Behavioral Physiology	Andrew S. French et al
1.2 D	5659480288115	Springer Nature	Journal of Comparative Physiology A: Neuroethology, Sensory, Neural, and Behavioral Physiology	Prof. Dr. Friedrich G. Barth et al



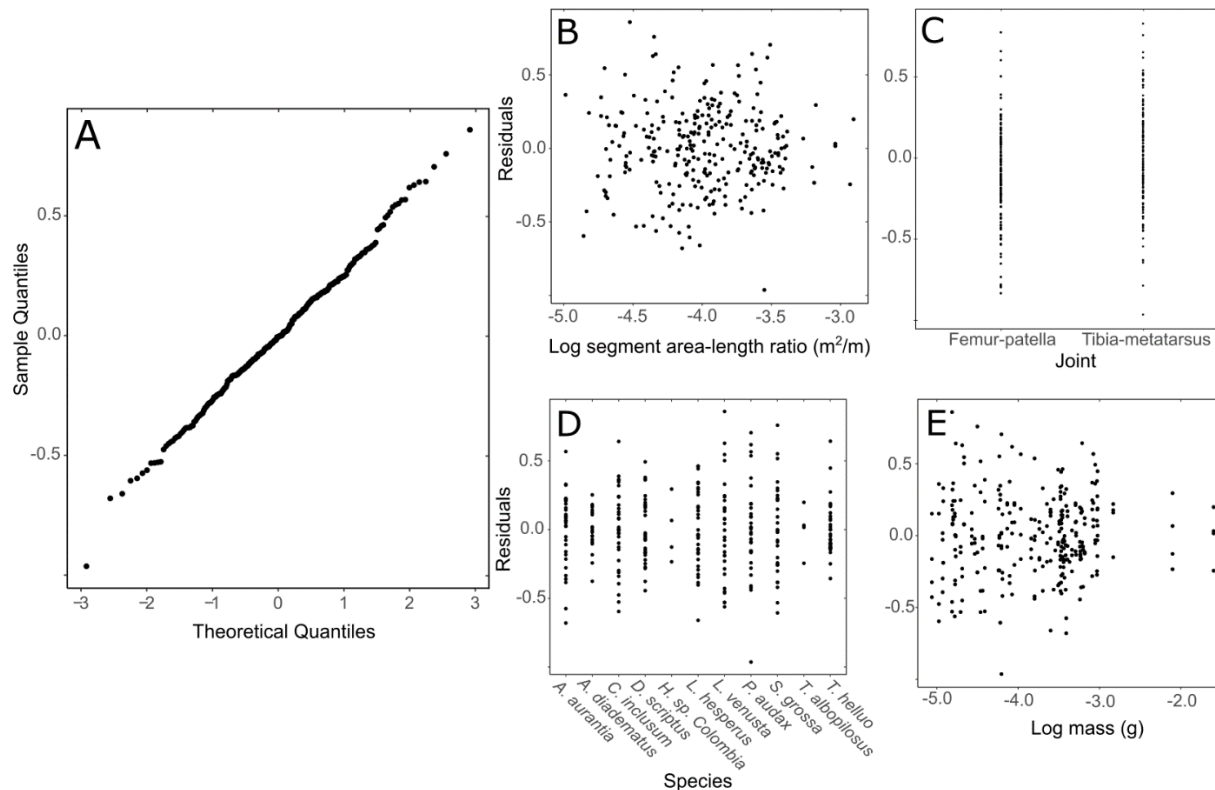
**Appendix 2.** Dead spiders hanging in webs with legs fully extended. (A) is *Argiope aurantia* and (B) is *Latrodectus hesperus*. The legs attached to the leg have fully extended because the passive stiffness of the joint is not sufficient to support the weight of the abdomen.



**Appendix 3.** Spider holders used in measurements for Chapter Two. (A) The proximal segments to the joint were immobilized by gluing the segments to a splint with liquid latex and the spider body was surrounded by cotton to restrict movement and prevent the spider from pulling the leg into the holder once awake. (B) For small spiders, two weigh plates were used as the holder. (C and D) For medium and large spiders, a holder was designed in Autodesk Fusion 360 (version 2.0.11894, Autodesk, USA) and printed using a 3D resin printer. Spider silhouettes show which holder was used for each species.

**Appendix 4.** Mean and standard deviation of the initial joint angle for each species ( $\xi$  = eight individuals per species, \*= one individual per species).

<b>Species</b>	<b>Femur-patella starting angle (deg)</b>	<b>Tibia-metatarsus starting angle (deg)</b>
<i>L. venusta</i> $\xi$	116.2 $\pm$ 22.9	154.0 $\pm$ 14.4
<i>C. inclusum</i> $\xi$	97.9 $\pm$ 15.6	140.8 $\pm$ 21.7
<i>S. grossa</i> $\xi$	92.8 $\pm$ 22.1	141.2 $\pm$ 16.0
<i>P. audax</i> $\xi$	107.1 $\pm$ 24.1	151.1 $\pm$ 15.9
<i>L. hesperus</i> $\xi$	103.2 $\pm$ 13.5	154.0 $\pm$ 14.4
<i>A. diadematus</i> $\xi$	115.5 $\pm$ 14.6	149.0 $\pm$ 15.5
<i>A. aurantia</i> $\xi$	105.4 $\pm$ 18.8	143.1 $\pm$ 22.3
<i>T. helluo</i> $\xi$	113.6 $\pm$ 17.3	149.2 $\pm$ 12.6
<i>D. scriptus</i> $\xi$	118.6 $\pm$ 18.8	166.1 $\pm$ 13.7
<i>H. sp. Colombia</i> *	114.1 $\pm$ 13.7	144.3 $\pm$ 18.0
<i>T. albopilosus</i> *	129.9 $\pm$ 4.8	146.6 $\pm$ 8.2



**Appendix 5.** Checking mixed effects model assumptions for the best model. (A) shows a quantile-quantile plot checking for normality. The residuals follow a linear trend which indicates this assumption is met. (B-E) Model residuals are shown on the vertical with each x-variable on the horizontal axis. Certain patterns, for example, a cone-shape pattern indicates systematic residual variation in the x-variable which is not accounted for by the model. No such patterns are seen in any of the x-variables included in the best model (B-D). In addition, no pattern is seen in the residuals of the excluded x-variable, mass (E). This indicates that including mass as an explanatory variable in the best model would not improve the fit of the slopes observed in each species. However, I find that the intercept is explainable by the mass.

**Appendix 6.** Tables of the parameters for the multi-body models for each species. All parameters are symmetric for each side.

<b>Rigid body dimensions for body segments (x-y-z (mm))</b>								
<i>Species</i>		<i>Cephalothorax</i>	<i>Abdomen average</i>	<i>Abdomen lower range</i>	<i>Abdomen upper range</i>			
<i>A. diadematus</i>		3.6 x 3.6 x 4.0	3.7 x 3.7 x 4.9	2.3 x 2.3 x 3.1	3.8 x 3.8 x 5.1			
<i>L. hesperus</i>		4.3 x 3.6 x 3.1	5.4 x 4.4 x 4.4	3.4 x 2.8 x 2.8	5.6 x 4.5 x 4.5			
<i>P. phalangioides</i>		1.5 x 1.4 x 1.4	1.9 x 1.3 x 1.3	1.2 x 0.8 x 0.8	2.0 x 1.4 x 1.4			

<b>Rigid body dimensions for leg segments (length x radius (mm))</b>								
<i>Species</i>	<i>Leg</i>	<i>Segment</i>						
		<i>Cx</i>	<i>Tro</i>	<i>Fem</i>	<i>Pat</i>	<i>Tib</i>	<i>Met</i>	<i>Tar</i>
<i>A. diadematus</i>	1	1.4 x 0.4	0.5 x 0.4	5.3 x 0.5	2.1 x 0.3	4.8 x 0.3	4.5 x 0.1	1.7 x 0.1
	2	1.5 x 0.5	0.5 x 0.4	4.5 x 0.4	2.0 x 0.3	4.1 x 0.3	3.9 x 0.1	1.5 x 0.1
	3	1.2 x 0.4	0.5 x 0.3	3.6 x 0.3	1.6 x 0.3	2.7 x 0.3	3.0 x 0.1	1.5 x 0.1
	4	1.4 x 0.5	0.6 x 0.4	4.7 x 0.3	1.7 x 0.3	3.6 x 0.2	3.5 x 0.1	1.3 x 0.1
<i>L. hesperus</i>	1	1.2 x 0.3	0.5 x 0.3	5.7 x 0.4	1.8 x 0.3	4.6 x 0.3	5.4 x 0.1	1.8 x 0.1
	2	1.1 x 0.3	0.4 x 0.3	4.1 x 0.3	1.5 x 0.3	2.6 x 0.3	3.8 x 0.1	1.3 x 0.1
	3	1.0 x 0.3	0.4 x 0.3	3.1 x 0.3	1.3 x 0.3	2.0 x 0.3	2.8 x 0.1	1.1 x 0.1
	4	1.4 x 0.4	0.5 x 0.3	5.1 x 0.4	1.7 x 0.3	4.0 x 0.3	5.1 x 0.2	1.7 x 0.1
<i>P. phalangioides</i>	1	0.9 x 0.1	0.1 x 0.1	5.7 x 0.1	0.4 x 0.1	6.4 x 0.07	8.9 x 0.05	1.6 x 0.03
	2	0.4 x 0.1	0.3 x 0.1	4.3 x 0.09	0.3 x 0.09	4.4 x 0.07	5.9 x 0.05	1.1 x 0.03
	3	0.3 x 0.1	0.1 x 0.1	3.5 x 0.1	0.3 x 0.08	3.2 x 0.07	4.4 x 0.05	0.8 x 0.03
	4	0.4 x 0.1	0.1 x 0.1	4.9 x 0.1	0.3 x 0.09	4.4 x 0.08	6.0 x 0.05	1.0 x 0.03

Joint parameters		
<i>Silk</i>	<b>Stiffness (N/m)</b>	<b>Damping coefficient (N/(m/s))</b>
	0.3	0.06
<i>Abd-Ceph joint</i> <sup>1</sup>	<b>Stiffness (Nm/rad)</b>	<b>Damping coefficient (Nm/(rad/s))</b>
	$3 \times 10^{-4}$	$15 \times 10^{-6}$

Leg joint stiffness		
<i>Species</i>	<b>Stiffness distribution mean (Nm/rad)</b>	<b>Stiffness distribution standard deviation</b>
<i>A. diadematus</i>	$4.19 \times 10^{-6}$	$3.78 \times 10^{-6}$
<i>L. hesperus</i>	$1.25 \times 10^{-5}$	$1.25 \times 10^{-5}$
<i>P. phalangioides</i>	$3.15 \times 10^{-7}$	$3.76 \times 10^{-7}$

Joint damping ( $\times 10^{-7}$ (Nm/(rad/s)))								
<i>Species</i>	<i>Leg</i>	<i>Joint</i>						
		<i>Ceph-Cx</i>	<i>Cx-Tro</i>	<i>Tro-Fem</i>	<i>Fem-Pat</i>	<i>Pat-Tib</i>	<i>Tib-Met</i>	<i>Met-Tar</i>
<i>A. diadematus</i>	1	4.71	4.71	4.53	4.98	3.51	3.01	1.52
	2	5.28	5.28	4.26	4.5	3.36	3	1.69
	3	4.33	4.33	3.43	3.92	3.25	2.8	1.94
	4	4.94	4.95	4.27	3.9	3.4	2.78	1.83
<i>L. hesperus</i>	1	3.79	3.79	3.64	4.24	3.67	3.36	1.76
	2	3.86	3.86	3.32	3.78	3.43	3.13	1.78
	3	3.49	3.49	3.14	3.52	3.19	3.14	1.74

<sup>1</sup> Parameter values for this joint are based on previous work (Mhatre et al., 2018), were the same for each species, and were not varied during model simulation

	4	4.31	4.31	3.8	4.03	3.82	3.9	2.26
<i>P. phalangioides</i>	1	1.36	1.36	1.29	1.09	1.01	0.75	0.56
	2	1.28	1.28	1.2	0.98	0.97	0.74	0.53
	3	1.36	1.36	1.19	1.02	0.87	0.71	0.52
	4	1.41	1.41	1.24	1.07	0.96	0.87	0.54

---

**Joint equilibrium angles (degrees)<sup>2</sup>**


---

<i>Species</i>	<i>Leg</i>	<i>FemPat</i>	<i>TibMet</i>
<i>A. diadematus</i>	1	-61	-50
	2	-60	-61
	3	-72	-30
	4	-38	-39
<i>L. hesperus</i>	1	-32	-55
	2	-54	-67
	3	-65	-35
	4	-51	-46
<i>P. phalangioides</i>	1	-43	-38
	2	-67	-80
	3	-71	-96
	4	-94	-50

---

**Variation in leg position<sup>3</sup>**


---

<i>Leg</i>	<i>Distribution mean</i>	<i>Distribution standard deviation (species)</i>
1	0	1 ( <i>A. diadematus</i> ), 0.7 ( <i>L. hesperus</i> ), 0.5 ( <i>P. phalangioides</i> )

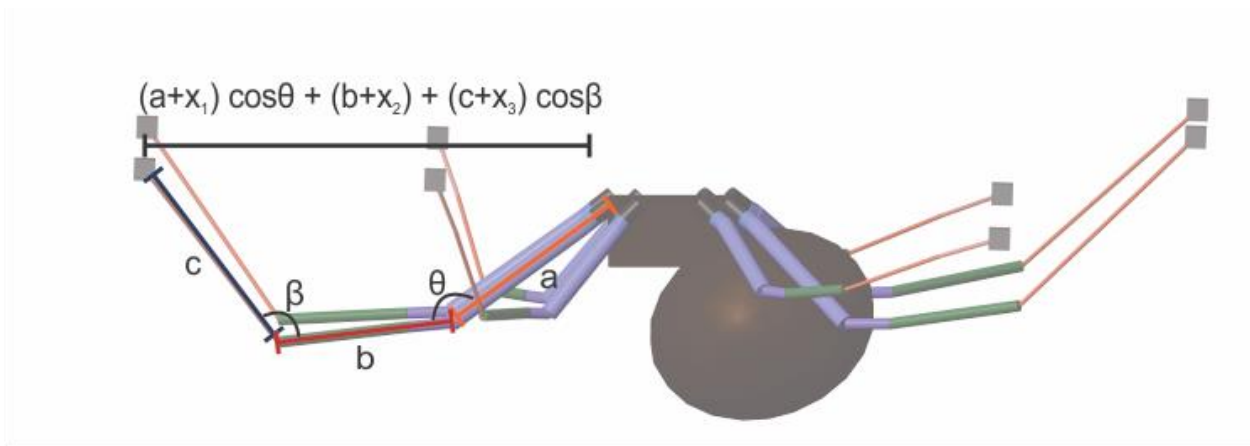
---

<sup>2</sup> Equilibrium angles of all unlisted joints were 0 degrees.

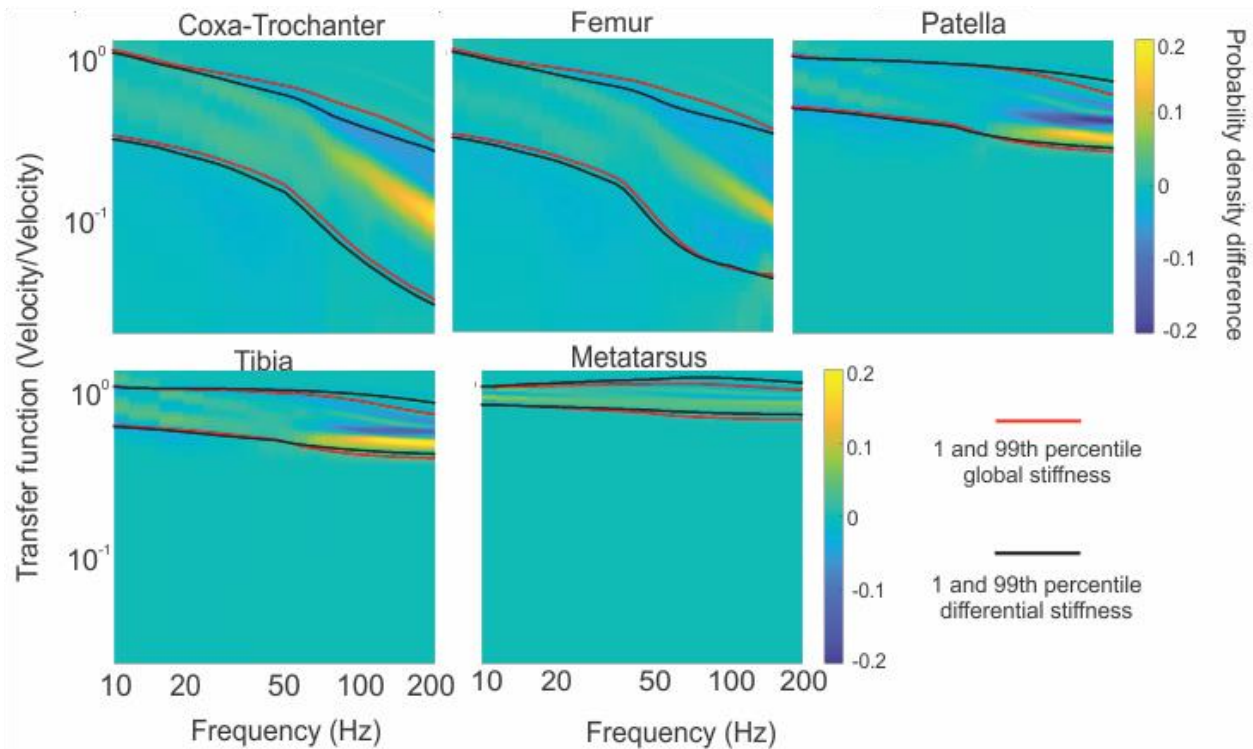
<sup>3</sup> See Appendix 7 for detail of how the leg position was varied.

2	0	0.5 (all species)
3	0	0.3 ( <i>A. diadematus</i> ), 0.5 ( <i>L. hesperus</i> ), 0.2 ( <i>P. phalangioides</i> )
4	0	1 ( <i>A. diadematus</i> ), 0.2 ( <i>L. hesperus</i> ), 0.2 ( <i>P. phalangioides</i> )

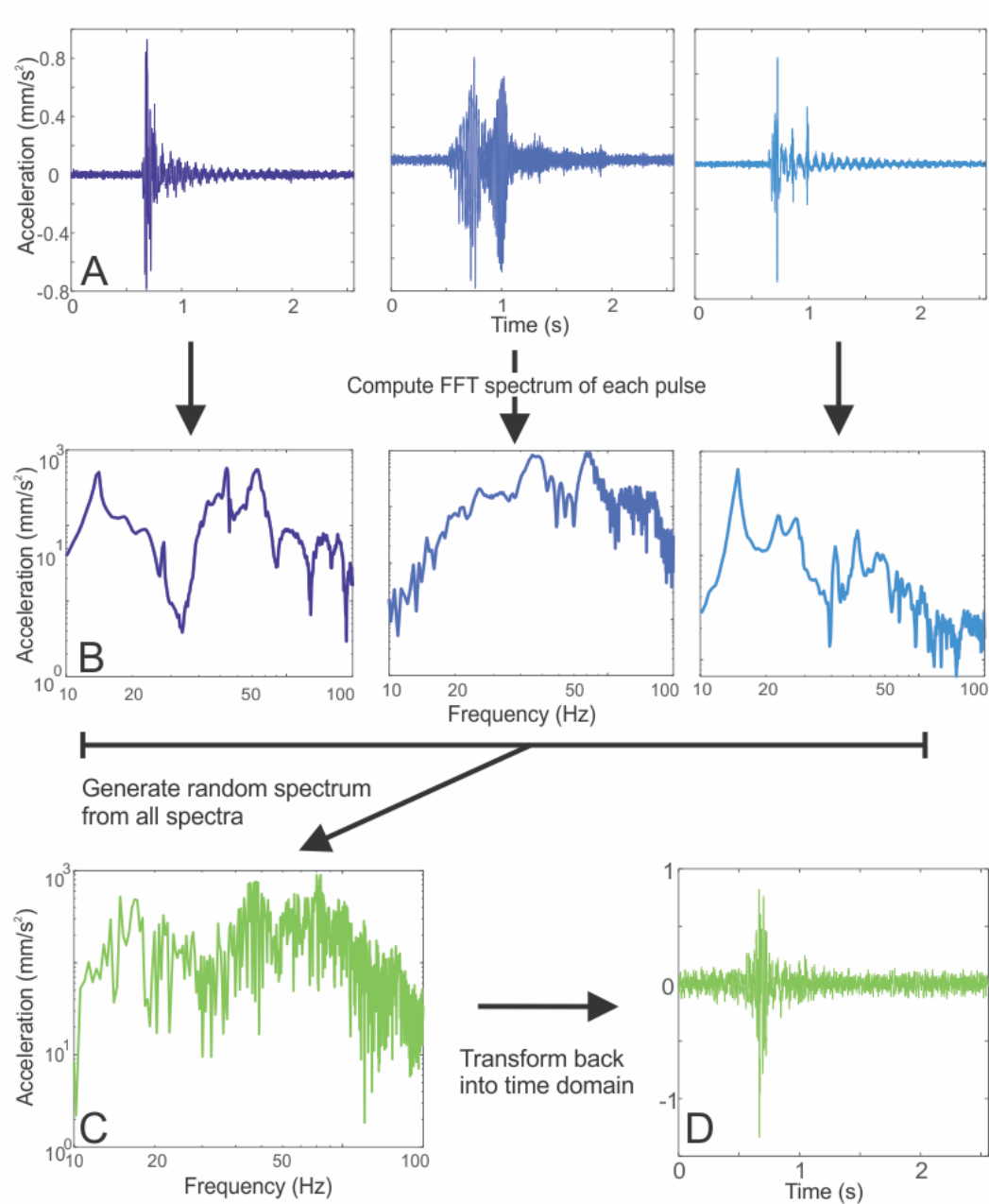
---



**Appendix 7.** The spider posture is defined by the joint angle between two adjacent leg segments and where the leg connects to the web. The location of the leg-web connection is calculated using the leg lengths and the femur-patella ( $\Theta$ ) and tibia-metatarsus ( $\beta$ ) joint angles. The spider leg at rest roughly makes a trapezium with the web. The sides of the trapezium are determined by the lengths of the leg segments and the base of the trapezium is calculated using the equation shown. I varied the sides of the trapezium by adding a number ( $x_i$ ) chosen with a random number generator in Matlab (*normrnd*). Note that the added variation does not change the actual dimensions of the rigid bodies, only dimensions of the trapezium that are used to calculate the distance of the leg tip placement. The generated numbers were determined from normal distributions (see Appendix 6). The distribution mean was chosen to include both negative and positive generated numbers to reflect the possibility that the leg tip is closer or farther from the cephalothorax respectively. The distribution standard deviation ( $\sigma$ ) was determined by running the model and observing its behaviour as this parameter was gradually changed. If the model posture was unnatural,  $\sigma$  was decreased. If the posture was not visually different between successive runs,  $\sigma$  was increased. The standard deviation was higher in the front legs, which also reflects their possible sensory function. These legs are thought to be sensory legs that are used to probe the environment and thus may have higher placement variation in static postures (Foelix, 2011).

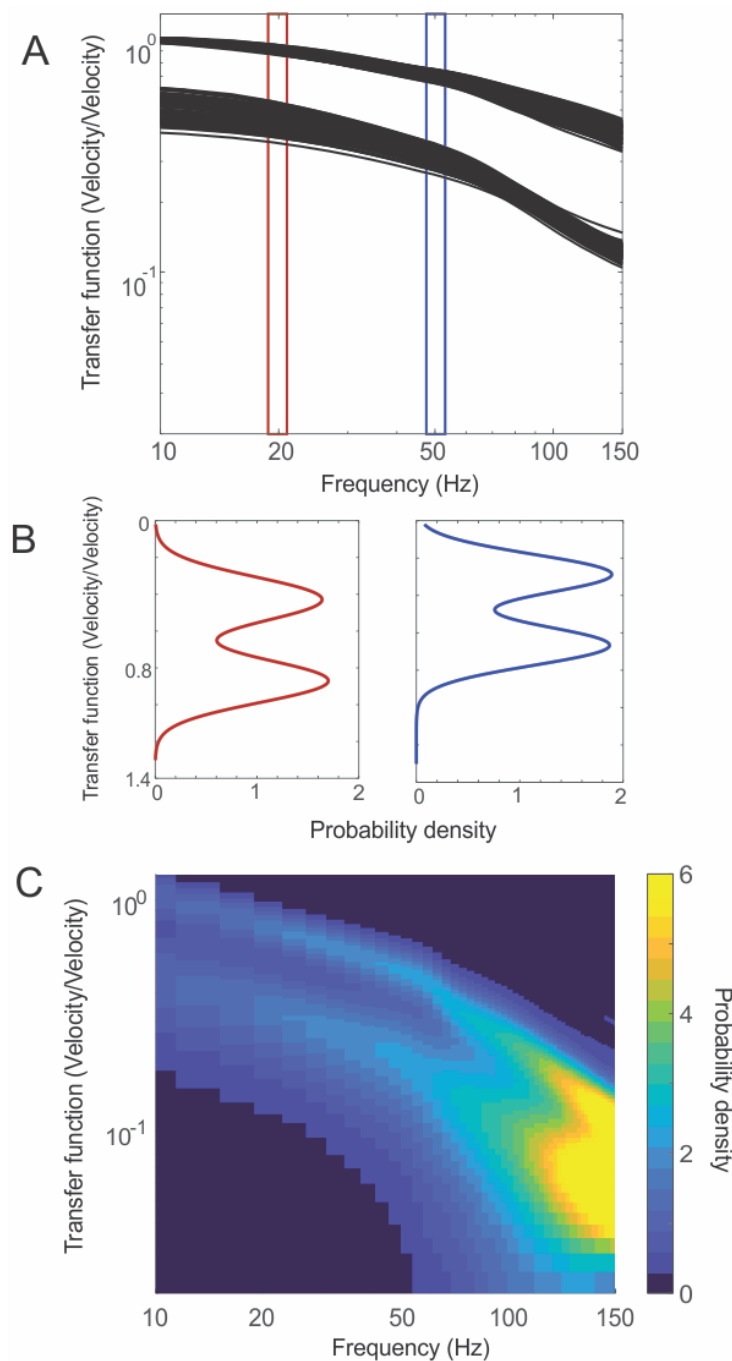


**Appendix 8.** Effects of varying the stiffness of different joint types independently. In Chapter Two, stiffnesses of different joint types were found to be statistically different, but it is unknown if this makes a difference functionally for mechanical filtering by the body mechanics. To test if varying each individual joint's stiffness had a functional impact on mechanical filtering, I ran the *L. hesperus* model in two different ways. I varied the joint stiffness but assigned each joint the same value. This is termed 'global stiffness'. I then varied the femur-patella and tibia-metatarsus stiffness independently. This is termed 'differential stiffness'. Subtraction of the heatmap results of the differential stiffness from the global stiffness heatmaps shows very minimal differences between the two. The red lines are the 1 and 99<sup>th</sup> percentiles of the global stiffness model and black is the same for the differential stiffness model. Percentiles are essentially the same in the two model versions. The difference in probability density is also quite small. Therefore, varying each joint's stiffness independently does not appear to have a functional impact on the mechanical filtering by the body. Based on this result, all joints were assigned the same stiffness value for all models in Chapter Three.



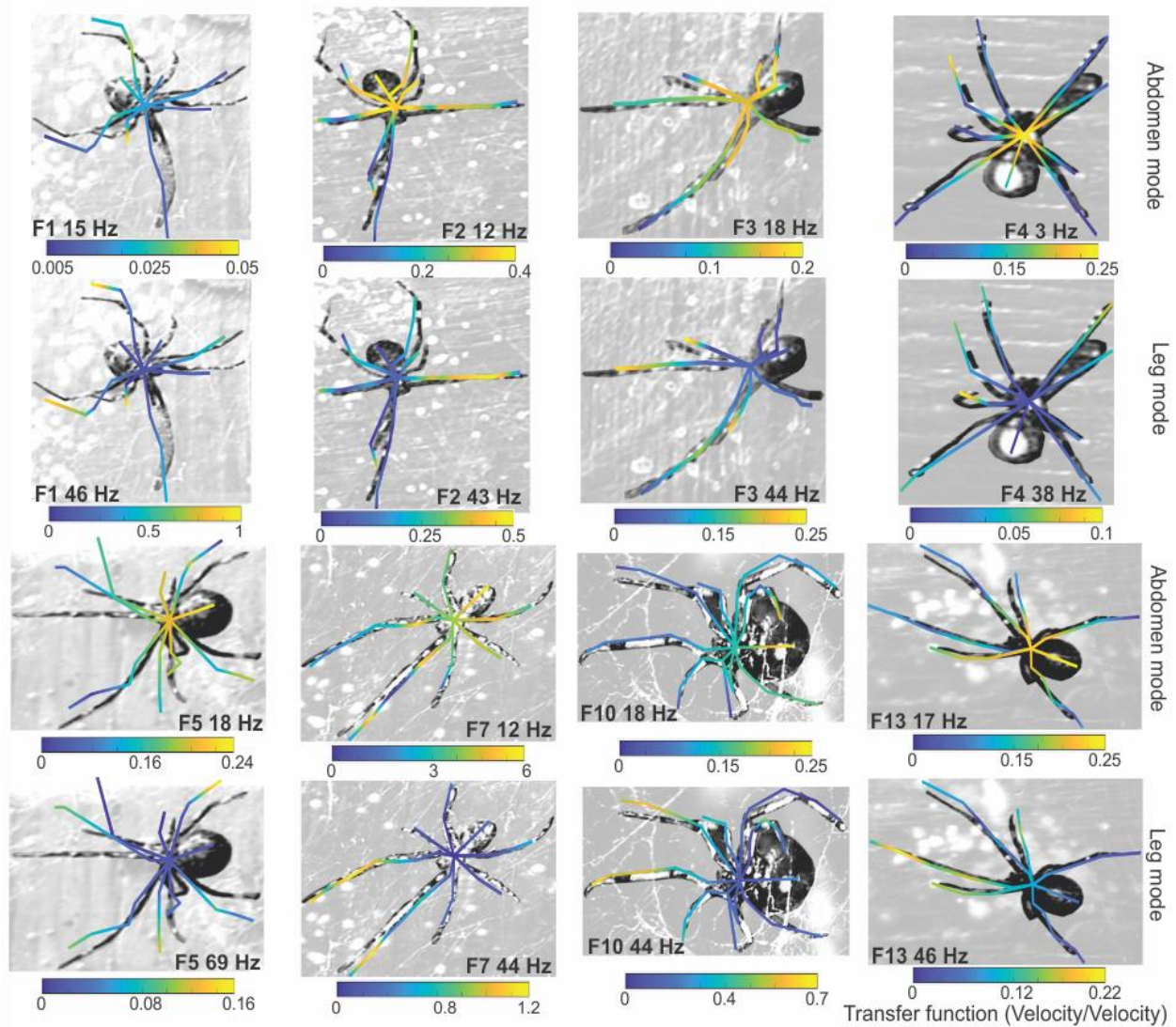
**Appendix 9.** Creating variable pulses for model stimulation. I obtained the vibration velocity of the tarsus over time from each measured individual. This represented the vibration entering a real spider and causing it to vibrate. (A) In Polytec Presentation (version 10), I calculated the acceleration of this point, which would be proportional to the applied force, by computing the derivative of the measured velocity signal. I applied a low-pass filter, which filters out high frequency vibrations, to reduce noise due to frequencies above 500 Hz in the signal. (B) In Matlab, I converted each signal of the tarsus' acceleration over time into the frequency domain

using the fast Fourier transform (FFT, sampling frequency = 25.6 kHz). I calculated the minimum and maximum amplitude and mean phase of each leg tip spectra at each frequency. (C) I created a spectrum by choosing a number from a uniform distribution based on the amplitude range using a random number generator. I used the mean phase for each spectrum rather than changing the phase because I found it reduced the noise in the generated spectrum. (D) I performed an inverse FFT to convert the generated spectrum back into time to be used for model simulation. 200 spectra were generated for each species and used for each model run.



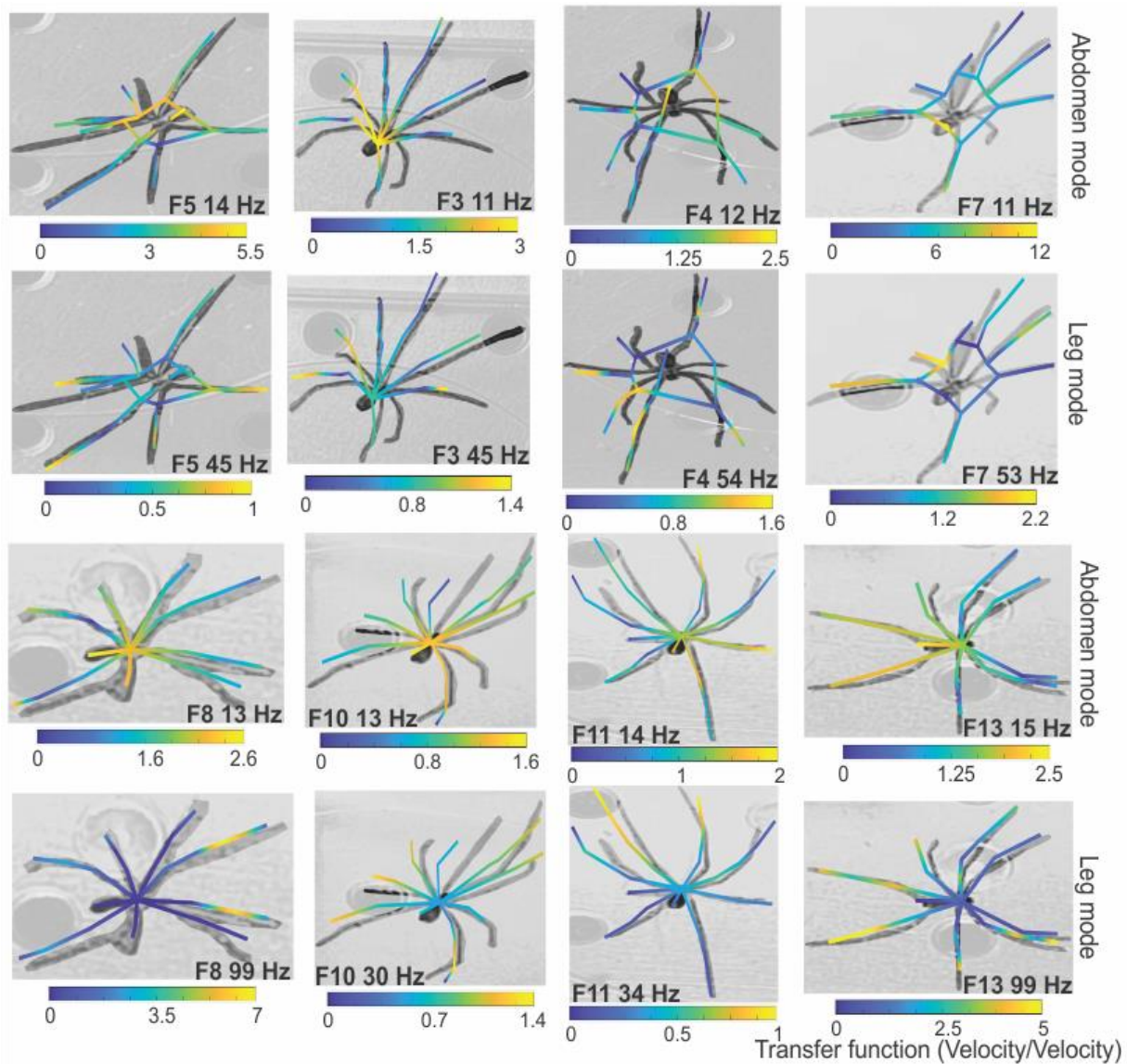
**Appendix 10.** Creating a probability density heatmap. (A) I took the 200 transfer functions of the model output of a single segment's motion relative to the leg tip. (B) I then calculated the probability density function (pdf) of the segment's motion at each frequency. To estimate the pdf, I fit a Kernel distribution to the model run amplitudes using the Matlab functions *fitdist* and *pdf*. I chose a Kernel distribution because it is a bimodal distribution which reflects the way the model output groups together due to the abdomen-web connection. (C) The pdfs at each

frequency were then concatenated and plotted as a 2D heatmap with frequency on the horizontal, transfer function magnitude on the vertical axis and the heatmap colours indicate the values of the pdf at each frequency. This was then repeated for each leg segment.

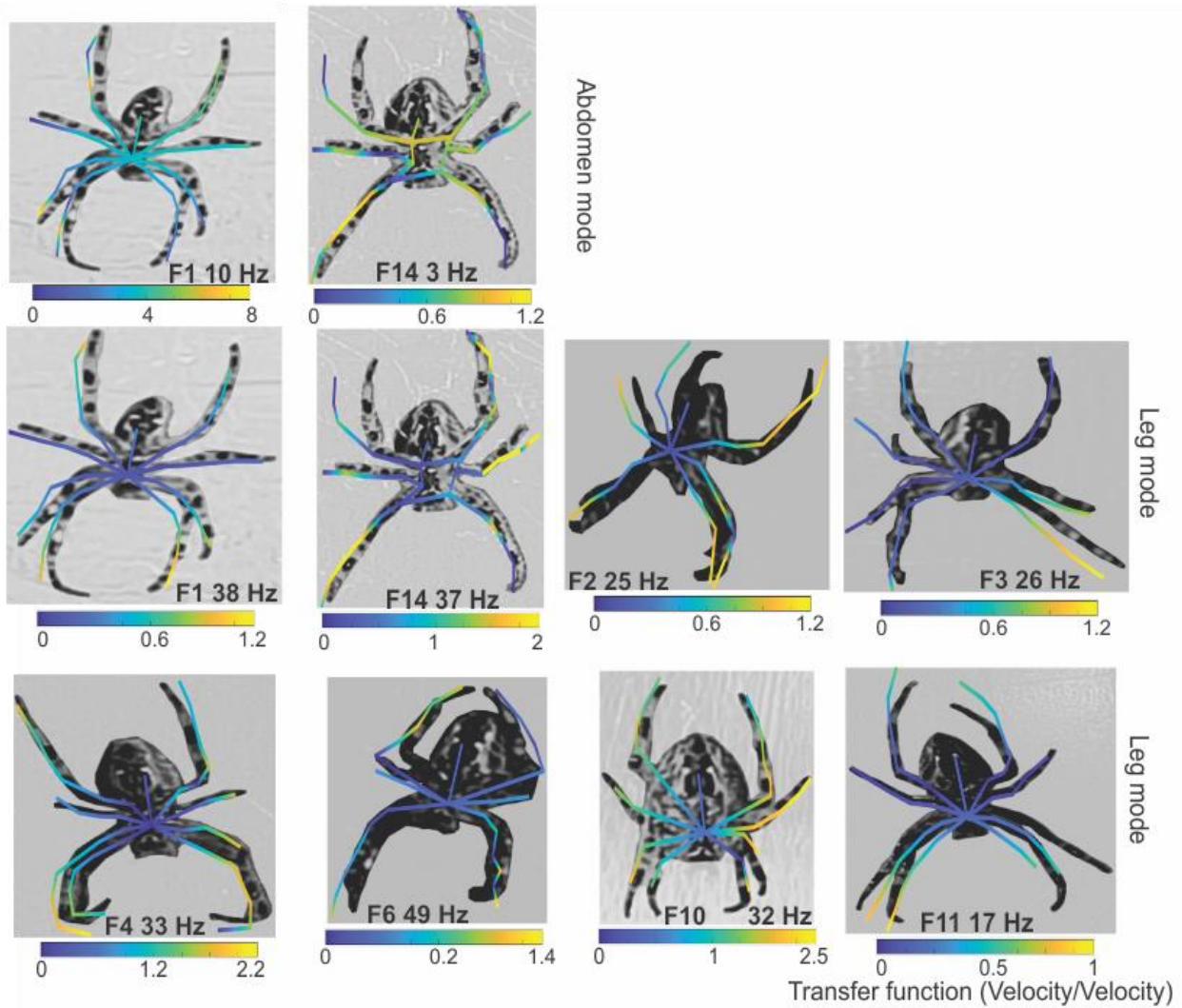


**Appendix 11.** Modes of vibration observed from the vibrometry measurements of *L. hesperus*.

Two modes of vibration were found for each measured individual ( $n = 8$ ). In the first mode, the abdomen had a high velocity amplitude and legs were relatively motionless (abdomen mode). In the second, the legs exhibited high velocity amplitudes, and the abdomen was relatively motionless (leg mode). Each row shows one mode type with individuals grouped by column. For each plot, the individual identification (e.g., F1) and the frequency at which the mode occurred is indicated. The lines overlaid on the spider photo indicate the pattern of movement of the spider body at the indicated frequency. The line colour indicates the magnitude of the transfer function, yellow indicating higher velocity, purple indicating lower velocity relative to the leg tips. The background is made partially transparent to make the spider more visible.



**Appendix 12.** Modes of vibration observed from the vibrometry measurements of *P. phalangioides*. The abdomen mode and leg mode were also found in this species (n=8). Each row shows one mode shape with individuals grouped by column. For each plot, motion of the body is represented in the same way as *L. hesperus*. Some individuals did not have a data point on the cephalothorax, so a box was drawn connecting the most proximal leg segment datapoints. The background is made partially transparent to make the spider more visible.



**Appendix 13.** Modes of vibration observed from the vibrometry measurements of *A. diadematus*. Unlike *L. hesperus* and *P. phalangioides*, only the leg mode was found (n=8). Only two individuals showed a pattern that resembled the abdomen mode found in *L. hesperus* and *P. phalangioides*. Each row shows one mode shape with individuals grouped by column. For each plot, motion of the body is represented in the same way as *L. hesperus*.

# Curriculum Vitae

## Reese Gartly

### Post-secondary Education and Degrees

**M.Sc. Biology**, September 2021 – Present

*University of Western Ontario, London, ON*

**B.Sc. Honors Specialization in Integrated Sciences with Biology**, April 2021

*University of Western Ontario, London, ON*

### Relevant Work Experience

Teaching Assistant, *University of Western Ontario, London, ON, 2021 – 2023*

Pre-Graduate Student Researcher, *University of Western Ontario, London, ON, 2021*

Student Researcher, *University of Western Ontario, London, ON, Summer 2018 & 2019*

### Honours and Awards

Queen Elizabeth II Award Graduate Scholarship in Science and Technology 2021 & 2022

Brian K. Hall Award, *Canadian Zoological Society, 2022*

Dean's Honour List, *University of Western Ontario, 2018 – 2021*

### Conference Presentations

**Gartly, R.**, Fisher, L., Elganga, M., Rubin, BR., Mhatre, N. (2023) Does spider leg joint stiffness vary with leg size? Invertebrate Sound and Vibration, Lincoln, UK [Poster]

**Gartly, R.**, Mhatre, N. (2022) Modeling whole-body vibrational tuning in spiders of different body sizes. Canadian Zoological Society, Moncton, NB [Oral – Virtual]

**Gartly, R.**, Mhatre, N. (2021) Testing the parameter sensitivity of biomechanical models of black widow spiders. Biology Graduate Research Forum, London ON [Poster]

**Gartly, R.**, Mhatre, N. (2021) Modeling the effect of morphology on spider vibration perception. Ontario Ecology, Ethology, and Evolution Colloquium, Guelph ON [Poster]